MONASH University

Evaluating rock physics–fracture mechanics relationship by quantifying fracture process zone

Saeed Aligholi
B.Sc, M.Sc.

A thesis submitted for the degree of Doctor of Philosophy at
Monash University in 2021
Department of Civil Engineering

Copyright notice

Abstract

In this thesis, the length of Fracture Process Zone (FPZ) of four rock types including a red sandstone, a white coarse-grained marble, a fine-grained granite and a coarse-grained granite are quantified. This selection covers sedimentary, metamorphic and igneous rock types with different grain sizes. The length of FPZ of a moving crack or the cohesive length ℓ_c is quantified by post mortem roughness analysis of the fracture surfaces of the studied rocks using statistical physics and multifractal framework. Then, this critical length, ℓ_c, is imported into non-linear fracture mechanics models to connect rock physics and fracture mechanics, which leads to determination of the cohesive stress σ_c or intrinsic tensile strength of rock materials.

By means of 3D image processing techniques using Mathematica software (Wolfram programming language and MASSIVE HPC facility) very high quality fractured surfaces are extracted from 3D X-ray CT data acquired at the Australian Synchrotron. A novel model based on multifractal analysis is developed that can quantify both ℓ_c and the roughness of rock materials at a wide range of length scales. Moreover, some methods for quantifying anisotropy and heterogeneity of materials using 3D X-ray CT data are developed. Electron microscopy techniques are also used to further decipher the intermittent behaviour of rock fracture and its corresponding rough surface.

To verify the quantified ℓ_c from mechanical side ring and semi-circular bend experiments are conducted on four rock types under a wide range of quasi-statics and dynamic loading rates. Brittle nature of rock materials is a major issue for fabricating sharp notch in SCB specimens to successfully determine fracture toughness. In this study, notch mechanics and practical developments in similar materials were introduced to circumvent this difficulty. Based on the presented analyses, it is concluded that if the notch root radius is smaller than the ℓ_c, the ISRM suggested method [Kuruppu et al. 2014] is a reliable method for determining fracture toughness of rock materials. The notch tip radius of the studied SCB specimens is 350 microns and is smaller than the ℓ_c of all studied rock types. Then, the Theory of Critical Distances (TCD), Coupled Finite Fracture Mechanics (CFFM) and Cohesive Zone Model (CZM) are modified and combined for failure analysis of the performed experiments.

Following such analyses, the ℓ_c is verified from two different mechanical models required completely different experimental inputs. This verification not only make a relationship between fracture toughness and roughness, and solve a forty-year-old dilemma, but also clarify some ambiguities in solid mechanics including the effects of geometry and experimental rate on tensile strength of rock materials.

Finally, the physics of fractured surfaces are also investigated at length scales smaller than ℓ_c, and the order of intermittency of rough rock fractured surfaces is discovered at intermediate length scales. However, this kind of disorder is more complicated than simple fractal or even multiscaling behaviours. Accordingly, some parameters are introduced that can perfectly take into account such systematic behaviour and fully quantify intermittency of the studied rock fractured surfaces.

Thesis including published works declaration

I hereby declare that this thesis contains no material which has been accepted for the award of any other degree or diploma at any university or equivalent institution and that, to the best of my knowledge and belief, this thesis contains no material previously published or written by another person, except where due reference is made in the text of the thesis.

This thesis includes one published original papers in peer reviewed journals and two manuscripts that will be submitted. The core theme of the thesis is fracture mechanics and physics of rock materials. The ideas, development and writing up of all the papers in the thesis were the principal responsibility of myself, the student, working within the department of civil engineering under the supervision of Drs. Qianbing Zhang, Laurent Ponson and Ali Reza Torabi.

The inclusion of co-authors reflects the fact that the work came from active collaboration between researchers and acknowledges input into team-based research.

In the case of *Chapter 3* my contribution to the work involved the following:

Thesis Chapter	**Publication Title**	**Status** *(published, in press, accepted or returned for revision, submitted)*	**Nature and % of student contribution**	**Co-author name(s) Nature and % of Co-author's contribution***	**Co-author(s), Monash student Y/N***
3	*A new methodology inspired from the Theory of Critical Distances for determination of inherent tensile strength and fracture toughness of rock materials*	*Published*	*60%. Performing experiments, analysing data and writing first draft*	*1) Laurent Ponson, improving the manuscript and data analysis 20%* *2) Ali Reza Torabi idea, input into manuscript 10%* *3) Qianbing Zhang providing fund, input into manuscript 10%*	*No*

Acknowledgements

I wish to acknowledge the support from Australian Government Research Training Program (RTP) Scholarship and the Monash International Tuition Scholarship (MITS). This research is supported by the Australian Research Council (DE200101293), Australian Synchrotron, the MASSIVE HPC facility (www.massive.org.au), and the Monash Centre for Electron Microscopy (MCEM).

I also would like to acknowledge my supervisors Drs. Qianbing Zhang, Laurent Ponson and Ali Reza Torabi for their great support and directions throughout my PhD journey. Without their great knowledge and experience doing this work was not possible, and I learned a lot from them.

Table of Contents

Chapter 1: Introduction

1.1. Research background

So far, many researchers have tried to quantify microstructures at different scales to provide some models to predict behaviours of materials. Two recent review papers have presented the applications and shortcomings of these models (Bargmann et al. 2018; Bostanabad et al. 2018). Although existing computational science and engineering capabilities for modelling nonlinear material behaviour are impressive, it is unclear how much impact they have had on materials engineering and design in general. Moreover, an integrated vision and/or framework that would be widely usable in multiscale computational materials engineering is lacking. Therefore, establishing microstructure-statistics-property relations underpinned by integrated computational materials engineering, based on an image-based (data-driven) multiscale modelling framework with co-designed simulations and experiments, has the potential to transform the materials science and engineering field (Matous et al. 2017). In the field of geo-mechanics, one of the ultimate aims is to provide some predictive models to bridge between different scales and predict response of rock materials and their nonlinear fracture mechanics.

Quasi-brittle materials, including rocks are not following Linear Elastic Fracture Mechanics (LEFM) at some small enough length scales (Irwin 1958; Barenblatt 1962) and Griffith fracture theory fails. This is because of the heterogeneous nature of such materials and existence of a fracture process zone (FPZ) at the tip of cracks or notches before crack propagation inside them. According to Cohesive Zone Model (CZM), if the length of FPZ (l_{pz}) ahead of a crack tip is ignored, the actual stress at which material fails cannot be determined by means of analytical solutions and all of the analysis and measurements including fracture toughness would have significant errors. Therefore, measuring the size of this zone is of prime importance to analyze the fracture behaviour of quasi-brittle materials, and is the key to understanding the relationship between multiscale physical properties and fracture mechanics of rock materials. However, quantifying the FPZ is a challenging task. Although different methodologies have been used for measuring FPZ (Dutler et al. 2018), it is inconclusive yet to

develop an internationally accepted norm for quantifying it. The outline of this thesis designed to tackle this issue is presented in Fig. 1.1.

In this thesis, fracture of rock materials is being investigated from physical, mechanical and dynamical points of view. Experimental measurements along with theoretical analysis and analytical solutions as well as statistical physics methods and roughness analysis are employed to quantify l_{pz}. Different theories, including Coupled Finite Fracture Mechanics (CFFM), Theory of Critical Distances (TCD), CZM, and notch mechanics are employed and coupled together to measure l_{pz} from experimental side. Statistical physics methods including correlation of local slopes and multifractal analysis of fractured surfaces as well as homogenization of 3D X-ray tomography data are employed to determine some length scales at which rock can be considered homogeneous. It is supposed that there is a correlation between heterogeneity and FPZ. Therefore, if the length scale at which rock can be considered as a homogeneous material is determined, then we can estimate the order of magnitude of l_{pz}. After analyzing various data it has turned out there is a very good agreement between all of the applied method and l_{pz} have been successfully quantified under quasi-static loading.

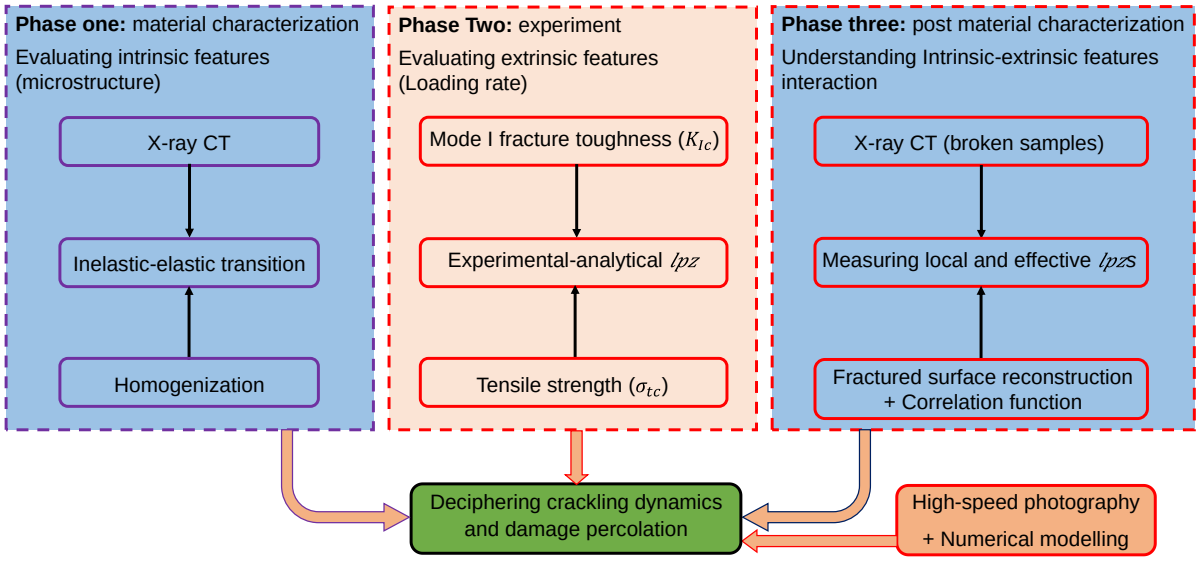

Fig. 1.1. Outline of the workflow.

High-tech facilities have been used to investigate the effect of loading rate on l_{pz} under a wide range of dynamic loads as well. This analysis can provide us with some important clues considering the effect of external and environmental conditions on fracture behavior and

mechanical response of rock materials. It will be shown that there is a transition zone from heterogeneous to homogeneous length scales according to 3D homogenization of X-ray tomography data of rock materials. It is supposed that under different loading and environmental conditions different length scales in transition zone will be activated and control l_{pz} that is the subject of our current research.

By proving the link between rock physics and fracture mechanics, it is possible to identify weakest points or directions in a body, which have the smallest fracture toughness. This would be a valuable tool for any project dealing with fracture controlling, such as geothermal energy, hydrocarbon reservoirs, induced seismicity, waste disposal, mining, and tunnelling in geo-mechanics, and plethora of other fields in material science and mechanical engineering. Moreover, such micro-mechanistic model could be combined with other techniques to understand multiscale materials behaviour under different loading and environmental conditions. This can integrate, for instance, with large scales seismic tomography and numerical modelling to predict rock mass behaviour at plenty of large scales rock engineering projects. This approach can also solve many fracture related problems in other grounds as well.

1.2. Research schedule

Following the outline of the thesis workflow (Fig. 1.1), the work has been conducted in three major phases. First of all, microstructure properties of different rock materials have been investigated by different techniques including Scanning Electron Microscopy (SEM) and 3D X-Ray Computed Tomography (CT). At the same time, some data analysis methods have been developed to analyse rock microstructure by processing the 3D X-Ray CT images.

In the second phase, experiments are performed following the research plan. Then, in the third stage, roughness of some of the broken samples are reconstructed and analysed by means of statistical physics methods. Finally, all results and analyses are used to understanding the rock physics and fracture mechanics by quantifying the l_{pz} of a moving crack based on percolation theory and developed mechanical models.

1.3. Materials

Four rock types including a red sandstone, a white coarse-grained marble, a Fine-Grained granite (FG granite) and a Coarse-Grained granite (CG granite) are selected for this study. This selection covers sedimentary, metamorphic and igneous rock types with different grain sizes. Fig. 1.2 is presenting the prepared rock samples from the selected rock types. The basic physical and mechanical properties of the studied rock materials including Uniaxial Compressive Strength (UCS), Brazilian Tensile Strength (BTS), Static elastic moduli including Young modulus (E_s) and Poisson' ratio (ν_s), compressional wave velocity (V_p), shear wave velocity (V_s), and dynamic elastic moduli including Young modulus (E_d), Bulk modulus (K_d), shear modulus (μ_d) and Poisson' ratio (ν_d) are determined following ISRM suggested metods (ISRM 2007) and reported in Tables 1.1 and 1.2.

Fig. 1.2. The prepared rock specimens for this research.

1.4. Thesis outline

This thesis consists of six chapter. In the first chapter a general background, research significant, aims and planned research, the characteristics of the studied rock materials, and outline of the thesis chapters has been presented. Second chapter is presenting a literature review.

Quantification of the l_{pz} of the studied rock materials by means of some mechanical models is the core of the third chapter. Moreover, Point Method (PM) form of the Theory of

Critical Distances (TCD) is used to determine the tensile strength and the fracture toughness of the studied rock materials. In chapter four, robust determination of the l_{pz} by combining physics and mechanics is presented. A novel multifractal roughness analysis is developed to determine the length of FPZ of the studied rock materials that is further verified by two different mechanical models required completely different experimental inputs. It is discussed how Coupled Finite Fracture Mechanics CFFM and PM form of TCD are modified and combined with Cohesive Zone Model (CZM) for such verification.

Table1.1 The basic mechanical properties of the studied rock materials.

Rock type	UCS [MPa]	E_s [GPa]	ν_s	BTS [MPa]
Sandstone	92.28	17.77	0.35	5.00
Marble	117.58	54.43	0.45	4.09
FG granite	138.08	55.34	0.23	12.32
CG granite	135.32	45.09	0.32	8.67

*FG: fine-grained; CG: coarse-grained

Order of intermittent rock fractured surfaces at length scales smaller than the length of fracture process is discussed and quantified in chapter five. Physics of these length scales is discussed. According to chaos theory, some underlying patterns can disclose order of disordered systems. It is shown that intermittency of rough rock fractured surfaces are such orderable disorders at intermediate length scales. Accordingly, intermittency of the studied surfaces is successfully quantified at length scales smaller than length of FPZ.

Table 1.2 The basic physical properties and dynamic elastic moduli of the studied rock materials.

Rock type	V_p [m/s]	V_s [m/s]	ρ [kg/m^3]	E_d [GPa]	ν_d	μ_d [GPa]	K_d [GPa]
Sandstone	3307	2195	2407	25.66	0.11	11.60	10.87
Marble	3785	2600	2830	40.31	0.05	19.13	15.05
FG granite	4559	2822	2611	49.45	0.19	20.79	26.54
CG granite	4500	2766	2612	47.81	0.20	19.98	26.26

Finally, in chapter six, the most important conclusions and future work are presented. Results of experimental tests performed under dynamic loading rates for both NSCB and ring tests of different rock types are presented. The reason behind dynamic increase factor is discussed from physics of some homogenised rock materials. Finally, the need for future work on roughness analysis of our reconstructed rock fractured surfaces broken under different loading rates for further understanding of this phenomenon is emphasised.

Chapter 2: Literature review

2.1. Introduction

This chapter reviews the literatures that have studied physics and mechanics of fracture process zone. All mentioned analytical fracture mechanics models in Chapter 1, for instance Dugdale–Barenblatt model Eq. (2-1) as the most popular method to determine the length of cohesive zone ahead of crack tip or the cohesive length ℓ_c, have shown there is a relationship between this length, the intrinsic tensile strength or cohesive strength (σ_c) and mode I fracture toughness (K_{Ic}) Eq. (2-2).

$$\ell_c = \frac{\pi}{8}\left(\frac{K_{Ic}}{\sigma_c}\right)^2 \tag{2-1}$$

Therefore, quantifying the length of fracture process zone or the cohesive length of a moving crack, is very important for quantyfing intrinsic properties of materials including cohesive or intrinsic tensile strength as well as material fracture toughness.

$$K_{Ic} \propto \sigma_c\sqrt{\ell_c} \tag{2-2}$$

Different techniques including Acoustic Emission (AE), Digital Image Correlation (DIC) and automatic fractography have been used for measuring FPZ and investigating into the relationship between these three important parameters. DIC is being introduced as a very popular method to measure FPZ. For instance, Dutler et al. (2018) have used notched semi-circular bending and Brazilian disk specimens to measure fracture toughness and tensile strength of an anisotropic granite. They have also used DIC technique to follow fracture process zone on the surface of the notched specimens. They have argued none of the proposed analytical solutions can have a good estimation of the length of fracture process zone, but (Eq. 2-2) has a good agreement between analytical solutions and the experiments at directions perpendicular and parallel to the bedding of the tested rock samples.

However, before applying the full-field measurement methods (e.g., digital image correlation), a proper understanding of the rupture propagation and separation of fractured

interfaces is necessary. Based on experimental observations in this study, firstly a rupture propagates, and failure of the studied rock materials takes place. After that, the separation of the two fractured surfaces and physical crack propagation is visible. A more promising approach would be the use of statistical fractography to determine ℓ_c of quasi-brittle materials (Bonamy et al. 2006; Vernede et al. 2015).

The rest of this chapter is organised as follows. The effect of FPZ on mechanical properties of different materials have been addressed in old literatures as the size effect on material strength. This is still an ongoing research topic in scientific communities. Therefore, first of all, size effect on material strength and its relation with FPZ is reviewed. Then, the work of some researchers who have tried to experimentally measure the FPZ to have a better understanding of its physics and its effect on mechanical response of different materials is summarised. Next, studies to understand and evaluate the cause of FPZ from different points of view is reviewed. It is notable that there is an agreement between different scientific societies that the cause of FPZ is heterogeneous nature of materials at small enough length scales. Finally, some fundamental researches that have been conducted in order to understand the relationship between FPZ, material heterogeneity and roughness of fractured surfaces are presented.

2.2. Size effect on material strength

One of the most important and challenging issues in the study of mechanical behaviour of materials and structures including rock materials and rock masses is the scale in which we want to study material's behaviour. It is well known that materials show different properties at different sizes (Carpinteri and Pugno 2005; Weinan 2011). There are some explanations for this phenomenon. First, from a (micro-) structural point of view, natural materials show scale dependent heterogeneity and anisotropy. Therefore, their structural features at every size, location and direction are different. Furthermore, constitutive behaviour of a material depends on the scale we want to study its behaviour. All brittle materials (i.e., materials in which the crack growth is governed by LEFM) become quasi-brittle on a small enough scale and all quasi-brittle materials become perfectly brittle on a large enough scale (Bazant et al. 2004).

Damage, spaning all length scales and governing the ultimate behaviour of any material, is one of the most difficult subjects in multiscale mechanics. Phenomenological models exist,

but real understanding is gained from analyses at heterogeneous microstructural scales (Matous et al. 2017). A description of a heterogonous structure in terms of micromechanics not necessarily leads to desirable estimation of fracture characteristics: transitions over a set of scale levels is a complicated problem. Furthermore, transition to averaged (effective) macro properties, correctly estimating general behaviour of material, can result in an inadequate prediction of the crack morphology and of peculiarities in crack evolution (Silberschmidt 1996). From an internal point of view, multiscale behaviour of materials is related to their multiscale physical properties in terms of configuration and phases. These intrinsic physical properties are nominally constant at certain scales and locations, but their mechanical response could change under different external parameters. Environmental conditions including in situ stresses, water content, temperature as well as loading condition are among the most important external parameters that can affect the response of materials with same nominal intrinsic features under mechanical loading.

Prediction of fracture behaviour in rock (or rock-like) materials is essential for a wide range of engineering problems, such as tunnel excavation, mineral and energy extraction and protective structure design in civil engineering (Wang et al. 2019). The absence of spatially accurate predictive models seriously degrades hydrocarbon recovery, protection and remediation of groundwater aquifers, and risk assessment of hazardous waste repositories (Leary 2003). Direct determination of mechanical behaviour of rock masses using mechanical tests is almost impossible. Moreover, for modelling their behaviour, we cannot use the parameters we have obtained from laboratory tests using small specimens unless we know how they would change at larger scales. This is usually called size effect or scale effect. The former mostly used by engineers in the concept of phenomenological failure criteria of solid quasi-brittle materials by means of some theoretical or experimental failure criteria while the latter is being used by scientists in the ground of fracture physics and mathematical mechanics. However, it is not convincing to use upscaling methods to determine rock mass properties by means of laboratory experiments since structural properties of rock masses are not the same as laboratory specimens and varies at different locations and directions.

Experimental studies on quasi-brittle materials have frequently shown there is an inverse relationship between, for instance, specimen size and its strength (Bieniawski 1975; Bazant 1997; Hoek and Brown 1997; Van Vliet and Van Mier 2000; Darlington et al. 2011). The general explanation for this behaviour is that by increasing the size of the specimen its defects density will increase, and consequently its strength against any type of mechanical load will

decrease. However, this decrease is not linear and by increasing the size of the specimen it would be reduced and after a quite representative size, it would remain almost constant for statistically homogeneous materials (Weibull 1939). A good survey regarding the size effect on strength of laboratory quasi-brittle specimens can be found in (Masoumi et al. 2016). Regarding the scale dependent behaviour of materials, there is a similar idea among fracture mechanics and fracture physics researchers with different definitions (Carpinteri et al. 2006; Taylor 2007; Ponson et al. 2007; Vernede et al. 2015). They all believe that there is a Characteristic Length (CL) for any material, which is not perfectly brittle. This characteristic length is related to microstructural features of quasi-brittle materials and controls scale dependent behaviour of such materials. In general, nominal homogeneous and isotropic materials, which have finer micro-structural features, have smaller characteristic length scales.

2.3. Fracture process zone quantification

As described by Ponson (2016), two model have been proposed for fracture propagation in heterogeneous materials. First approach is a continuous model based on Linear Elastic Fracture Mechanics (LEFM), in which the Fracture Process Zone (FPZ) is much smaller than the microstructural features of the material. However, the second discontinuous approach considers a damage zone at the crack tip, which is much larger than the microstructural features of the material. Many experimental studies have shown scale dependent fracture properties of materials are related to the size of fracture process zone and the ratio of the sample size to FPZ should be large enough to obtain valid fracture properties from laboratory tests (Ponson 2016; Bazant and Kazemi 1990; Karihaloo et al. 2006; Muralidhara et al. 2013; Kuruppu et al. 2014). Zietlow and Labuz (1998) have claimed the FPZ is quite same for large enough sample sizes and under same loading condition. Measuring the FPZ and its mechanical and physical properties is one of the most challenging tasks to understanding fracture properties of quasi-brittle materials. Different methods including AE, DIC and automatic fractography have been used for measuring FPZ e.g. (Vernede et al. 2015; Otsuka and Date 2000; Fakhimi et al. 2018; Kietov et al. 2019). Some researchers have used numerical modelling to estimate the size of FPZ considering the microstructural properties of quasi-brittle materials (e.g. Fakhimi and Tarokh 2013; Parisio et al. 2019). A good survey regarding the current progresses and challenges to quantifying FPZ using different methodologies can be found in Dutler et al. (2018).

It has been proved that there is a relationship between CL, FPZ and material heterogeneity. For instance, Bonamy et al. (2006) have shown their defined CL based on multiscale quantification of fractured surfaces has a direct relationship with the length of FPZ ahead of crack tip and varies depending on material heterogeneity. Taylor (2007), using experimental-analytical studies has shown FPZ and CL are almost the same. However, he has claimed there are many fundamental questions that are needed to be answered to understand the relationship between CL and fracture properties of materials. This is an easy to answer but hard to understand and quantification problem. The failure of quasi-brittle materials is being formed with coalescence of micro-fractures ahead of pre-existing defects such as cracks and pores. The micro-structural features of materials around these defects are different. Therefore, when we want to move from micro to macro scales the effects of these disorders should be considered as well. These multiscale mechanical behaviour of materials are extremely important in both solid and fluid mechanics engineering including mechanical behaviour of rock masses and fluid flow in fractured rock masses.

One way to study the behaviour of natural anisotropic heterogeneous materials is to define some representative features for them with few assumptions like using the effective medium theories. Effective Medium Theory (EMT) can be used to homogenise a heterogeneous material to determine its elastic constants and mechanical behaviour. However, heterogeneity and anisotropy of materials change at different length scales. Researchers have attempted to use multiscale modelling to solve this problem. Gao et al. (2015) and Hu and Oskay (2019), for instance, have proposed homogenization algorithms based on multiscale methods for simulating elastic wave propagation in anisotropic heterogeneous elastic media; a good survey can be found in the review paper by Matous et al. (2017). Multiscale mechanics aims to identify and quantify relationships bridging various length scales in heterogeneous materials. The ultimate goal is to extract effective properties at the scales of application (Matous et al. 2017). Therefore, we need to define a *multiscale effective medium*, which its constants are some functions of scale. These are some nonlinear heterogeneous functions depending anisotropy and heterogeneity of materials.

2.4. FPZ and Scale dependent heterogeneity

The first step towards this end is to have a deep and insightful understanding of the (micro-) structure of a material. It is also important to understand how the physical properties of the

material are changing with respect to size of the sample from micro to macro scales. Many researchers have attempted to address this issue. For instance, Carpinteri and Chiaia (1995) and Carpinteri et al. (1995), proposed two equation for fracture energy and tensile strength by means of multifractal scaling law. This means that for smaller scales a self-similar distribution of Griffith cracks is prevalent, whereas for larger scales the disorder is not visible, the size of the defects and heterogeneities being limited. In practice there may be a dimensional transition from disorder to order (Carpinteri et al. 1995). Therefore, materials can be considered linear elastic at large enough scales and their effective properties can be introduced into predictive models. However, if materials show large amounts of heterogeneity and anisotropy these formulas are not valid anymore. For instance, sedimentary rock masses are formed of different layers with different properties at different locations. Therefore, it is almost impossible to determine some multifractal scaling laws for them that can determine their behaviour at every scale, location and direction.

There is also a similar concept in mathematical theory of asymptotic homogenisation, which has been developed to characterise effective properties of heterogeneous materials (Bakhvalov and Panasenko 1989; Cioranescu and Donato 1999; Tartar 2010). The basic idea is that if the unique structure of a material could be find, by considering boundary conditions, it is possible to estimate effective elastic properties of the material. This theory has been used to estimate the effective properties of periodic materials like biological tissues, synthetic composites and metamaterials. Same concept has been used by material scientists and mechanical engineers (e.g. Kanit et al. 2003; Kanoute et al. 2009) to estimate mechanical properties of materials with the aid of identification of their Representative Volume Element (RVE). However, there is no single solution for different materials or same materials at different conditions, or even it is not completely true if we say there is a self-affine fractal characteristic or same RVE that could describe material microstructure at different directions. Too many variables in terms of both configuration and phases could change multiscale physical properties of materials and their response to mechanical loading, so there are different answers for such a multiscale problem.

This is a big gap and different scientific societies are trying to introduce new theories that could bridge between different scales. Regarding this issue with quantifying the length of FPZ, which takes scale dependent physical properties of materials into account, seems to be a practical solution. The amount of heterogeneity and anisotropy of materials and structures depend on length scales. In other word, there is no effective model that can describe effective

properties of a body at all length scales, and when we want to investigate into smaller details, we need to consider scale dependent local changes of the body.

A rapidly moving crack in a brittle material is often idealized as a one-dimensional object with a singular tip, moving through a two-dimensional material. However, in real three-dimensional materials, tensile cracks form a planar surface whose edge is a rapidly moving one-dimensional singular front. The dynamics of these fronts under repetitive interaction with material heterogeneities and the morphology of the fracture surface that they create are not yet understood (Sharon et al. 2001). Indeed, even what determines in which direction a section of crack front will advance is not understood, although it is clear that this involves physics on smaller scales than the regime of continuum elasticity theory. Until 1990s, except for the uniform motion of a straight crack front in an ideal elastic solid, there has not been, much theoretical analysis of these problems (Ramanathan and Fisher 1997). There seems to be no material so brittle that the process zone always remains featureless. It remains to be seen whether a simple continuum limit exists, or whether a crucial ingredient in understanding fracture is the discreteness of the underlying atoms (Fineberg and Marder 1999). Therefore, it is necessary to quantify multiscale physical properties of materials, which are controlling scale dependent materials behaviour.

Appendix A is showing the post-mortem fracture surface of different rock types at different scales. From these micrographs, it is obvious that rock materials are showing a considerable scale-dependent heterogeneity. Therefore, when we want to investigate materials behaviour it is necessary to determine the scale of application as well as the mechanisms that are related to the scale of application at other scales. For instance, if we need to understand underlying mechanisms that have created the form of rock fractured surfaces at grain scale, which is related to intergranular cracks, we should understand which scales are contributing to make this form. However, if we need to investigate the roughness at sub-grain scales we need to consider different underlying mechanisms at different length scales. Local changes are the second important aspect of multiscale mechanics that can be explained by means of these images. However, for engineering applications, usually effective properties of materials should be determined and used as the input into predictive models.

Other important considerations are the kind of problem we want to solve and the precision we need. For instance, intergranular cracks in polycrystalline materials like rocks or ceramics have been considered problematic in applying the EMTs coming from the theory of linear

elasticity. Some researchers have tried to address this issue by applying some modifications into EMTs by restricting pre-existing cracks to the grain boundaries (Bruno et al. 2019; Sevostianov and Kachanov 2019). In applications, however, both intergranular and intragranular cracks may appear in dependence on the strength of the interfaces between the grains (Zhang and Zhao 2013; Paggi et al. 2018). Therefore, if we need to predict both intergranular and intragranular cracks we should use multiscale approaches and consider the crystallographic cleavages as well. As another example, Aligholi et al. (Aligholi 2017a; Aligholi et al. 2019) have used statistical approaches to understand the relationship between rock physics properties at grain scale and mechanical behaviour. They have used multiple regression methods, which integrate modal composition, grain size and grain shape of igneous intact rocks to obtain statistical correlation between these features and a wide range of mechanical properties. The results were different for different mechanical properties. For instance, their results have revealed it is possible to classify strength of the tested rock materials under quasi-static loading, but it is not possible to determine their surface hardness against penetration of rotary drill bits. Interestingly, when they used rebound surface hardness data to classify strength of igneous rocks by means of basic physical and dynamic properties, their models have significantly improved (Aligholi 2017b). They have concluded that more details at finer length scales are required to predict surface hardness of igneous rocks.

2.5 FPZ and roughness analysis

Scale dependent problem that we are addressing here is the roughness of fractured surfaces of rock as a quasi-brittle anisotropic heterogeneous material. This is because of local changes of toughness of rock materials that lead different sections of a crack front to the different directions. Scale dependent fracture properties of rock materials are mainly related to the size of inelastic FPZ ahead of crack tip and its proportion to the size of the sample or the scale of application. Therefore, quantifying three-dimensional FPZ and understanding the cause of this phenomenon can lead to understanding the relationship between rock physics and fracture mechanics.

Toughness of materials including rocks can be determined by means of laboratory tests. Jiang and Vecchio (2009), and Zhu and Joyce (2012) reviewed dynamical and statistical test methods for toughness measurements of materials. International Society for Rock Mechanics (ISRM) have suggested two test methods for measuring Mode I statistic and dynamic fracture

toughness (Kuruppu et al. 2014; Zhou et al. 2012) using notched semi-circular bending samples. Considering the heterogeneity of tested rocks, there is always variation between the toughness test results for different samples from same rock. There is not quantitative approach that can decipher the origin of these variations and engineers usually use the minimum conservative values as input into their models. From microscopic images presented in Appendix A, it can be deduced that fracture behaviour of a material is a function of its multiscale physical properties in terms of configuration and phases. Therefore, when we use different samples to determine the toughness of a material the results are different since even under exactly same testing conditions different samples have different physical properties. However, this is a challenging task to understand the local changes of materials' microstructure and its relationship to global (effective) and local toughnesses.

In general, there are three ways to understand interaction of microstructure and crack front: direct methods, indirect methods and numerical modelling. Direct methods are not applicable to all materials, and they are limited to small specimen sizes and cannot provide us with three-dimensional data. Kumar and Curtin (2007) reviewed progresses and challenges of both direct and numerical methods. The main indirect approach to study fracture properties of materials is fractography. It can be used to study the post-mortem fracture surfaces to understand the effect of microstructural features on fracture propagation. In recent years, quantitative fractography has been used to study fracture propagation in heterogeneous materials (e.g. Bouchaud et al. 1993; Ponson et al. 2006a; Bonamy et al. 2008; Guerra et al. 2012; Vogler et al. 2017). There are comprehensive review papers on this (Bouchaud 1997; Alava et al. 2006; Bonamy and Bouchaud 2011). Determining the relationship between toughness of materials and roughness of their fractured surfaces has been one of the most important aims of these studies (e.g. Mandelbrot et al. 1984; Srivastava et al. 2014).

It has been proved that quasi-brittle materials are not following Linear Elastic Fracture Mechanics (LEFM) (Irwin 1958; Barenblatt 1959 and 1962; Dugdale 1960). This is because of existence of a FPZ at the crack tip before crack propagation in these materials. Therefore, measuring the size of this zone is of prime importance to analyse fracture behaviour of quasi-brittle materials. Fractography has been recently used to determine length of FPZ of quasi-brittle materials (Vernede et al. 2015). This procedure can be used to understand the relationship between toughness, roughness and microstructure. In this thesis, this procedure is further developed to quantify length of FPZ of rock materials.

Chapter 3: Quantifying the length of FPZ using TCD

In the first two chapters, the importance of quantifying length of FPZ in failure analysis of quasi-brittle materials is explained. It is also explained that it is a main research gap in the field of fracture mechanics and there is no internationally accepted norm for quantifying it. Chapter 3 of this thesis employs Point Method (PM) form of the Theory of Critical Distances (TCD), which is a practical solution for analyzing failure of materials, and combines it with the well-developed theoretical concepts of the CZM to quantify length of FPZ of the studied rock materials. Moreover, notch mechanics is employed to have a close estimation of fracture toughness of the studied notched semi-circular bending specimens for further verifications of the novel presented PM. Finally, it is emphasized this method provides just an acceptable estimation of the length of FPZ, which is good enough for practical purposes, and more sophisticated schemes are required for a better quantification of this critical length. One of these schemes is based on quantitative fractography and roughness analysis of the fractured surfaces that is successfully employed in this study as explained in Chapters 4 and 5.

This chapter is presented in the form of following publication (Aligholi et al. 2022) with permission from Elsevier, International Journal of Rock Mechanics and Mining Sciences.

International Journal of Rock Mechanics & Mining Sciences 152 (2022) 105073

Contents lists available at ScienceDirect

International Journal of Rock Mechanics and Mining Sciences

journal homepage: www.elsevier.com/locate/ijrmms

A new methodology inspired from the Theory of Critical Distances for determination of inherent tensile strength and fracture toughness of rock materials

S. Aligholi [a,*], L. Ponson [b], A.R. Torabi [c], Q.B. Zhang [a]

[a] Department of Civil Engineering, Monash University, VIC, 3800, Australia
[b] Fracture Lab, Institut Jean le Rond d'Alembert, CNRS – Sorbonne Université, Paris, France
[c] Fracture Research Laboratory, Faculty of New Science and Technologies, University of Tehran, Tehran, Iran

ARTICLE INFO

Keywords:
Critical distance
Intrinsic tensile strength
Fracture toughness
Point method
Notch mechanics

ABSTRACT

Measuring the intrinsic fracture properties of quasi-brittle materials like rocks is of great importance and at the same time a major issue for engineers. In this study, we explore the ability of the Theory of Critical Distances (TCD) to determine accurately both the tensile strength and fracture toughness. To this end, we conduct ring tests and semi-circular bend tests on four rock types including a red sandstone, a white coarse-grained marble, a fine-grained granite and a coarse-grained granite. This selection covers sedimentary, metamorphic and igneous rock types with different grain sizes. The experimental data are analysed using a new methodology developed from the so-called Point Method (PM), a particular form of the TCD, from which we infer the intrinsic tensile strength and the fracture toughness of the studied rock materials. Our results are compared with those obtained from ISRM suggested methodology that is modified to take into account the finite notch root radius used in our experiments. The comparison is successful, supporting that the newly developed methodology is suitable to determine the intrinsic tensile strength and fracture toughness of rock materials.

1. Introduction

Rocks are archetypes of quasi-brittle materials. Under compression, they generally show a rather extended non-linear regime owing to the spreading of micro-fractures before final failure takes place. Under traction, they fail through the propagation of a crack that grows through the coalescence of micro-cracks localized at the crack tip vicinity in the so-called process zone. If the spatial extent of the process zone is small with respect to the specimen size, this phenomenon is then appropriately described by the theory of Linear Elastic Fracture Mechanics (LEFM).[1] Within the LEFM framework, we introduce the fracture toughness K_{Ic} that quantifies the ability of the material to resist crack growth. Alternatively, one can seek to determine the stress level at which the material fails in traction, thus defining the material tensile strength. This is of particular relevance in absence of an initial crack in the structure.[2,3] However, defining an intrinsic (specimen independent) tensile strength for quasi-brittle solids is a rather difficult challenge, as the load-bearing capacity of quasi-brittle specimens is known to strongly depend on its size,[4,5] and often overlooked in engineering practice.[6]

Owing to their quasi-brittle nature, rock made structures can give rise to catastrophic failures. Therefore, the accurate determination of their failure properties is key to assessing the structural resistance of rock masses, an important issue in many rock engineering practices such as tunnelling, rock cutting processes, hydraulic fracturing and rock slope stability.[7] In the following, the term *structural* properties is used when the geometrical features of the specimens or bodies do play a significant role on top of the *intrinsic* properties that depend only on the microstructural features of the rock materials as well as the surrounding environment.[8]

A suitable solution for defining the tensile strength of rocks consists in considering the characteristic stress level at which the material fails within the process zone of a stress concentrator or a running crack. According to the Cohesive Zone Model (CZM) for brittle cracks,[9,10] the so-called cohesive strength σ_c of the material is then related to the material fracture toughness via the cohesive length ℓ_c (or process zone size along the crack propagation direction) through the relation $K_{Ic} \propto \sigma_c \sqrt{\ell_c}$.[9] Although appealing, this definition raises serious experimental issues: how to determine the stress level at the tip of stress concentrators,

* Corresponding author.
E-mail addresses: saeed.aligholi@monash.edu, saeed.aligholi@monash.edu (S. Aligholi).

https://doi.org/10.1016/j.ijrmms.2022.105073
Received 7 July 2021; Received in revised form 11 February 2022; Accepted 16 February 2022
Available online 24 February 2022

as the process zone is hardly larger than 1 mm in most quasi-brittle materials.

Theoretically speaking, specimens with a sharp notch and without a stress concentrator can be used to determine the toughness of a material and its tensile strength, respectively. However, in practice, such a procedure is neither reliably achievable nor practical. On the one hand, preparing sharp cracks in rock specimens is a challenging task and there is a systematic effect of the notch radius on the measured apparent fracture toughness. On the other hand, specimens without stress concentrators at all do not provide reliable measurements of the intrinsic tensile strength of rock materials. The reasons behind this observation relate to the stochastic (defect driven) nature of tensile failure in brittle solids that have been thoroughly documented, see e.g. Refs. 4,11,12.

To circumvent these difficulties, a natural yet challenging approach consists in using specimens with round notches. Contrary to the failure load of specimens with sharp notches that reflect the toughness of the material only, the mechanical strength of round notch specimens also reflects the material cohesive strength σ_c. Yet, measuring σ_c from such a methodology requires a reliable, accurate (and if possible simple) failure criterion that relates the intrinsic mechanical strength of the material to the structural strength of the specimen. To address this issue, several theories belonging to the realm of Finite Fracture Mechanics have been proposed (see e.g. Ref. 13 for a recent review). They all share the same concept that consists in determining the failure load of the specimen through the comparison of the local stress applied at a *finite* distance L to the notch with an intrinsic (material dependent) critical stress at failure. However, they differ in the way this critical distance is computed.

Among these different models, the so-called Theory of Critical Distances (TCD)[14] is one of the most successful ones, as it is both simple and has been shown to predict rather accurately the mechanical strength of notched specimens for a large range of materials including composites,[15,16] metals,[17–19] polymers,[20,21] and rocks.[22–25] In its simplest form, the so-called point method (PM), the critical distance L is determined from the intersection of the stress profile ahead of two notched specimens with different radii at their respective failure load. Here, we examine the validity of this approach by testing Semi-Circular Bend (SCB) and ring specimens with four different inner radii in four different rocks. We show that the specimens with the highest stress concentrator (the specimen with almost a sharp notch) and the lowest one (the ring specimen with the largest possible inner radius) are the most suitable for measuring accurately both K_{Ic} and σ_c. It is notable that notch mechanics[26–29] is applied to modify the effect of a round-tip notch on measured fracture toughness of the studied materials. We also modify the original PM so the obtained value of the critical stress corresponds to the cohesive strength σ_c of the material, as defined in cohesive zone models. Ultimately, our work provides a new and simplified methodology for the determination of the intrinsic fracture properties of rocks, opening a new perspective for the extensive mechanical characterization of these materials under different conditions (temperature, loading rate, environment, etc.).

This paper is organized as follows. First, we present the studied rock materials as well as the experimental and analytical methods adopted for this study. A brief theoretical background on the methodology employed to analyse the ring tests and bending tests carried out in this study is provided in Section 2. Section 3 presents our main results including a discussion. Finally, the conclusions are drawn in Section 4.

2. Materials and methods

Four different rock types including a red sandstone, a white coarse-grained marble, a fine-grained granite and a coarse-grained granite are selected for this study. This selection covers sedimentary, metamorphic and igneous rock types with different grain sizes. The PM form of the TCD is applied to measure accurately the failure properties of these rock materials including tensile strength and fracture toughness. To check the validity of the proposed PM, the fracture toughness of the tested rocks is also measured according to the ISRM Suggested Method[30] modified to take into account the finite radius of the notch used in our experiments.

2.1. A modified version of the PM based on CZM

The PM is the simplest form of the TCD.[31] Its failure criterion has been defined by Taylor[32] as follows: 'Failure will occur when the stress at a distance $L/2$ from the notch root is equal to σ_0'. This translates as:

$$\sigma(L/2) = \sigma_0 \tag{1}$$

where L is a characteristic distance, and σ_0 is the inherent tensile strength of the material. If the stress distribution ahead of a stress concentrator and the characteristic distance are known, then the inherent tensile strength can be determined. As justified in Appendix A, the material fracture toughness K_{Ic} can finally be estimated from the relation:

$$L = \frac{1}{\pi}\left(\frac{K_{Ic}}{\sigma_0}\right)^2 \tag{2}$$

Although this approach has been successfully applied to a large range of fracture problems, it remains a phenomenological method. Interestingly, it is intimately connected to the CZM of failure, which rigorously extends LEFM to elasto-damageable solids. In its simplest version, CZM introduces a cohesive stress σ_c, below which the material behaves elastically and beyond which it does not sustain any mechanical load. This approach predicts the spatial extent of the fracture process zone, also called the cohesive zone, through the Dugdale–Barenblatt (D–B) formula (see Appendix A):[9,33]

$$\ell_c = \frac{\pi}{8}\left(\frac{K_{Ic}}{\sigma_c}\right)^2 \tag{3}$$

This formula is almost identical to Eq. (2) up to a constant $\pi^2/8 \approx 1.23$. On top of it, considering the tensile stress distribution $\sigma(r) = K_I/\sqrt{2\pi r}$ ahead of a running crack as predicted by LEFM, one infers the relation $\sigma(4\ell_c/\pi^2) = \sigma_c$ that is similar to Eq. (1). In the following, we use Eq. (3) instead of Eq. (2), as it derives from a well-identified assumption, namely the existence of a unique stress level that provides both the elastic limit and the failure threshold of the material, but we use the following PM based methodology to determine both σ_c and. ℓ_c.

Specimens with different notch geometries are loaded up to failure. Following Eq. (1), the point of intersection of the stress distribution ahead of the stress concentrators at the onset of failure is expected to provide the material tensile strength. Following the previous interpretation of the PM based on CZM, two extreme stress concentrators, i.e. a sharp notch (very high-stress concentration) and a flat free surface (no stress concentration), are best suited. However, in practice, machining very sharp notches and initiating a crack from a flat free surface are quite difficult to achieve in rock materials.

Instead, SCB specimens with a notch root radius of about 350 μm and ring specimens with an inner radius of around 14 mm are used to produce the highest and lowest possible stress concentrations, respectively. Despite the discrepancy between these specimens and the perfect concentrators expected theoretically, our method provides accurate values of tensile strength, as we will show in Section 3.

2.2. Ring test

Rock rings are used in the following as the low-stress concentrator specimens. This test geometry has been used in the past to measure the apparent tensile strength of rocks and other brittle materials.[34,35] However, the apparent tensile strength is a structure-dependent property rather than an inherent material property.[11,36] The difference between the value of the apparent tensile strength and σ_c results from the

combination of three factors: (1) the probabilistic nature of the resistance of materials to tensile loading; (2) the complexity of the failure process involving the initiation of a crack by damage accumulation before it can propagate; and (3) the calculated stress following a linear elastic assumption may not be the 'real' stress experienced by the material.[11]

The minimum diameter of the internal hole that could be drilled into the sandstone and the marble is about 3 mm, while it is about 6 mm for granites (Fig. 1-c). Rings with four different inner diameters are prepared for the sandstone and the marble, whereas three different ring specimens are prepared for granites. Moreover, normal disk specimens with no hole are also prepared and tested for all rock types. At least three different specimens for any geometry are tested and the average of calculated tensile strengths for each rock type/geometry is used for further analyses. The outer diameter and thickness of the rings/disks are around 75 and 30 mm, respectively. Note that, following the analysis of Fillon,[37] the ratio of the inner to the outer diameter of our ring specimens is less than or equal to 0.4 so that the tensile mode of failure dominates over the compressive one.[34] The driving rate of the cross-head for all our tests is set to 0.05 mm/min.

The apparent tensile strength σ_{max} is defined as the maximum stress level applied locally to the material at the onset of failure, assuming that it behaves elastically everywhere. It then follows:[34]

$$\sigma_{max} = \frac{P_{max}}{\pi B R_0}\left[6 + 38(R/R_0)^2\right] \tag{4}$$

that provides the tensile stress applied to the inner surface of the specimen at the applied failure load P_{max}. For disk specimens for which $R = 0$, the maximum applied stress is located at the centre of the specimen and follows:

$$\sigma_{max} = \frac{P_{max}}{\pi B R_0} \tag{5}$$

Here, B is the ring thickness, while R and R_0 are the inner and outer radii of the ring, respectively.

Following Torabi et al.,[38] Kirsch's solution together with Hobbs' correction[34] are used to determine the tensile stress distribution $\sigma_y(x)$ along the loading axis x (see the schematic of the ring specimen shown in Fig. 1-a for the definition of the axes x and y):

$$\sigma_y(x) = \frac{\sigma_{max}}{2}\left(2 - 2\frac{R^2}{x^2} + 12\frac{R^4}{x^4}\right)F_{corr} \tag{6}$$

Here, F_{corr} is a correction factor that should be taken into account for sufficiently large R/R_0 ratios, which follows:

$$F_{corr} = 1 + \frac{19}{3}\left(\frac{R}{R_0}\right)^2. \tag{7}$$

In the course of the ring experiments, we observe an interesting phenomenon that we would like to discuss. As shown in Fig. 2-b and 2-d, the mechanical response of the ring specimen with the largest inner radius shows two peaks, the first one being larger than the second one. It turns out that full failure of the ring specimen took place in two steps. First, as the load is increased, the tensile strength of the material is reached and failure takes place at point A (see Fig. 2-c). After stress drop, the sample is still able to sustain load. As a result, the applied load increases again, starting from a lower level until it reaches a second time the tensile strength of the material at point C (see Fig. 2-c). It is interesting to notice that each half of the sample can still bear some compressive load until the tensile strength of the material is reached a second time at point C, and providing good evidence that the sample has been split under pure tension at point A.

The first and second peaks in Fig. 2-d corresponds to the fractures labelled in Fig. 2-c and are located at points A and C, respectively. From this observation, it can be concluded that the ring test is suitable to measure the tensile strength. From recorded videos by high-speed cameras, we do observe that rings with smaller internal holes are always separating from point A in a tensile mode as well (Fig. 3), as expected from direct numerical simulations of failure in such specimens.[35]

2.3. Semi-circular bending test

The notched semi-circular geometry is used for preparing rock specimens with high-stress concentrators. Various methods have been used to determine the fracture toughness of rock materials.[e.g.30,39–41] The method suggested by ISRM[30] relies on SCB specimen that is rather simple to machine and provides good repeatability (see e.g. Refs. 42–45).

Herein, SCB specimens are prepared and tested according to ISRM. Multiple SCB specimens for each rock type are tested and the average generalized (or apparent) fracture toughness K_{Ic}^{U} is calculated as follows:

$$K_{Ic}^{U} = Y' \frac{P_{max}\sqrt{\pi a}}{DB} \tag{8}$$

Here a, B, D, and P_{max} are the notch length, the specimen thickness, the diameter of the SCB specimen and the maximum applied load, respectively (see Fig. 4). The notch length of the tested SCB specimens is comprised between 14 and 16 mm while the notch tip radius is 350 μm. The diameter and the thickness of the SCB specimens range from 74 to 76 mm and 29–31 mm, respectively. Finally, Y' gives the non-dimensional Stress Intensity Factor (SIF) derived using the finite element method while assuming plane-strain conditions.[30] Its expression follows:

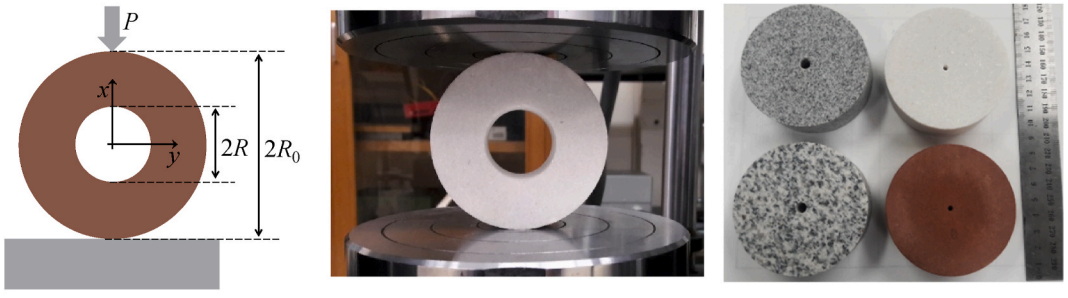

Fig. 1. Ring experiment: (a) Schematic of the ring specimen; (b) A marble ring with an inner radius of 15 mm under compression; and (c) Specimens with the minimum inner radii before testing.

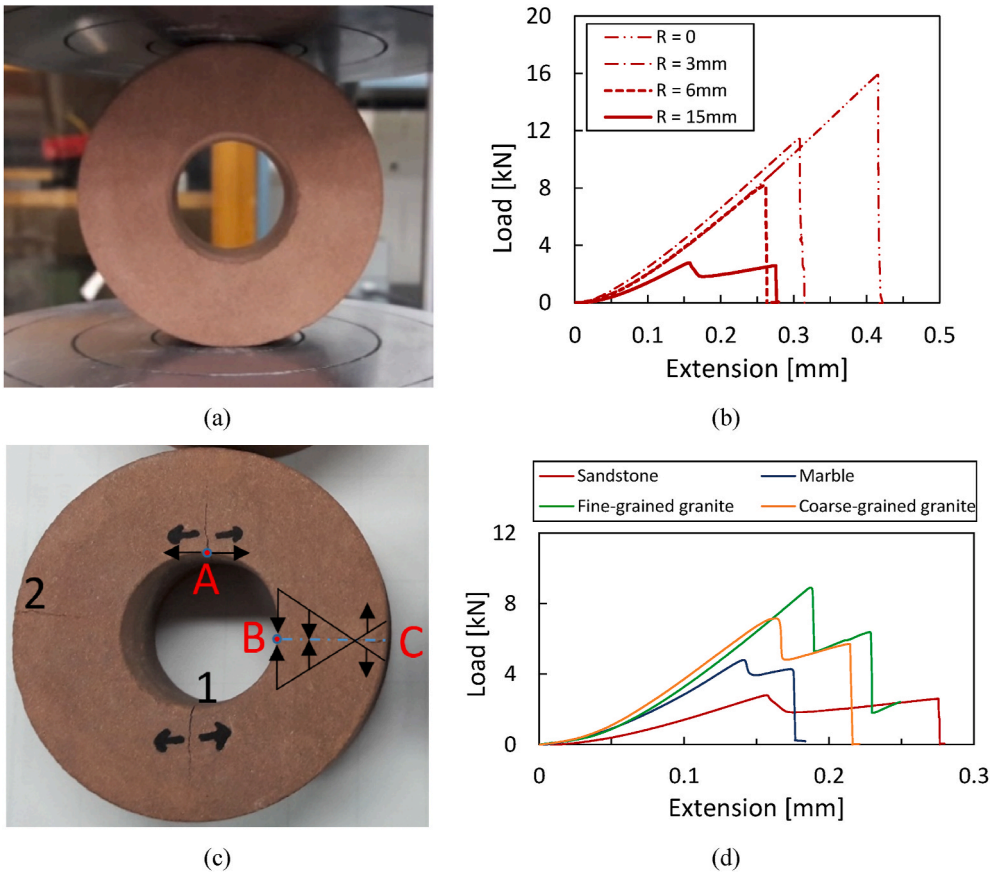

Fig. 2. a) Sandstone ring specimen under compression; b) Mechanical response of the sandstone ring specimens with different inner radii; c) Schematic illustration of the two steps failure behaviour of ring specimens; and d) Mechanical response of the ring specimens made of different rocks for the largest inner radii (13–15 mm).

$$Y' = -1.297 + 9.516(s/D) - (0.47 + 16.457(s/D))\beta + (1.071 + 34.401(s/D))\beta^2 \quad (9)$$

where s is the span length which is between 37 and 38 mm for all our tests while β is equal to $2a/D$.

Failure of SCB specimens is recorded by means of a high-speed camera (Fig. 5-a). It can be clearly seen that the fracture initiates from the notch tip and propagates parallel to the axis of application of the forces, as expected. Typical load-extension curves obtained for different rock types are shown in Fig. 5-b.

Creager–Paris solution[26] provides the stress distribution in SCB specimens with a blunted notch of radius ρ:

$$\sigma(x,0) = \frac{2K^{U}}{\sqrt{\pi}} \frac{x+\rho}{(2x+\rho)^{3/2}} \quad (10)$$

using the coordinate system depicted in Fig. 4-b. K^{U}, the apparent stress intensity factor, is provided by Eq. (8) after replacing the failure load P_{max} by the current applied load P.

2.4. Direct fracture toughness measurement using SCB tests

To test the ability of the proposed methodology to accurately measure the fracture toughness of rock materials, we proceed to an independent measurement of K_{Ic} using the failure load of the semi-circular bending tests. The basic idea is to consider that at the onset of failure, the imposed stress intensity factor (determined from Eqs. (8) and (9) at the tip of the notch) reaches the fracture toughness value K_{Ic}. However, in our experiments, the notch tip radius is too large to be neglected. Compiling a large set of experimental data, Gomez et al.[27] determined the ratio of the apparent fracture toughness (resulting from the finite notch root radius) over the actual material fracture toughness:

$$\frac{K_{Ic}^{U}}{K_{Ic}} = \sqrt{1 + \frac{\pi}{4}\frac{\rho}{(K_{Ic}/\sigma_c)^2}} \quad (11)$$

Here, the intrinsic tensile strength σ_c is determined using the PM based methodology while ρ measured from 2D slices of SCB specimens scanned by means of X-ray tomography, is found to be close to 350 μm (Fig. 4-d). K_{Ic}^{U} corresponds to the apparent fracture toughness measured experimentally. As the material fracture toughness K_{Ic} appears on both sides of this equation, Eq. (11) must be solved iteratively as follows. First of all, Eq. (11) can be divided into the following two formulas:

$$\frac{K_{Ic}^{U}}{K_{Ic}} = \sqrt{1 + \frac{\pi}{4}\frac{\rho}{l_{ch}}} \quad (12)$$

where l_{ch} is a characteristic length given in Eq. (13):

$$l_{ch} = (K_{Ic}/\sigma_c)^2. \quad (13)$$

Then, an iterative process for estimating K_{Ic} can be presented in four steps as follows:

a) estimating the l_{ch} using Eq. (13) by assuming K_{Ic} is equal to the measured generalized fracture toughness from the experiment;
b) estimating the material fracture toughness by replacing the measured generalized fracture toughness from experiment, notch tip radius ρ, and the calculated l_{ch} from the first step into Eq. (12);
c) updating the l_{ch} by replacing the estimated material fracture toughness from the second step into Eq. (13); and
d) repeating this loop several times until old and new l_{ch} values and accordingly material fracture toughness values converge.

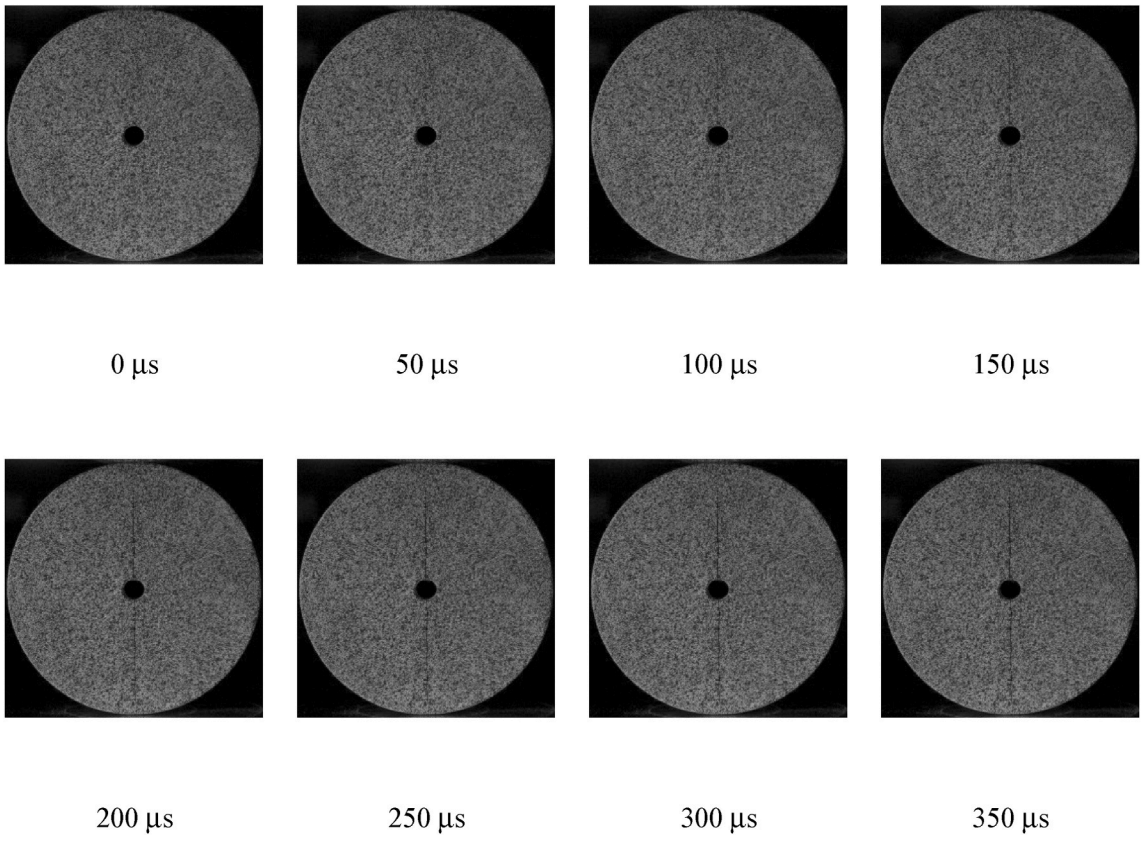

Fig. 3. Sequence of high-speed images taken from a sandstone ring with an inner radius of 3 mm showing symmetric fracture propagation from point A, as depicted in Fig. 2-c.

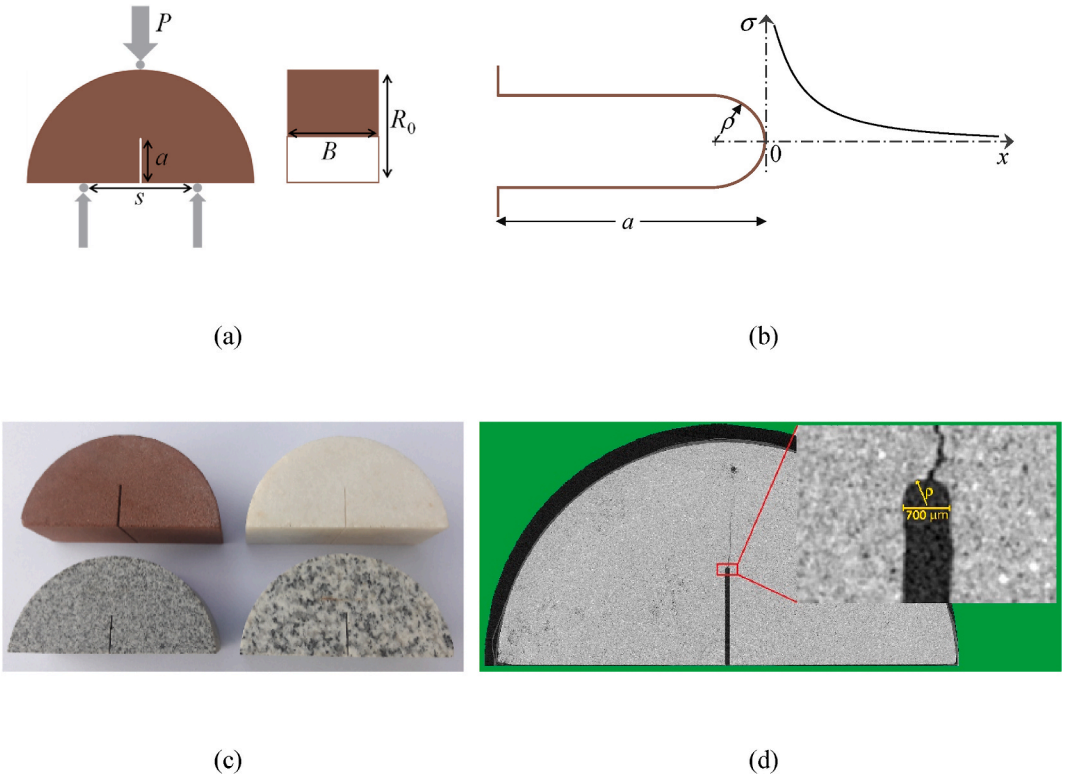

Fig. 4. SCB fracture tests: (a) Schematic of SCB specimen under three point bending; (b) Schematic of the stress distribution on the bisector line of a blunted notch under opening mode loading conditions; (c) SCB specimens before testing; and (d) 2D image slice of a sandstone SCB specimen scanned by means of X-ray tomography after failure. Note the radius $\rho \approx 350$ μm of the initial notch.

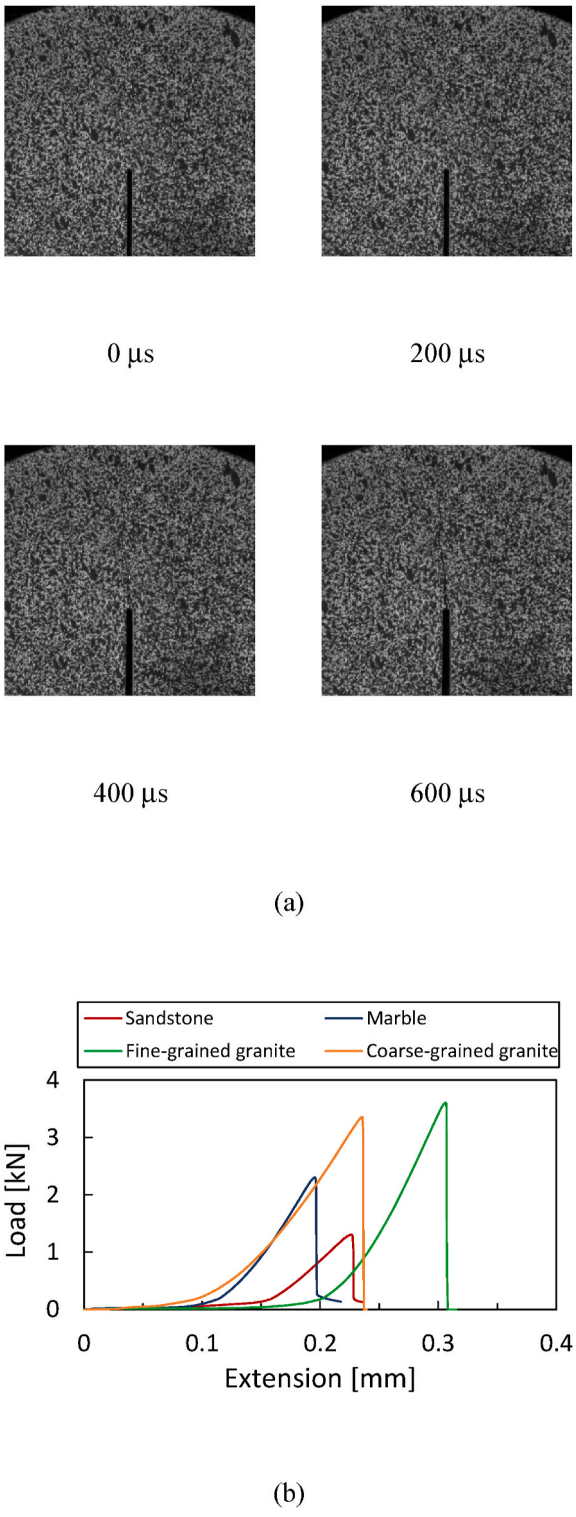

Fig. 5. (a) Sequence of high-speed images taken from a fine-grained granite SCB specimen showing crack initiation and growth from the initial notch tip; (b) Mechanical response of the notched SCB specimens for the four rocks investigated.

The larger the notch tip radius ρ, the greater the number of required iterations for convergence (Fig. 6-a and 6-b). It turns out that the ratio K_{Ic}/K_{Ic}^{U} is close to 0.95 for the four materials investigated. Beyond the particular cases of the fracture tests carried out in this study, Fig. 6-c and 6-d depict the effect of the cohesive length in comparison to the notch root radius on the ratio K_{Ic}/K_{Ic}^{U}. In particular, it can be seen that small notch radii compared to cohesive length give rise to $K_{Ic} \approx K_{Ic}^{U}$.

3. Results and discussion

3.1. Size effect on tensile strength measurements using ring specimens

A natural first step in assessing the structure-independent tensile strength of the rock materials investigated is to determine the apparent (structure dependent) tensile strength σ_{max} as a function of the ring geometry. Ring specimens with various inner radii as well as disk specimens from different rock types are tested for such a purpose. Fig. 7-a shows the value of P_{max} as a function of the inner hole radius as obtained after averaging over different samples. It appears that the apparent tensile strength strongly depends on the hole radius (Fig. 7-b). This calls for a more advanced method of analysis to determine the inherent tensile strength.

3.2. Intrinsic tensile strength and material fracture toughness

The methodology described in Section 2.1 is applied in Fig. 8 for the four rocks investigated using the highest stress concentrator (the SCB specimens with a notch root radius of 350 μm) and the lowest concentrator (the ring specimens with inner radii of 13–15 mm) as justified below. Equations (6) and (10) are used to predict the stress profile ahead of each concentrator at failure for the ring and the SCB specimen, respectively. According to Eq. (1), the intersection point of the tensile stress distributions at the onset of failure for both ring and SCB specimens provides both the cohesive strength and the cohesive zone length. The fracture toughness value is then obtained from Eq. (3) using the D–B relationship. The results obtained for the four rocks investigated are summarized in Table 1.

The validity of the proposed methodology is now evaluated. First, we compare the fracture toughness value predicted by Eq. (3) with the fracture toughness value measured directly from the notched SCB specimen, after taking into account the effect of its finite notch root radius. For this purpose, the value of σ_c determined previously is used in Eq. (11), providing the ratio K_{Ic}/K_{Ic}^{U} between the inherent fracture toughness and the apparent one, as explained in Sec. 2.4. The comparison shown in Table 2 is excellent. We then compare in Table 3 the cohesive zone length as measured from our method using the intersection point between both stress distributions at the onset of failure (see Fig. 8) with the one predicted from D–B Formula using the fracture toughness determined directly from the notched SCB tests and modified for the rounded notch tip effect. Here also, the agreement is very good. Last but not least, we did proceed to an independent measurement of the process zone length from statistical fractography, a technique that consists in analysing the statistics of fracture surface roughness to extract the characteristic size of the damage processes taking place at the crack tip vicinity during propagation, and found values comparable to the one determined in this study.

These results call for a few comments. First, the intrinsic tensile strength varies in the range of 8–25 MPa for the different rock materials investigated. This is somehow larger, however comparable to the values reported in the literature for such materials.[6,46] Note that using a ring specimen with a smaller hole radius instead gives larger values of σ_c, as inferred from Fig. 9 where the tensile stress distribution at the onset of failure is represented for the different specimen geometries. First, considering a stronger stress concentrator is not compatible with the justification of Eq. (1) that requires the combination of a high and a low-stress concentrator (see Section 2.1). Second, it leads to smaller values of cohesive length, of the order of a few hundred microns, that do not match with the results inferred from the statistical analysis of the fracture surfaces.

We then would like to discuss the fracture toughness values measured for the four rocks investigated. Our methodology provides

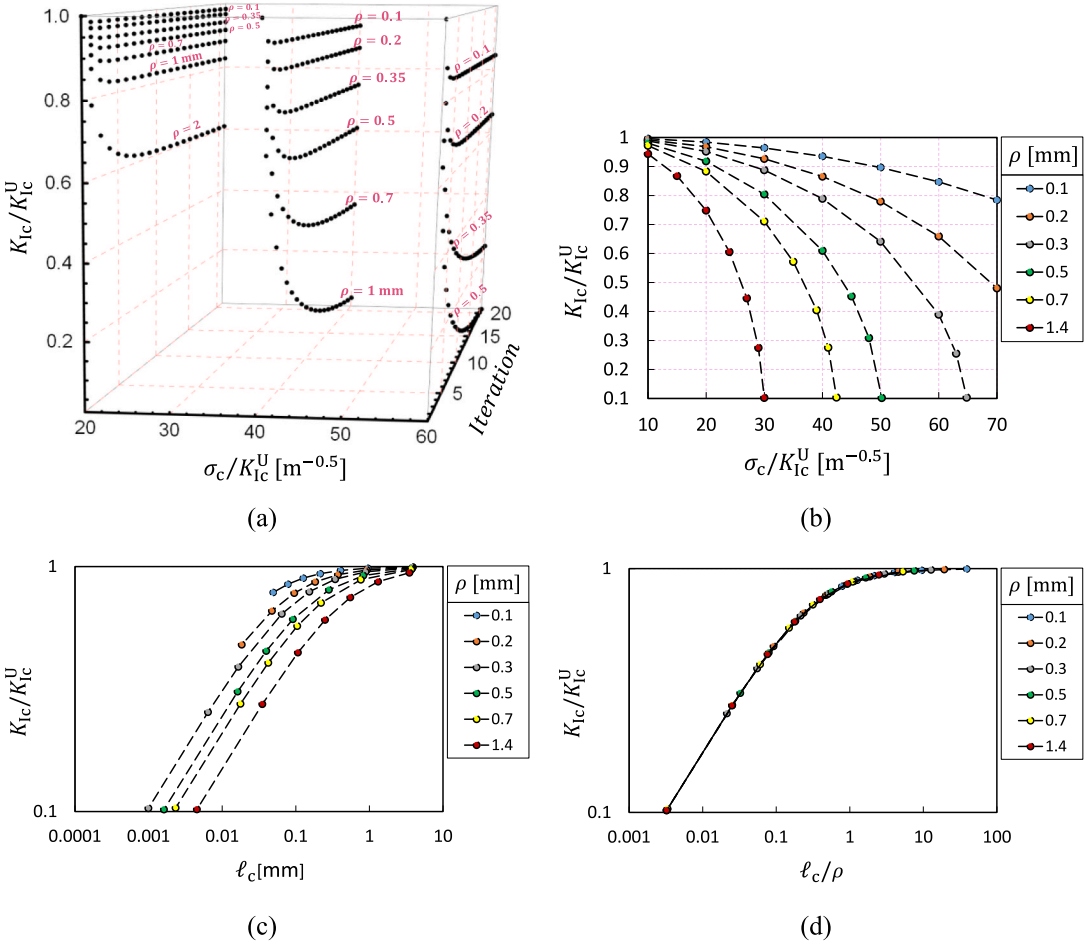

Fig. 6. Graphical guides for modifying the notch root radius effect on material fracture toughness: a) A 3D guide showing the iterative process; and b) A guide for estimating K_{Ic} as a function of notch tip radius, intrinsic tensile strength and generalized fracture toughness. c) K_{Ic} as a function of notch tip radius, the cohesive length and generalized fracture toughness; and d) a single master curve for evaluating K_{Ic} as a function of ℓ_c/ρ ratio and generalized fracture toughness.

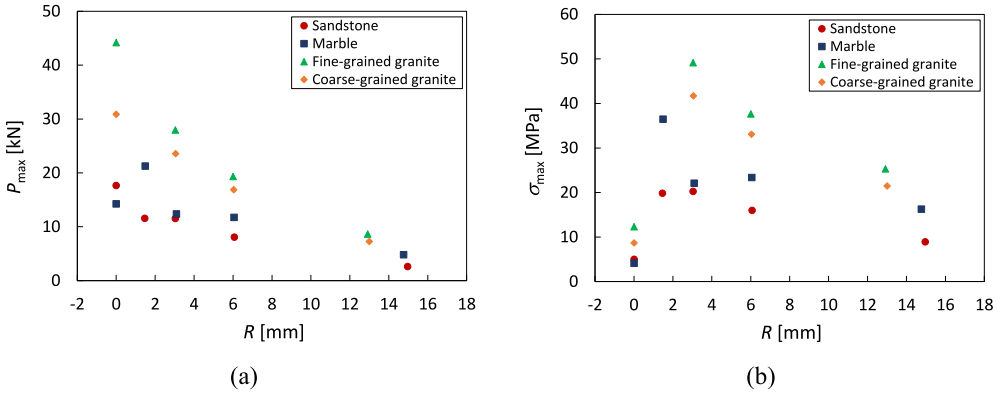

Fig. 7. Failure load P_{max} (a) and apparent tensile strength σ_{max} (b) of the different rocks investigated as obtained from the different fracture tests.

accurate fracture toughness values, in agreement with values of K_{Ic} determined directly from the notched SCB specimens using the ISRM suggested method. Afterwards, it turns out that the value of the apparent fracture toughness obtained with a notch root radius less than 500 μm as suggested by ISRM already provides a rather good estimate of K_{Ic} for the rocks investigated.

3.3. Discussion

We would like now to discuss the following points: Why PM might preferentially be applied to specimens with a low and a high stress concentrator? Why the CZM compatible version of the PM proposed in this study may give better results than the standard PM? Finally, what are the limitations of the proposed method?

To answer these questions, we first provide a brief background of the

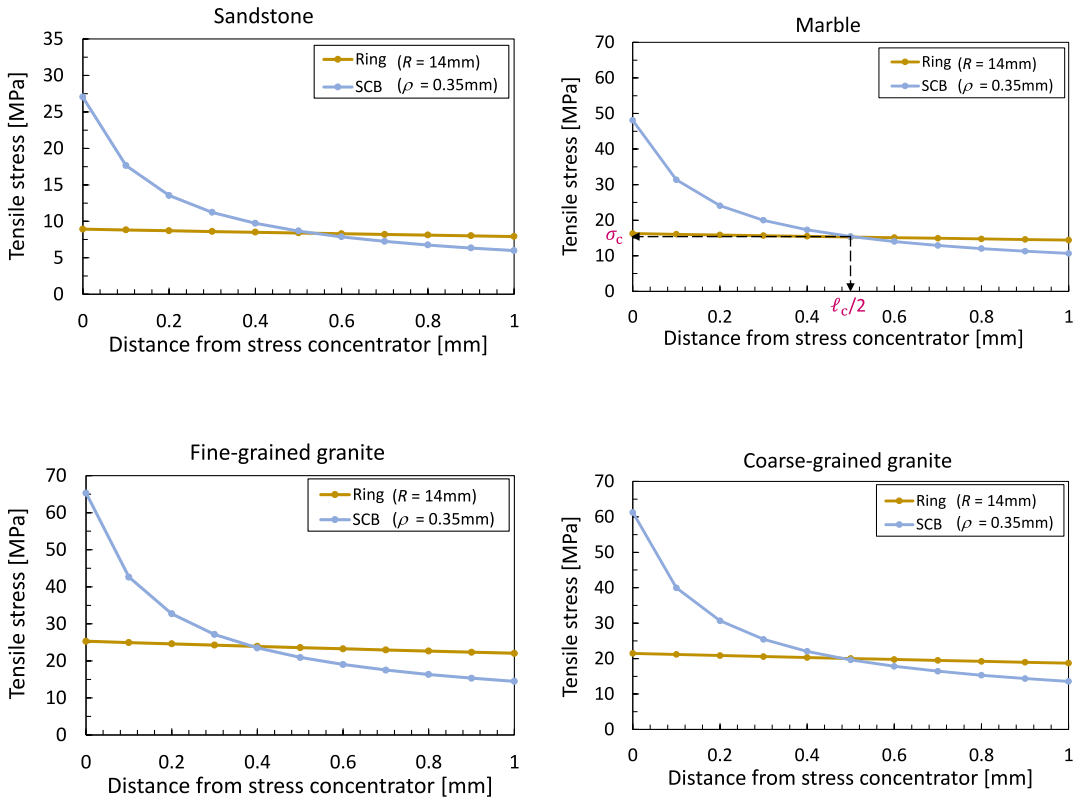

Fig. 8. Application of the PM for the determination of the tensile strength: Stress distribution against distance for the two geometries displaying the highest and the lowest stress concentrations for (a) sandstone, (b) marble, (c) fine-grained granite and (d) coarse-grained granite. The point of intersection of both curves provide the intrinsic tensile strength as well as the cohesive length, as illustrated for marble in the panel (b).

Table 1
The intrinsic tensile strength, the cohesive half-length and the material fracture toughness, determined by the developed PM.

Rock type	σ_c [MPa]	$\ell_c/2$ [mm]	K_{Ic} [MPa.m$^{0.5}$]
Sandstone	8.4	0.53	0.44
Marble	15.4	0.51	0.78
Fine grained granite	24.0	0.39	1.07
Coarse grained granite	19.8	0.48	0.98

Table 2
Comparison of measured generalized fracture toughness K_{Ic}^{U} [MPa.m$^{0.5}$] and modified fracture toughness K_{Ic} [MPa.m$^{0.5}$] values with those obtained using the common and developed PMs.

Rock type	K_{Ic}^{U} (ISRM[28])	K_{Ic} (Gomez et al.[25])	K_{Ic} (common PM)	K_{Ic} (modified PM)
Sandstone	0.45	0.43	0.49	0.44
Marble	0.80	0.76	0.86	0.78
Fine grained granite	1.08	1.00	1.19	1.07
Coarse grained granite	1.02	0.97	1.11	0.98

Table 3
The cohesive length ℓ_c [mm] as per D–B formula determined both from SCB tests modified for the rounded notch tip effect and the developed PM.

Rock type	Experimental	Developed PM
Sandstone	1.03	1.07
Marble	0.96	1.01
Fine grained granite	0.68	0.78
Coarse grained granite	0.94	0.96

PM. As discussed in Section 2, Eq. (1) is the cornerstone of the PM. This formula assumes that the stress level applied at failure at a (material dependant) distance $L/2$ from the concentrator is equal to the inherent tensile strength of the material. In this approach, L is assumed to be a characteristic length that depends on the material microstructure, but that is independent of the specimen geometry. Therefore, the intersection point of the stress profile ahead of the concentrator of two different specimens (irrespective of their geometry) is expected to provide both L and the intrinsic tensile strength σ_c. In practice, this is not the case. As illustrated in Fig. 9, the stress profiles corresponding to different stress concentrators do not intersect at the same point. Understanding this behaviour would require the cohesive zone modelling of the crack initiation process in these different geometries, a study that is beyond the scope of the present work. Here, instead, we seek to provide a simple procedure that allows for an estimation of the intrinsic fracture properties of the material. As a result, we proposed to use the lowest and the highest stress concentrators for applying the PM. From an experimental perspective, these two cases are not achievable, but can be fairly well approximated by the thin notch SCB and the large inner radius ring specimens used in our experiments.

What are the limitations of this approach? First, our method in particular (and the PM in general) relies on the calculation of the *elastic* stress field without considering that damage may start to grow in the neighbouring of the stress concentrators prior to crack initiation. This means that the real stress field emerging from the damage growth and its

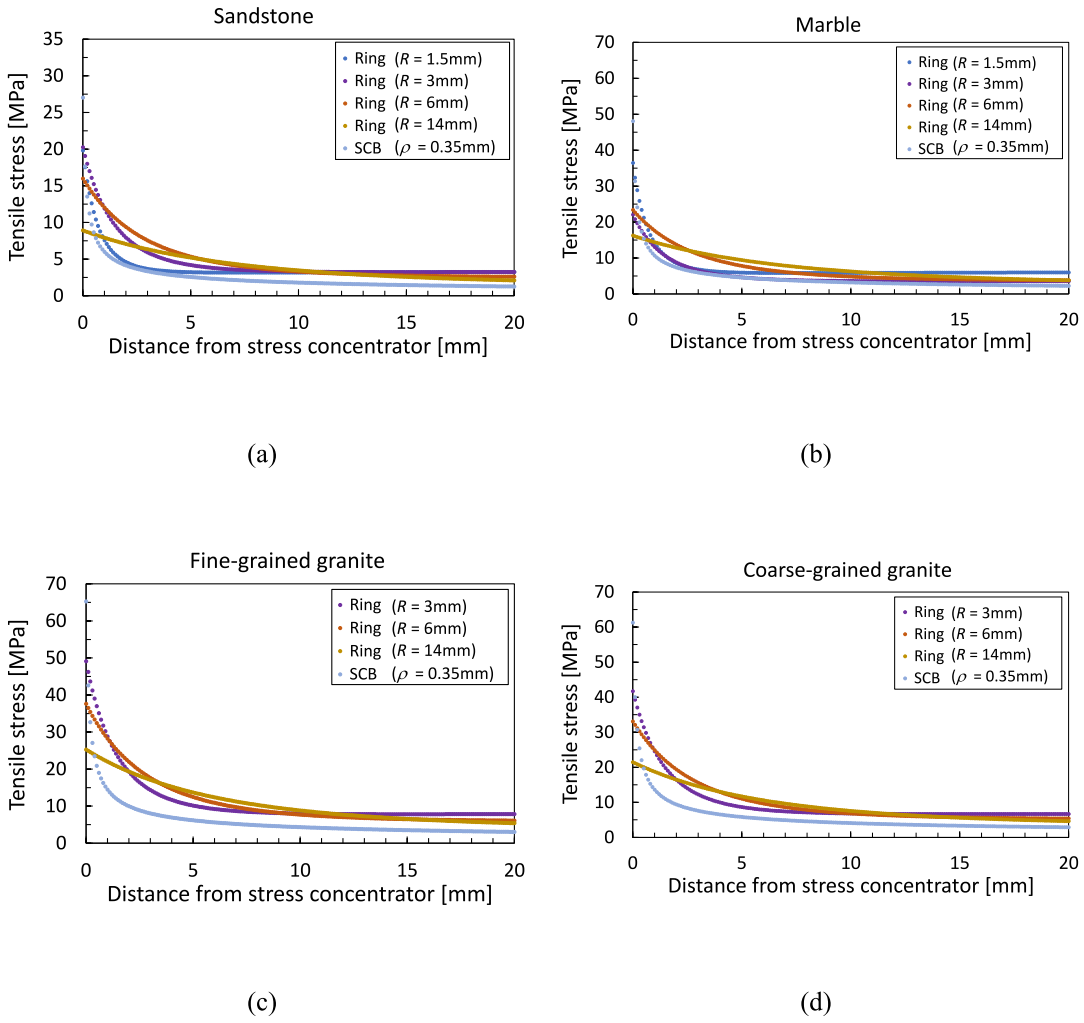

Fig. 9. Tensile Stress distribution against distance at the onset of failure for different fracture test geometries and different materials: a) sandstone; b) marble; c) fine-grained granite; and d) coarse-grained granite.

coupling with the elastic field is never computed. This could be done numerically using the CZM of crack initiation. Such an approach may improve the accuracy of the measurement of both σ_c and ℓ_c in comparison to the modified point method, but at the expense of a much more complex methodology. Then, we have assumed here that the rocks investigated all follows a D–B cohesive zone law. A more realistic law could be used instead (e.g., Refs. 47,48 the experimentally determined cohesive zone laws), which may (slightly) modify the constant $8/\pi$ involved in Eq. (3), and thus the fracture properties determined by our methods. However, before applying the full-field measurement methods (e.g., digital image correlation), a proper understanding of the rupture propagation and separation of fractured interfaces is necessary. Based on our experimental observations, firstly a rupture propagates and failure of the studied rock materials takes place. After that, the separation of the two fractured surfaces and physical crack propagation is visible. A more promising approach would be the use of statistical fractography to determine ℓ_c of quasi-brittle materials.[49,50] Then, the equivalent stress corresponding to this length can be calculated using LEFM and provide σ_c.

4. Conclusions

In this study, a TCD based methodology is examined to determine two key mechanical properties of rock materials namely intrinsic tensile strength and material fracture toughness. The first and foremost conclusion is that the PM form of TCD is a suitable means to reliably determine intrinsic tensile strength and material fracture toughness of different rock types. According to our results, PM is very reliable if the cohesive length ℓ_c is considered as the characteristic length L in this method.

The size and geometry of the flaws in natural rocks might obviously be different from the holes and the notches used in the specimens prepared for laboratory tests. Therefore, the proposed method will be more reliable for obtaining the intrinsic fracture properties of rock materials as compared to the existing methods. Notably, the developed methodology can be further used for more complicated external loads as long as it includes one test with strong stress concentration and another one with weak stress concentration. Then the same methodology applies using the corresponding stress field at the tip of the stress concentrators for the fracture load of each experiment.

Following the results of this study, it turns out that plane disk specimens without stress concentrators cannot be used to measure

tensile strength of rock materials, and tensile strength is underestimated if plane specimens are used. However, it could provide engineers with a safe and conservative estimation despite the fact that it would often increase the costs of a project. From the observations in the course of ring experiments, it can be concluded that the ring test is a suitable means to measure the apparent tensile strength of rock materials. The tensile strength of rocks is revealed to depend on their structural properties due to the facts discussed by Hudson.[11] However, if a specific value should be reported for a particular rock type and is needed by analytical or numerical solutions, then the intrinsic tensile strength of the rock can be determined following the procedure in this study with the aid of newly developed PM.

Brittle nature of rock materials is a major issue for fabricating sharp notch in SCB specimens to successfully determine material fracture toughness. In this study, notch mechanics and practical developments in similar materials were introduced to circumvent this difficulty. From the experimental observations and comparison with different methods, it is being suggested that Gomez et al.[27] formula can be used to successfully rectify the notch root radius effect on determining fracture toughness of rock materials. However, if the notch root radius is smaller than the cohesive length, the ISRM suggested method[30] is a reliable method for determining fracture toughness of rock materials. Based on the results of this study, the cohesive length is around 1 mm for rock materials. Therefore, if the notch width is less than 1 mm or notch root radius is less than 500 μm, as specified in the ISRM suggested method,[30] then the material fracture toughness measured by this method is reasonably close to the real value.

Although the results are satisfying, there is a mismatch between the actual location and the considered intersection point for estimating the intrinsic tensile strength because of material heterogeneities and theoretical assumptions. This is why fracture toughness values estimated from SCB tests modified for notch root effect and developed PM are a bit different. The question remains open in this study is that how this issue can be rectified and if there is any way to measure L or ℓ_c for different materials to get the best possible results. In other words, the length of the fracture process zone in the direction of crack propagation or the cohesive length ℓ_c should be quantified to determine the actual stress at the tip of the cohesive zone right before failure of a material to precisely measure the material fracture toughness. Further investigations are required to exactly quantify the length of the fracture process zone and answer this question.

Declaration of competing interest

The authors declare the following financial interests/personal relationships which may be considered as potential competing interests: Saeed Aligholi reports financial support was provided by Australian Government Research Training Program (RTP) Scholarship. Qianbing Zhang reports financial support was provided by Australian Research Council (DE200101293). Qianbing Zhang reports equipment, drugs, or supplies was provided by Australian Synchrotron. Saeed Aligholi reports equipment, drugs, or supplies was provided by The MASSIVE HPC facility (www.massive.org.au). Saeed Aligholi reports equipment, drugs, or supplies was provided by Monash Centre for Electron Microscopy (MCEM).

Acknowledgements

S. A. wishes to acknowledge the support from Australian Government Research Training Program (RTP) Scholarship and the Monash International Tuition Scholarship (MITS). This research was financially supported by the Australian Research Council (DE200101293), Australian Synchrotron, the MASSIVE HPC facility (www.massive.org.au), and the Monash Centre for Electron Microscopy (MCEM).

Appendix A

Following Taylor,[32] derivation of Eq. (2) starts by Westergaard's equation[51] that provides an estimation of tensile stress $\sigma(r)$ in the direction of crack propagation as a function of distance r from the crack tip, for a through-thickness crack of a half-length a in an infinite body. The equation can be read as:

$$\sigma(r) = \sigma\sqrt{\frac{a}{2r}} \tag{A1}$$

if $r \ll a$ i.e. for the comparatively close points to the crack tip for an applied tensile stress σ.

According to LEFM for the same conditions Mode-I SIF K_I can be calculated:

$$K_I = \sigma\sqrt{\pi a} \tag{A2}$$

At the moment of failure K_I and σ can be replaced by critical Mode-I SIF or fracture toughness K_{Ic} and tensile failure stress σ_f, respectively:

$$K_{Ic} = \sigma_f\sqrt{\pi a} \tag{A3}$$

Finally, combining the PM criterion Eq. (1) with Eqs. (A1 and A3), σ_f^2 is equal to both side of Eq. (A4):

$$\frac{L{\sigma_0}^2}{a} = \frac{{K_{Ic}}^2}{\pi a} \tag{A4}$$

which is another form of Eq. (2).

Derivation of Eq. (3) can be summarized as follows. If a crack or notch with length a as shown in Fig. A1 is considered, then the distribution of $\sigma_c(x,0)$ along with ℓ_c ranged from the physical crack tip or notch tip to fictitious crack tip would be non-linear. The general formula for calculating Mode-I SIF associated with such cohesive stresses K_I^c for a straight crack in an infinite body can be formulated as follows:[1]

$$K_I^c = -2\sqrt{(c/\pi)}\int_0^c \frac{\sigma_c(x,0)}{\sqrt{c^2-x^2}}dx \tag{A5}$$

where $c = a + \ell_c$ and $\sqrt{c^2-x^2}$ is Green's function. There is no close form solution for this equation since the distribution of σ_c over ℓ_c is unknown. The

D–B formula is derived by simplifying this condition. If we consider σ_c over ℓ_c has a constant value (strip model), then Eq. (A5) will transform to:

$$K_I^c = -\sqrt{(2/\pi)}\int_a^c \frac{\sigma_c(x,0)}{\sqrt{x}}dx \tag{A6}$$

Fig. A2 shows this simplified situation for a crack of length $2(a+\ell_c) = 2c$ in an infinite body under uniaxial tensile stress σ. Then, using superposition of the problem, and right before crack propagation, the following equilibrium could be reached:

$$K_I = -K_I^c \tag{A7}$$

where K_I is given in Eq. (A2) and K_I^c can be solved using Eq. (A6). Now, the equilibrium can be rewritten as follows:

$$\begin{aligned}&\sigma\sqrt{\pi c} = 2\sigma_c\sqrt{\frac{c}{\pi}}\cos^{-1}\frac{a}{c};\rightarrow\sqrt{\pi c}\left(\sigma - \frac{2\sigma_c}{\pi}\cos^{-1}\frac{a}{c}\right) = 0;\\ &\therefore\frac{a}{a+\ell_c} = \cos\left(\frac{\pi\sigma}{2\sigma_c}\right)\end{aligned} \tag{A8}$$

Finally, by two reasonable assumptions including $\ell_c \ll a$ and $\sigma \ll \sigma_c$ this equilibrium can be solved for ℓ_c:

$$\begin{aligned}&1-\frac{\ell_c}{a} = 1-\frac{\pi^2\sigma^2}{8\sigma_c^2};\\ &\rightarrow\ell_c = \frac{\pi\sigma^2\pi a}{8\sigma_c^2}\end{aligned} \tag{A9}$$

that is another form of Eq. (3).

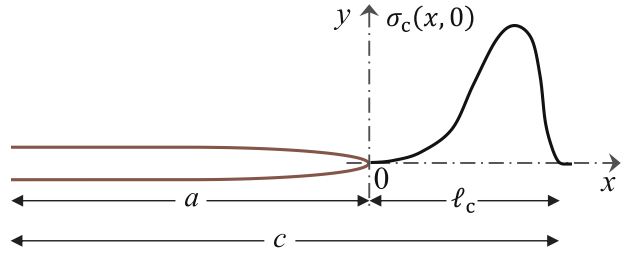

Fig. A1. Schematic of Barenblatt cohesive zone model

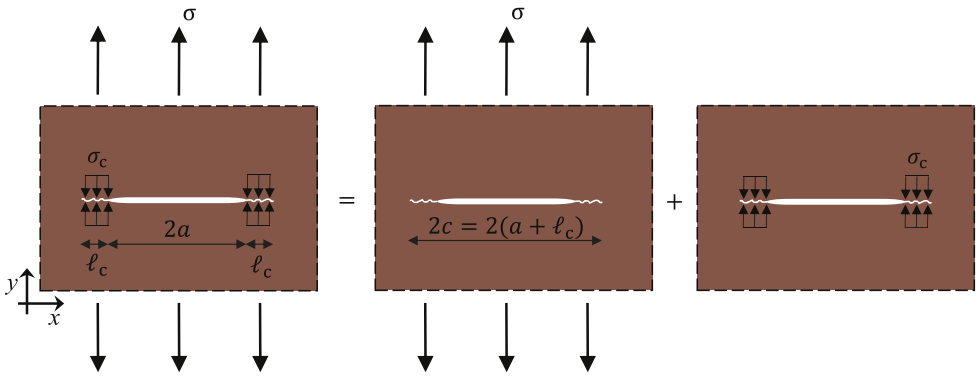

Fig. A2. Equilibrium for derivation of D–B formula as superposition of applied and cohesive stresses

References

1 Lawn B. *Fracture of Brittle Solids*. London: Cambridge University Press; 1993.
2 Myer LR, Kemeny JM, Zheng Z, Suarez R, Ewy RT, Cook NGW. Extensile cracking in porous rock under differential compressive stress. *Appl Mech Rev*. 1992;45(8):263–280.
3 Haimson BC, Cornet FH. ISRM suggested methods for rock stress estimation—Part 3: hydraulic fracturing (HF) and/or hydraulic testing of pre-existing fractures (HTPF). *Int J Rock Mech Min Sci*. 2003;40:1011–1020.
4 Weibull W. A statistical distribution function of wide applicability. *J Appl Mech*. 1951;18(3):293–297.
5 Bazant ZP, Planas J. *Fracture and Size Effect in Concrete and Other Quasibrittle Materials*. Boca Raton Florida: CRC Press; 1997.
6 Perras M, Diederichs M. A review of the tensile strength of rock: concepts and testing. *Geotech Geol Eng*. 2014;32:525–546.
7 Justo J, Castro J, Cicero S. Application of the theory of critical distances for the fracture assessment of a notched limestone subjected to different temperatures and mixed mode with predominant mode I loading conditions. *Rock Mech Rock Eng*. 2021;54(5):2335–2354.
8 Atkinson BK. Subcritical crack growth in geological materials. *J Geophys Res Solid Earth*. 1984;89(B6):4077–4114.
9 Barenblatt GI. The mathematical theory of equilibrium cracks in brittle fracture. *Adv Appl Mech*. 1962;7:55–129.
10 Xu XP, Needleman A. Numerical simulations of fast crack growth in brittle solids. *J Mech Phys Solid*. 1994;42(9):1397–1434.
11 Hudson JA. Tensile strength and the ring test. *Int J Rock Mech Min Sci Geomech Abstr*. 1969;6:91–97.
12 Newman DA, Bennett DG. The effect of specimen size and stress rate for the Brazilian test—a statistical analysis. *Rock Mech Rock Eng*. 1990;23:123–134.

13 Weissgraeber P, Leguillon D, Becker W. Arch Appl. Mech. A review of Finite Fracture Mechanics: crack initiation at singular and non-singular stress raisers. *Arch Appl Mech*. 2016;86:375–401.
14 Taylor D. The theory of critical distances. *Eng Fract Mech*. 2008;75:1696–1705.
15 Ibáñez-Gutiérrez FT, Cicero S, Carrascal IA, Procopio I. Effect of fibre content and notch radius in the fracture behaviour of short glass fibre reinforced polyamide 6: an approach from the Theory of Critical Distances. *Compos B Eng*. 2016;94:299–311.
16 Ibáñez-Gutiérrez FT, Cicero S, Carrascal IA. On the influence of moisture content on the fracture behaviour of notched short glass fibre reinforced polyamide 6. *Compos B Eng*. 2019;159:62–71.
17 Susmel L, Taylor D. Fatigue design in the presence of stress concentrations. *Int. J. Strain Analy*. 2003;38:443–452.
18 Susmel L, Taylor D. On the use of the theory of critical distances to predict static failures in ductile metallic materials containing different geometrical features. *Eng Fract Mech*. 2008;75:4410–4421.
19 Pereira JCR, de Jesus AMP, Xavier J, Correia JAFO, Susmel L, Fernandes AA. Low and ultra-low-cycle fatigue behavior of X52 piping steel based on theory of critical distances. *Int J Fatig*. 2020;134:1–9.
20 Cicero S, Torabi AR, Madrazo V, Azizi P. Prediction of fracture loads in PMMA Unotched specimens using the equivalent material concept and the theory of critical distances combined criterion. *Fatig Fract Eng Mater Struct*. 2017:1–12.
21 Peron M, Torgersen J, Berto F. A novel approach for assessing the fatigue behavior of PEEK in a physiologically relevant environment. *Materials*. 2018;11:1923.
22 Cicero S, García T, Castro J, Madrazo V, Andrés D. Analysis of notch effect on the fracture behaviour of granite and limestone: an approach from the theory of critical distances. *Eng Geol*. 2014;177:1–9.
23 Jenkins A, Fathi E, Belyadi F. Stress field behavior induced by hydraulic fracture in shale reservoirs: a practical view on cluster spacing. *J Nat Gas Sci Eng*. 2017;48:186–196.
24 Justo J, Castro J, Cicero S, Sánchez-Carro MA, Husillos R. Notch effect on the fracture of several rocks: application of the theory of critical distances. *Theor Appl Fract Mech*. 2017;90:251–258.
25 Justo J, Castro J, Cicero S. Notch effect and fracture load predictions of rock beams at different temperatures using the theory of critical distances. *Int J Rock Mech Min Sci*. 2020;125:104161.
26 Creager M, Paris P. Elastic field equations for blunt cracks with reference to stress corrosion cracking. *Int J Fract Mech*. 1967;3:247–252.
27 Gomez FJ, Guinea GV, Elices M. Failure criteria for linear elastic materials with U-notches. *Int J Fract*. 2006;141:99–113.
28 Lazzarin P, Filippi S. A generalized stress intensity factor to be applied to rounded V-shaped notches. *Int J Solid Struct*. 2006;43:2461–2478.
29 Tanné E, Li T, Bourdin B, Marigo JJ, Maurini C. Crack nucleation in variational phase-field models of brittle fracture. *J Mech Phys Solid*. 2018;110:80–99.
30 Kuruppu MD, Obara Y, Ayatollahi MR, Chong KP, Funatsu T. ISRM-suggested method for determining the Mode I static fracture toughness using semi-circular bend specimen. *Rock Mech Rock Eng*. 2014;47(1):267–274.
31 Taylor D. Predicting the fracture strength of ceramic materials using the theory of critical distances. *Eng Fract Mech*. 2004;71:2407–2416.
32 Taylor D. *The Theory of Critical Distances: A New Perspective in Fracture Mechanics*. Oxford, UK: Elsevier; 2007.
33 Dugdale DS. Yielding of steel sheets containing slits. *J Mech Phys Solid*. 1960;8:100–104.
34 Hobbs DW. An assessment of a technique for determining the tensile strength of rock. *Br J Appl Phys*. 1965;16:259–268.
35 Zhang XJ, Yi YN, Zhu HB, et al. Measurement of tensile strength of nuclear graphite based on ring compression test. *J Nucl Mater*. 2018;511:134–140.
36 Bai QS, Tu SH, Zhang C. DEM investigation of the fracture mechanism of rock disc containing hole(s) and its influence on tensile strength. *Theor Appl Fract Mech*. 2016;86:197–216.
37 Filon LNG. The stresses in a circular ring. *Sel. Engng. Pap. Instn. Civ. Engrs.*. 1924. Paper No. 12.
38 Torabi AR, Etesam S, Sapora A, Cornetti P. Size effects on brittle fracture of Brazilian disk samples containing a circular hole. *Eng Fract Mech*. 2017:496–503.
39 Isrm. The complete ISRM suggested methods for rock characterization, testing and monitoring: 1974–2006. In: Ulusay R, Hudson JA, eds. *Suggested Methods Prepared by the Commission on Testing Methods, International Society for Rock Mechanics, Compilation Arranged by the ISRM Turkish National Group*. Ankara: Kozan Ofset; 2007.
40 Nara Y, Kaneko K. Study of subcritical crack growth in andesite using the Double Torsion test. *Int J Rock Mech Min Sci*. 2005;42:521–530.
41 Ponson L. Depinning transition in the failure of inhomogeneous brittle materials. *Phys Rev Lett*. 2009;103, 055501.
42 Chong KP, Kuruppu MD. New specimen for fracture toughness determination for rock and other materials. *Int J Fract*. 1984;26(2):R59–R62.
43 Aliha MRM, Hosseinpour GR, Ayatollahi MR. Application of cracked triangular specimen subjected to three-point bending for investigating fracture behavior of rock materials. *Rock Mech Rock Eng*. 2013;46(5):1023–1034.
44 Zhang QB, Zhao J. Effect of loading rate on fracture toughness and failure micromechanisms in marble. *Eng Fract Mech*. 2013;102:288–309.
45 Nejati M, Aminzadeh A, Driesner T, Saar MO. On the directional dependency of Mode I fracture toughness in anisotropic rocks. *Theor Appl Fract Mech*. 2020;107:102494.
46 Li D, Wong LNY. The Brazilian disc test for rock Mechanics applications: review and new insights. *Rock Mech Rock Eng*. 2013;46(2):269–287.
47 Gain AL, Carroll J, Paulino GH, Lambros J. A hybrid experimen- tal/numerical technique to extract cohesive fracture properties for mode-I frac- ture of quasi-brittle materials. *Int J Fract*. 2011;169(2):113–131.
48 Réthoré J, Estevez R. Identification of a cohesive zone model from digital images at micron-scale. *J Mech Phys Solid*. 2013;61:1407–1420.
49 Bonamy D, Ponson L, Prades S, Bouchaud E, Guillot C. Scaling exponents for fracture surfaces in homogeneous glass and glassy ceramics. *Phys Rev Lett*. 2006;97:135504.
50 Vernede S, Ponson L, Bouchaud JP. Turbulent fracture surfaces: a footprint of damage percolation? *Phys Rev Lett*. 2015;114:21550.
51 Westergaard HM. Bearing pressures and cracks. *J Appl Mech*. 1939;6:49–53.

Chapter 4: Quantifying the length of FPZ by roughness analysis

Four decades ago, Mandelbrot et al. (1984) endeavoured to connect physics and mechanics of fracture by proposing a relationship between fractal dimension of metal fractured surfaces and fracture toughness. After a decade, however, new explorations reported universality of fractal dimension and roughness exponent of fractured surfaces (Bouchaud et al. 1990; Maloy et al. 1992). Regarding this paradox, new statistical physics models in the last two decades have considered fracture as a mixed-order phase transition from continuous damage percolation at small enough length scales to first order at a critical length scale ξ (Alava et al. 2006; Bonamy et al. 2006; Morel et al. 2008; Gjerden et al. 2013; Vernede et al. 2015). Following this line of thinking, ξ is also the length of fracture process zone of a crack or the cohesive length ℓ_c (Irwin 1958; Barenblatt 1962; Dugdale 1960). The new challenge, however, from both physical and mechanical points of view is experimental determination of $\xi \equiv \ell_c$. In this chapter, we employ a novel multifractal roughness analysis to determine ξ that is further verified by two different mechanical models required completely different experimental inputs. These results not only make a relationship between fracture toughness and roughness, and solve a forty-year-old dilemma, but also clarify some ambiguities in solid mechanics including determination of intrinsic tensile strength or the cohesive stress σ_c as well as the effects of geometry (Bazant and Planas 1997; Carpinteri and Pugno 2005; Torabi et al. 2017) and experimental rate (Needleman 1988; Zhang and Zhao 2014) on tensile strength.

Quasi-brittle materials including rocks are not following Linear Elastic Fracture Mechanics (LEFM) at some small enough length scales owing to the heterogeneous nature of such materials, and existence of a Fracture Process Zone (FPZ) at the tip of cracks or other stress concentrators within these materials before crack propagation inside them (Irwin 1958; Barenblatt 1962). According to Cohesive Zone Model (CZM) (Dugdale 1960; Barenblatt 1962), if the length of FPZ ℓ_{pz} ahead of a stress concentrator including cracks is ignored, the actual stress at which material fails cannot be determined by means of analytical solutions and all analyses and measurements including fracture toughness would have significant errors. Therefore, measuring ℓ_{pz} is of prime importance to analyze or predict failure of quasi-brittle

materials, and is the key to understanding the relationship between multiscale physical properties and fracture mechanics of such materials (Tanne et al. 2018). Although different methodologies have been employed for ℓ_{pz} measurement as surveyed by Dutler et al. (2018) it is inconclusive yet to develop an internationally accepted norm for quantifying it.

Here we quantify geometry dependent ℓ_{pz} of four different rock types including a red sandstone, a white coarse-grained marble, a fine-grained (FG) granite and a coarse-grained (CG) granite. This selection covers sedimentary, metamorphic and igneous rock types with different grain sizes (Figs. 4.1 and 4.2). For such a purpose, Notched Semi-Circular Bending (NSCB) specimens as well as ring specimens with different central hole radii are made from these rocks and broken under quasi-static loading rates. NSCB specimens are prepared and tested as per ISRM (Kuruppu et al. 2014) for fracture toughness measurement. Moreover, high-resolution 3D X-ray computed tomography data from fractured area of some NSCB specimens acquired at the Australian synchrotron are used for reconstructing roughness of their fractured surfaces (Fig. 4.1). The rough surfaces are further analyzed for determining the critical length scale ξ by applying a novel multifractal analysis. Finally, failure analysis of NSCB and ring specimens is used for validating $\xi \equiv \ell_c$. Further details of these procedures are specified in Methods.

Fracture and phase transition

Fractography on the post-mortem fracture surfaces is a failure analysis routine and provides useful information about interaction of a moving crack front with material's microstructure. Based on solid physical arguments, quantitative fractography has been employed to estimate ℓ_c for quasi-brittle materials (Vernede et al. 2015). This method considers two regimes with different scaling properties on fractured surfaces that conjectures a mixed-order phase transition. Fractured surfaces at length scales ϵ smaller than a critical length scale $\epsilon \ll \xi$ are multiaffine fractals (Barabasi et al. 1991) with significant intermittency, whereas at length scales $\epsilon \gg \xi$ are monoaffine fractals with universal roughness exponents (Santucci et al. 2007). Accordingly, there are two different mechanisms that control fracture roughness in these regimes.

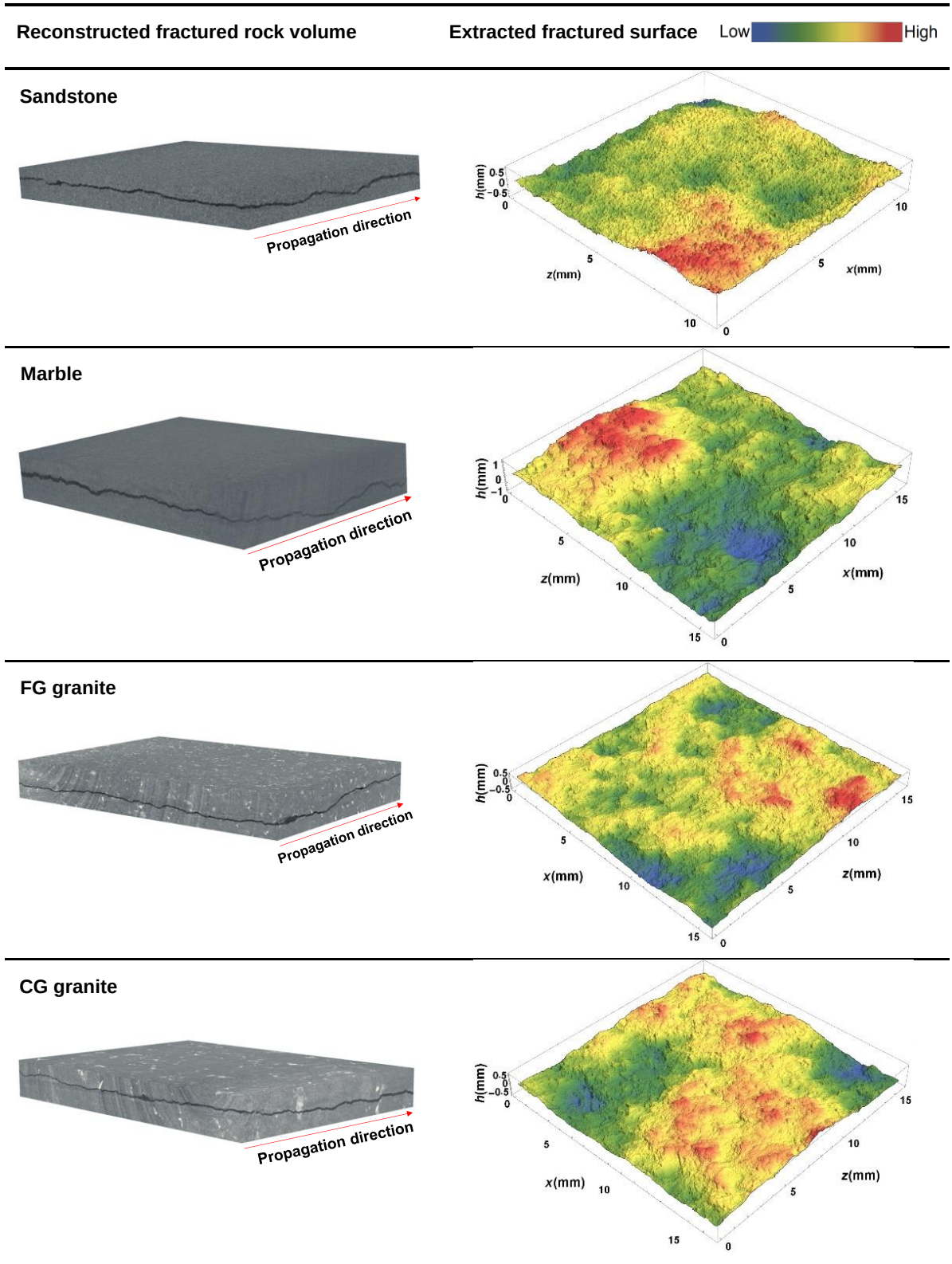

Fig. 4.1. 3D X-ray computed tomography images of fractured area and topographic images of fractured surfaces of different rock specimens. The x-axis and z-axis correspond to the crack propagation direction and the crack front direction, respectively. Real length of reconstructed CT images is around 18 mm in propagation direction.

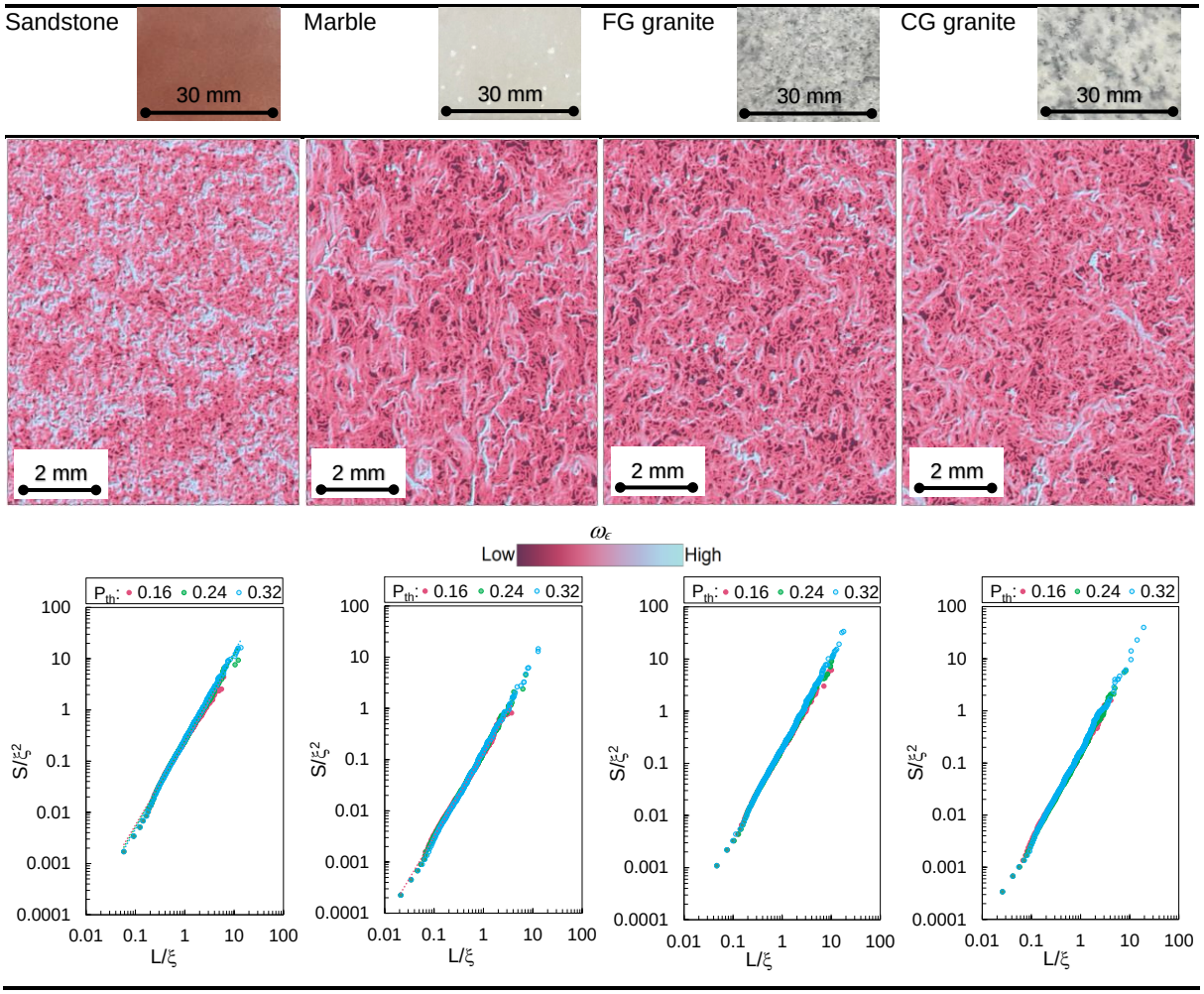

Fig. 4.2. Percolation analysis of different rock specimens. The universal fractal dimension ($D \sim \log(S/\xi^2) / \log(L/\xi) \approx 1.7$) of percolation clusters on ω_ϵ field calculated at a length scale ϵ = 33 μm, which is much smaller than ξ of the analysed rock specimens with considerably different microstructures, confirms damage percolation is the underlying mechanism of fracture initiation and depinning at small enough length scales $\epsilon \ll \xi$.

It was suggested by Mandelbrot et al. (1984) and later modelled by Hansen and Schmittbuhl (2003), and Shekhawat et al. (2013) that if damage percolation takes place before crack propagation, then fractal dimension of percolation clusters on fractured surfaces at length scales $\epsilon \ll \xi$ will be universal. Fig. 4.2 is showing the universality of fractal dimension of percolation clusters ($D \approx 1.7$) on ω_ϵ field calculated as per Vernede et al. (2015) (Eq. 4-1) at a length scale $\epsilon = 2.d$, which is much smaller than ξ of the analysed rock specimens (Table 4.2),

where d is the spatial resolution of the tomograph and is about 16.5 μm, Δh is ensemble average of height differences over all directions Θ, calculated for all X. Further details of this procedure is specified in Methods.

$$\omega_\epsilon(\mathrm{X}) = \frac{1}{2}\log(\langle \Delta h(\epsilon)^2 \rangle_\Theta) \tag{4-1}$$

From Fig. 4.2, it can be clearly seen that there is a meaningful correlation between grain size and percolation clusters of different rock types. This fact can be further clarified by normalizing calliper length L and size S of the clusters formed from different fractions of steep cliffs P_{th} on $\omega_\epsilon(\mathrm{X})$ by ξ and ξ^2, respectively. This correlation along with the universality of fractal dimension of the percolation clusters can be deciphered as follows. At a length scale $\epsilon \ll \xi$ depinning is a continues phase transition successfully described by damage percolation and has nothing to do with material microstructure. Moreover, grain size is a very important microstructural feature that controls ℓ_c and fracture mechanics of quasi-brittle materials. Therefore, continues damage percolation will transform to discontinue phase transition at ξ that is being controlled by material microstructure, and LEFM is valid for larger length scales $\epsilon \gg \xi$ where the crack front interact with material microstructure in an effective random medium (Bouchaud et al. 1993; Bouchaud et al. 2002).

ξ quantification

According to Bouchbinder et al. (2006) and our analyses roughness of fractures does not belong to any of the known kinetic roughening models. Consequently, it is very challenging to determine the critical cut-off length ξ. Multifractal spectra, $H(q) = \zeta_q/q$ versus q, of ensemble average of height differences $\Delta h(\delta r)$ on the fractured surfaces computed at different separations δr is calculated by means of qth-order structure functions $S_q(\delta r)$ (Santucci et al. 2007):

$$S_q(\delta r) = \langle |\Delta h(\delta r)|^q \rangle^{1/q} = \langle |h(\mathrm{X}+\delta r) - h(\mathrm{X})|^q \rangle_{\mathrm{X}}^{1/q} \propto \delta r^{\zeta_q * 1/q} \tag{4-2}$$

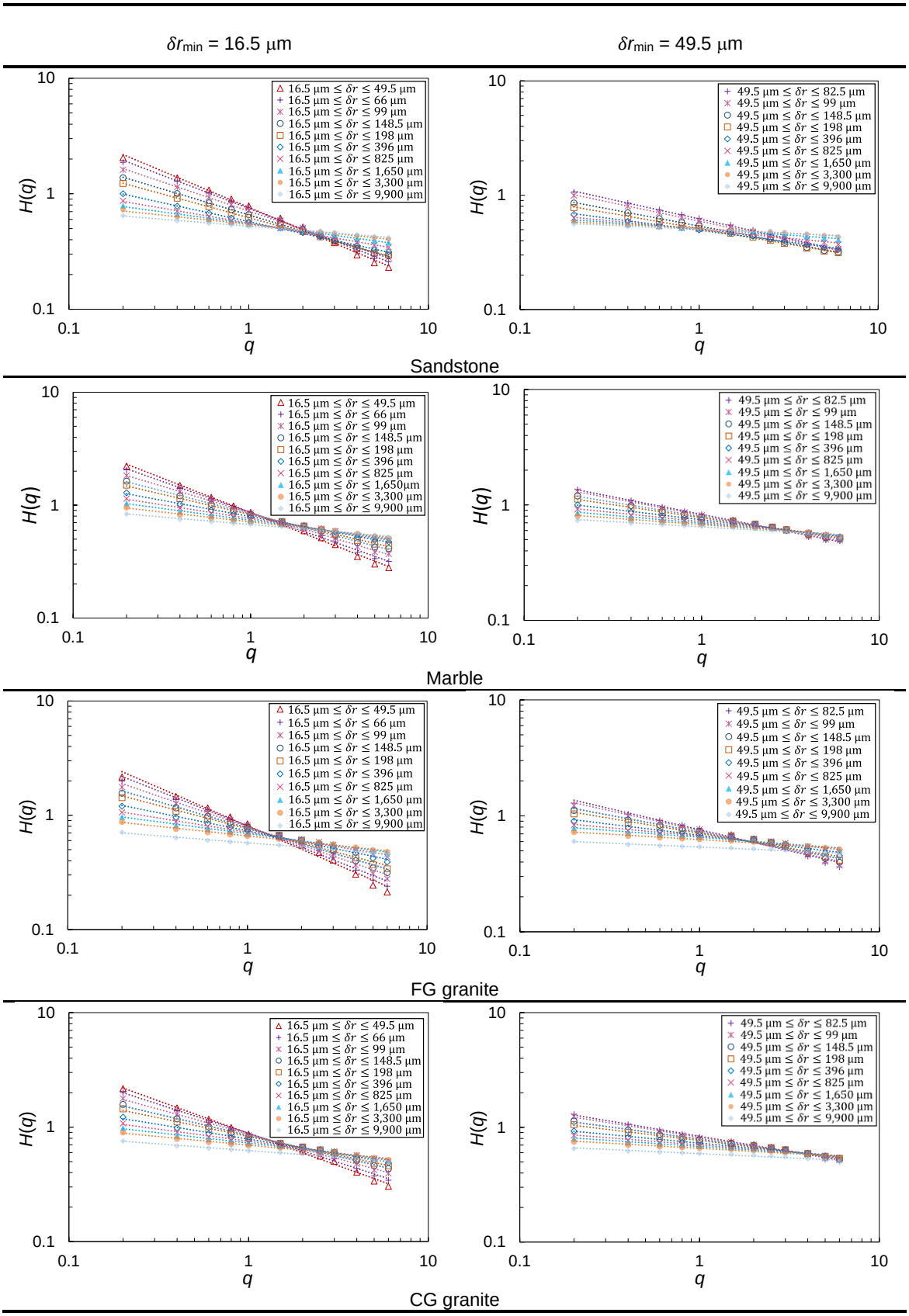

Fig. 4.3. Intermittency of the multifractal spectra of different rock types. R-squared of the fitted power laws are above 0.99 on average.

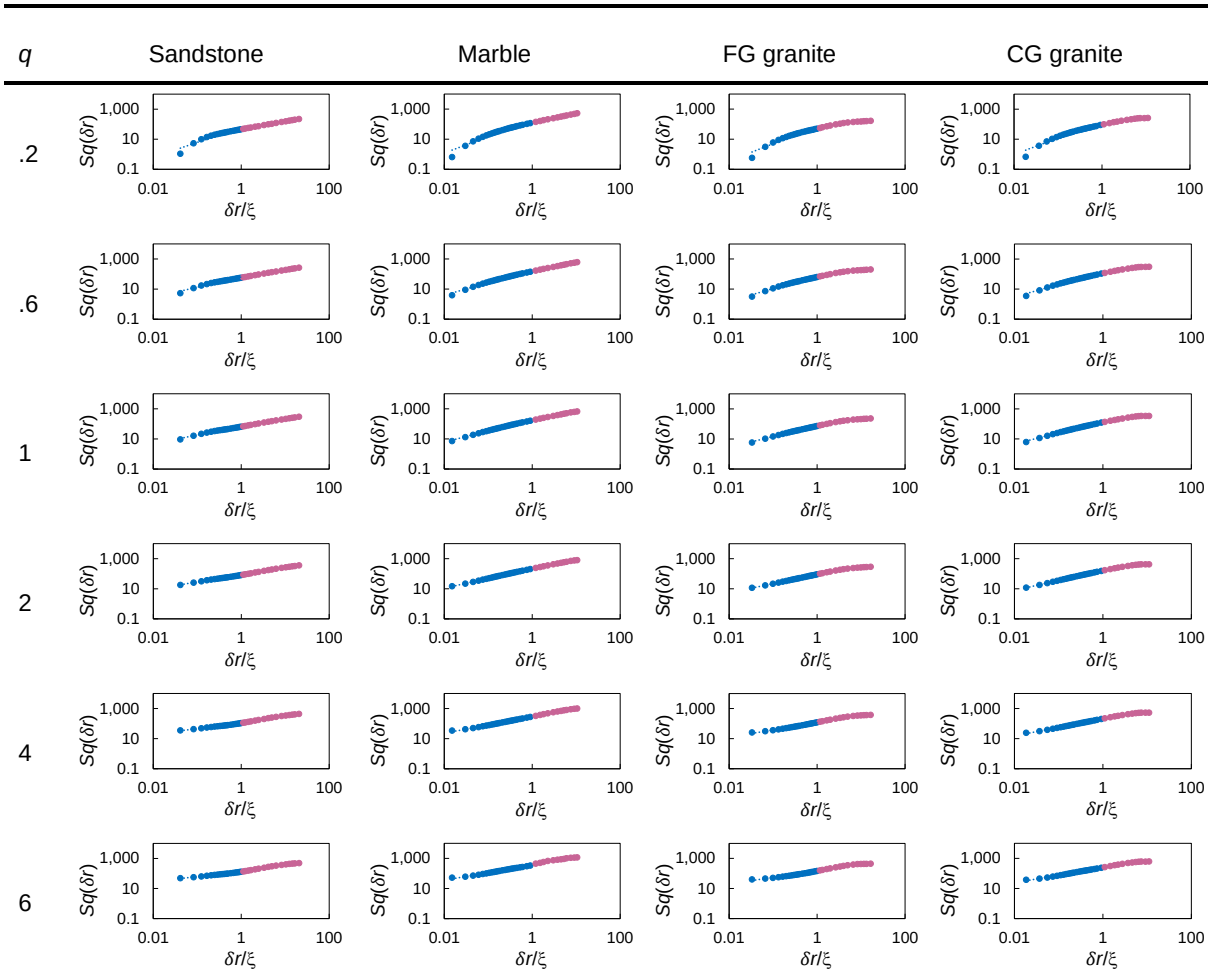

Fig. 4.4. *q*th-order structure functions for 6 different moments q and different rock types both below and above the critical length scale ξ.

Intermittency or deviation of $H(q)$ from a constant value can be formulated by perfect power laws for the rock fractured surfaces (Fig. 4.3). Thus, slope of the multifractal spectra λ is a measure of intermittency. However, such intermittency depends on the analyzed domain $[\delta r_{\min}, \delta r_{\max}]$, and there is an inverse relationship between $\delta r_{\max}$ and λ if $\delta r_{\min}$ is fixed. The discussed mixed-order phase transition is the root cause of this domain dependency since moment order q of the $S_q(\delta r)$ are not always showing perfect power laws for all moments or all separations δr (Fig. 4.4).

Monofractals are neither correlated nor intermittent. Therefore, ξ is the minimum of the domain that possesses a multifractal spectrum with a constant $H(q)$ and a power exponent λ

almost equal to zero. Table 4.2 reports these parameters for the identified monofractal domains on the studied rock fractured surfaces. An elaborate domain analysis for different pairs of δr_{min} and δr_{max} is conducted to identify such monofractal domain. Fig. 4.5 is presenting the outcome of this analysis for different rock types. Indeed, the coordinates of the $\lambda \approx 0$ in the $\delta r_{min} - \delta r_{max}$ space are the extremums of the monofractal domain. In addition, multifractal and monofractal spectra of the fractured surfaces below and above $\xi \equiv \ell_c$ is shown in Fig. 4.5.

Following the latest statistical physics fracture models (Shekhawat et al. 2013; Vernede et al. 2015), the quantified ξ is considered as ℓ_c and imported into two mechanical models, which are developed based on Point Method (PM) form of the Theory of Critical Distances (TCD) (Taylor 2007) and Coupled Finite Fracture Mechanics (CFFM) (Leguillon 2002; Cornetti et al. 2006), for verifying that the quantified length scale by means of quantitative fractography is the cohesive length or the length of FPZ of a crack in the direction of fracture propagation.

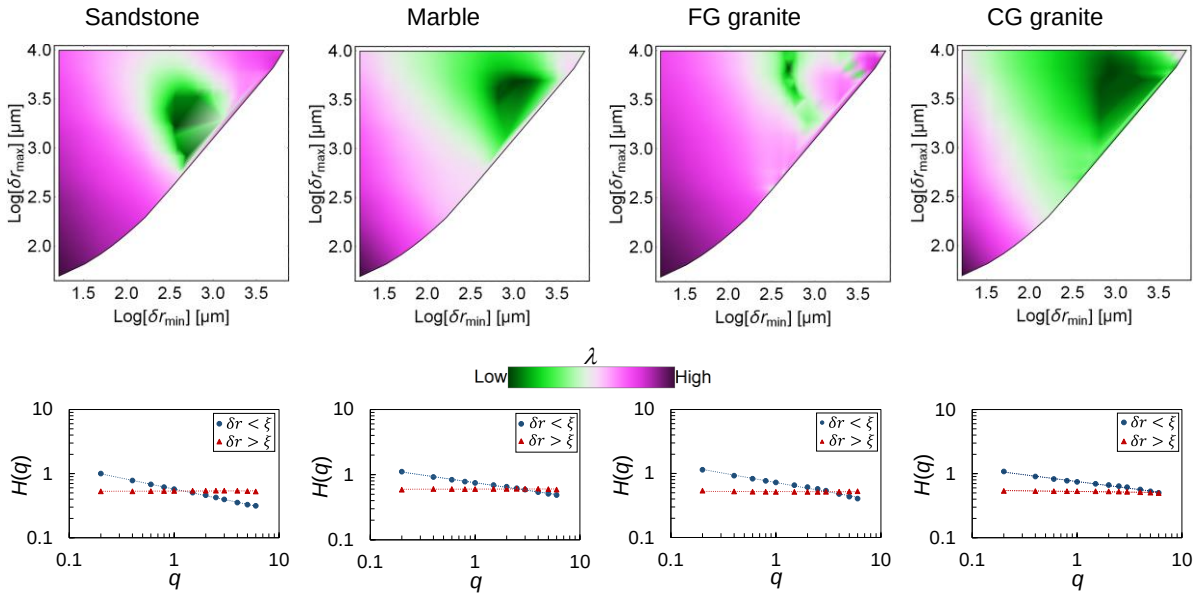

Fig. 4.5. Determining $\xi \equiv \ell_c$ as the minimum δr_{min} of the monofractal domain. The intermittency $\lambda \in (0, 0.7)$ of different δr_{min} and δr_{max} pairs is presented in $\delta r_{min} - \delta r_{max}$ space for different rock specimens. The coordinates of the minima on these plots $\lambda \approx 0$ are the extremums of the monofractal domain. Corresponding multiscaling graphs for both multifractal $\epsilon \ll \xi$ and monofractal $\epsilon \gg \xi$ domains are presented.

Validating $\xi \equiv \ell_c$ by PM

According to PM failure criterion the inherent tensile strength σ_0 of materials can be calculated at half of a characteristic distance $CL/2$ from the notch tip if the stress distribution and failure load are known. Creager – Paris (C – P) solution (Creager and Paris 1967) can perfectly modify the blunted notch effect and calculate stress distribution ahead of rounded notch tips as a function of notch tip radius ρ and stress intensity factor that can be measured experimentally (Methods and Fig. 4.6). Then, this LEFM based method can be used to calculate apparent fracture toughness K_{Ic}:

$$CL = \frac{1}{\pi}\left(\frac{K_{Ic}}{\sigma_0}\right)^2 \tag{4-3}$$

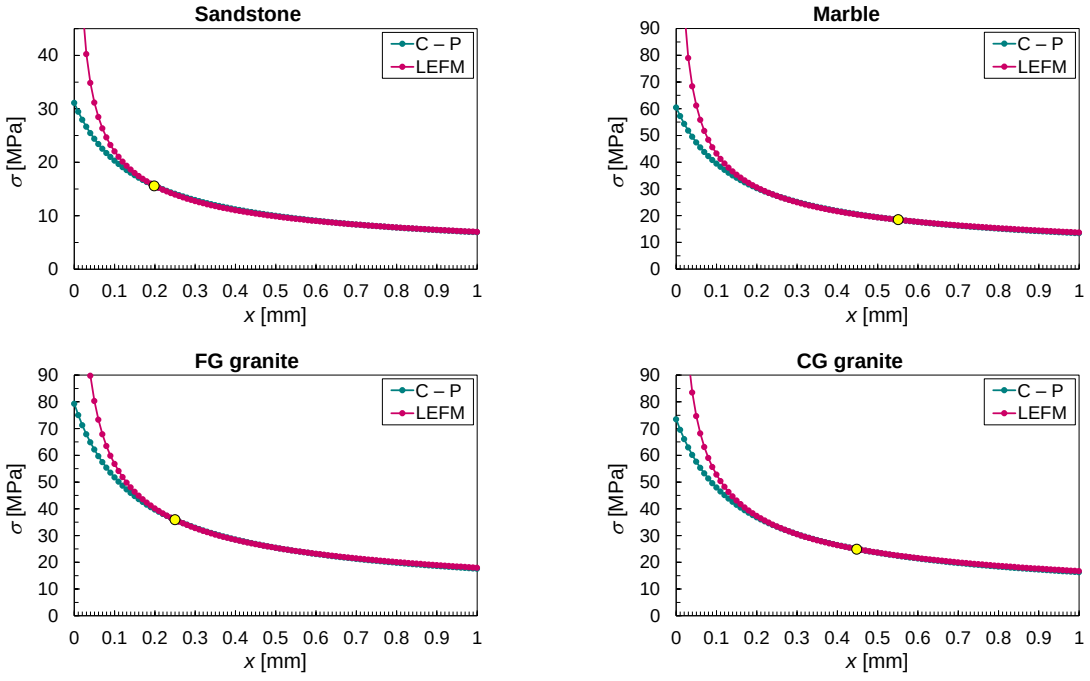

Fig. 4.6. Tensile stress $\sigma(x)$ against distance from stress concentrator x according to C – P and LEFM solutions. Four different rock specimens are shown: sandstone (SIS3), marble (MaS6), FG granite (GFS6) and CG granite (GCS4). Modification of the notch root radius according to C – P solution is very successful and at $\ell_c/2$ shown by yellow points the LEFM and C – P curves are overlapped. Therefore, C – P solution can be safely used to determine both cohesive stress σ_c and apparent fracture toughness K_{Ic}.

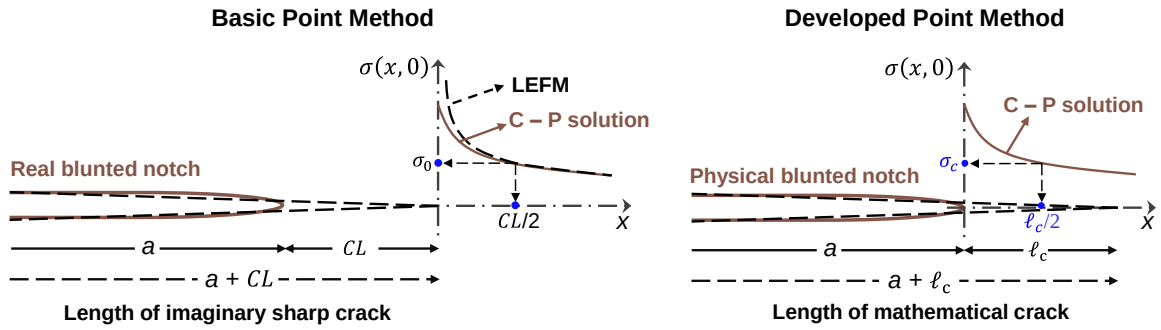

Fig. 4.7. Schematics of basic and developed PMs.

Indeed, the *CL* is estimating ℓ_{pz}, and *CL*/2 is the idealized radius of the zone of plastic deformation at the crack tip (Irwin 1958). PM estimates K_{Ic} by adding a characteristic length *CL* ahead of a notch with a length *a*, and applying LEFM to determine stress distribution ahead of the imaginary equivalent sharp crack with a length *a* + *CL* (Fig. 4.7). Derivation of Eq. (4-3) can be found in (Taylor 2007).

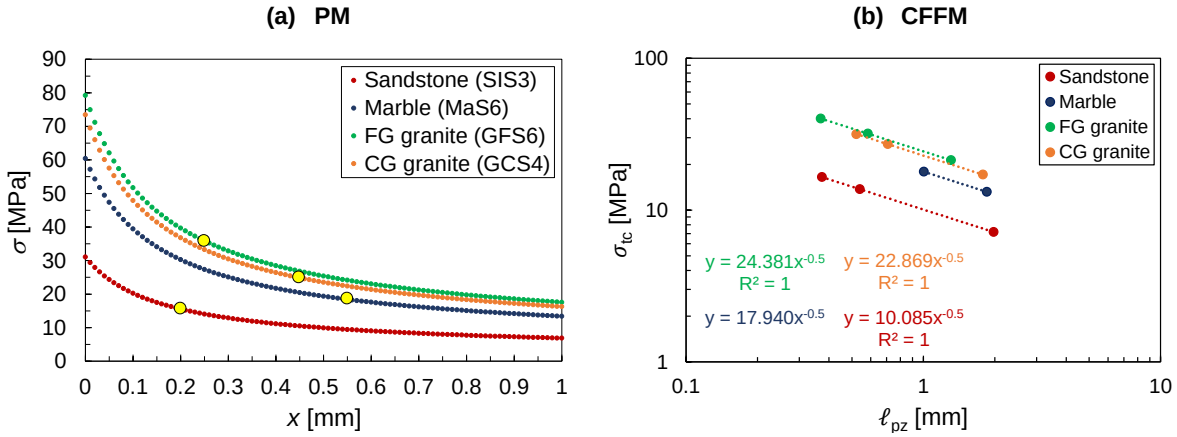

Fig 4.8. Cohesive stress σ_c approximation as a function of cohesive length ℓ_c quantified by roughness analysis. PM: the stress distribution is calculated using C – P solution [30] and experimentally measured failure load, then σ_c is approximated as the (ℓ_c) on this curve. CFFM: The ℓ_{pz} of different ring geometries have been calculated using energy criterion, then the perfect power law emerging from LEFM is used to approximate σ_c as the $\sigma_{tc}(\ell_c)$. There is a very good agreement between σ_c values approximated by PM and CFFM (Table 4.2).

There are two unknowns in this criterion: CL and σ_0. A new PM is developed that instead of replacing the blunted notch with an imaginary equivalent sharp crack to take into account nonlinear deformations close to crack tip, follows CZM and replaces $CL/2$ and σ_0 with $\ell_c/2$ and σ_c. In this way, according to CZM notch tip is the physical crack tip and the mathematical crack tip is located ahead of the cohesive length ℓ_c. The developed PM predicts the cohesive stress σ_c as a function of quantified ℓ_c using roughness analysis. The σ_c is equal to the tensile stress at a distance $\ell_c/2$ from the notch tip computed by means of C – P solution (Creager and Paris 1967) (Fig. 4.7). Fig. 4.8.a is showing the σ_c approximation using the developed PM for different rock specimens. Finally, the ℓ_c and σ_c pair is inserted into the Dugdale – Barenblatt (D – B) formula Eq. (4-4) (Dugdale 1960; Barenblatt 1962) to predict the critical stress intensity factor or apparent fracture toughness K_{Ic} that is showing a perfect agreements with the one measured experimentally for the same specimen following ISRM (Kuruppu et al. 2014). The experimental tests performed under 5 mm/min rate since under slower rates specimens were not completely separated and roughness reconstruction for such samples is challenging. Table 4.2 is reporting this surprising agreement for all rock types, which is verifying the quantified ℓ_c and σ_c values by the developed PM.

$$\ell_c = \frac{\pi}{8}\left(\frac{K_{Ic}}{\sigma_c}\right)^2 \tag{4-4}$$

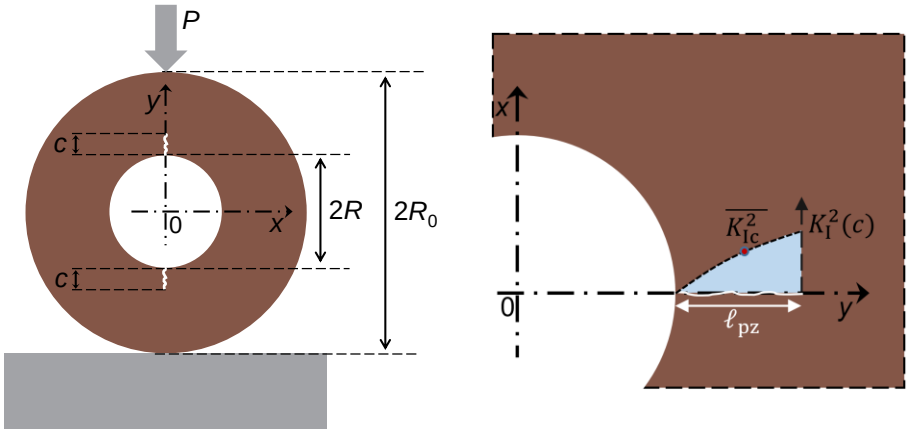

(a) (b)

Fig. 4.9. Schematics of ring experiment (a); and energy criterion (b).

Validating $\xi \equiv \ell_c$ by CFFM

The CFFM is a comprehensive failure criterion requiring fulfillment of both stress and energy criteria before fracture propagation (Cornetti et al. 2006):

$$\begin{cases} \int_0^{\Delta} \sigma_x(y)dy \geq \sigma_u \Delta \\ \int_0^{\Delta} G(c)dc \geq G_c \Delta \end{cases} \tag{4-5}$$

where (x, y) is the Cartesian coordinate system (centered at the ring center in our experiments as shown in Fig. 4.9). These two equations integrating the stress $\sigma_x(y)$ and crack driving force G over a critical crack advance Δ. The stress criterion needs an average critical tensile stress σ_u over Δ, while energy criterion ensures that the available energy $G_c\Delta$ can create the new fracture surface. The energy criterion can be rewritten in terms of the stress intensity factor K_I and intrinsic toughness K_{Ii} as well (Eq. (4-6)) (Irwin 1958).

The developed CFFM replaces the finite crack advance Δ with the length of process zone ℓ_{pz}, and determines this quantity for different ring specimens according to the energy criterion and the intrinsic fracture toughness K_{Ii} determined experimentally. K_{Ii} is determined as per ISRM (Kuruppu et al. 2014) with a slow experimental rate of 0.05 min/mm to avoid dynamics effects. All ring tests are also carried out under the same rate for minimizing the dynamic effects. Then, the ℓ_{pz} is imported into the stress criterion, and determines geometry dependent tensile strength σ_{tc} of rings using Kirsch's solution together with Hobbs' correction (Hobbs 1965).

$$\begin{cases} \int_0^{\ell_{pz}} \sigma_x(y)dy \geq \sigma_{tc}\ell_{pz} \\ \int_0^{\ell_{pz}} K_I^2(c)dc \geq K_{Ii}^2\ell_{pz} \end{cases} \tag{4-6}$$

Finally, by plotting ℓ_{pz} against σ_{tc} for different rings of the same rock type, a perfect power law $\sigma_{tc} \sim \ell_{pz}^{-0.5}$ emerging from linear elasticity will determine the intrinsic tensile strength or

the cohesive stress of crack σ_c corresponding to ℓ_{pz} of crack or the cohesive length quantified by roughness analysis $\xi \equiv \ell_c$ (Fig. 4.8.b). Table 4.2 is summarizing this results as well. The determined σ_c following the developed CFFM is identical with the one determined using the developed PM, within experimental error. This excellent agreement can further verify the accuracy of the cohesive length ℓ_c or the length of process zone of a moving crack determined by quantitative fractography on the post mortem fracture surfaces of the studied rock materials. Further details of the CFFM is specified in Methods.

Table 4.1. Results of ring tests and the developed CFFM for different geometries.

Rock type	R [mm]	R_0 [mm]	B [mm]	P_{max} [MPa]	σ_{max} [MPa]	K_{Ic} [MPa.m$^{0.5}$] ISRM	ℓ_{pz} [mm]	σ_{tc} [MPa]
Sandstone	1.46	37.43	30.08	11.57	3.30	0.45	7.14	4.09
	3.03	37.50	30.23	11.55	3.38	0.45	0.37	16.49
	6.07	37.42	30.10	8.08	2.66	0.45	0.54	13.72
	14.96	37.44	29.98	2.61	1.49	0.45	1.98	7.17
Marble	1.49	37.50	30.00	21.26	6.08	0.80	5.98	7.87
	3.09	37.41	29.88	12.39	3.68	0.80	21.22	4.28
	6.05	37.41	29.85	11.73	3.90	0.80	1.01	17.89
	14.76	37.48	29.98	4.82	2.71	0.80	1.85	13.19
CG granite	3.05	37.69	29.85	23.57	6.95	1.02	0.52	31.66
	6.04	37.74	30.03	16.88	5.51	1.02	0.71	27.18
	13.00	37.72	30.07	7.27	3.58	1.02	1.78	17.12
FG granite	3.04	37.70	30.01	27.96	8.19	1.08	0.37	40.13
	6.00	37.78	30.10	19.33	6.28	1.08	0.58	31.93
	12.92	37.80	30.10	8.66	4.22	1.08	1.31	21.32

Table 4.2. Summary of computed statistical physics parameters as well as mechanical properties.

Rock type	ℓ_c [mm]	λ ($\delta r < \ell_c$)	H ($\delta r > \ell_c$)	D (ϵ = 33 μm)	σ_c [MPa] PM	K_{Ic} [MPa.m$^{0.5}$] PM	K_{Ic} [MPa.m$^{0.5}$] ISRM	σ_c [MPa] CFFM
Sandstone	0.4	0.34	0.53	1.68 ± 0.06	15.57	0.497	0.498	15.95
Marble	1.1	0.23	0.60	1.69 ± 0.06	18.44	0.976	1.002	17.11
FG granite	0.5	0.29	0.52	1.68 ± 0.05	35.90	1.281	1.314	34.48
CG granite	0.9	0.21	0.53	1.72 ± 0.06	24.88	1.191	1.218	24.11

Geometry and rate effects on σ_c

The results presented in Fig. 4.8.b suggests a novel powerful method for analysing the effect of geometry including shape and size on material tensile strength by taking into account the ℓ_{pz} following CZM. Experimental measurements and results of the developed CFFM are summarised in Table 4.1. According to these results, if the radius of the ring central hole R is larger than the ℓ_{pz} quantified by energy criterion $\ell_{pz} \ll R$, then $\sigma_{tc} \sim \ell_{pz}^{-0.5}$. Otherwise, if $\ell_{pz} \gg R$, then the stress will not concentrated on expected parts of the ring and will distribute in a larger area, and analytical solutions will fail. The power exponent 0.5 is in agreement with other proposed size effect laws (Bazant and Planas 1997; Carpinteri and Pugno 2005) and emerges from linear elasticity since σ_{tc} is calculated as a function of failure load and linear elastic stress distribution $\sigma_x(y)$ that is totally acceptable for $y \geq \ell_{pz}$.

σ_c, however, has nothing to do with the applied stress, and its geometry dependent distribution. The cohesive stress is purely material dependent, and material will fail as soon as it reaches. In fact, the cohesive stress of material together with geometry of the sample or structure, environmental condition, and loading condition sets the ℓ_{pz} and the apparent tensile strength σ_{tc}. ℓ_{pz} values calculated by the energy criterion call for generalizing D – B formula

in order to approximate the length of FPZ by adding a new factor f that is a function of geometry as well as environmental and loading conditions (refer to Methods for more details):

$$\ell_{\mathrm{pz}} = \frac{\ell_{\mathrm{c}}}{f^2} = \frac{\pi}{8}\left(\frac{K_{\mathrm{Ic}}}{\sigma_{\mathrm{c}}}\right)^2 \tag{4-7}$$

According to our experimental observations after a threshold the apparent fracture toughness increase with loading rate. For the studied NSCB specimens the K_{Ic} values measured at 5 and 0.05 mm/min experimental rates are reported in Table 4.2 and Table 4.1, respectively. As it goes from its name K_{Ic} or critical stress intensity factor is a measure of stress concentration that can change as a function of geometry or loading rate, and change the behaviour of material in K dominance region that ℓ_{pz} is whitin it.

We have shown in quasi-statics loading rate cohesive stress is material dependent and independent of loading rate. However, it is suggested that at dynamic loading rates the properties of material will change. Zhao (2000) has suggested that the cohesion parameter in the Mohr–Coulomb strength criterion or the so-called cohesive strength is the cause of Dynamic Increase Factor (DIF) of material strength. Therefore, in a future research we will investigate into it by determining cohesive stress σ_{c} of fractured surfaces of the same rock types broken under dynamic loading rates using roughness analysis.

Methods

Roughness reconstruction

The topography of fractured surfaces, illustrated in Fig. 4.1, have been reconstructed from 3D X-ray computed tomography data with a spatial resolution d of about 16.5 μm acquired at the Australian synchrotron. This method is superior to contact methods affected by the tip geometry of probes (Mazeran et al. 2005; Lechenault et al. 2010). After reconstructing the fractured part of the NSCB samples broken under 5 mm/min experimental rate, a threshold is employed to separate the fractured area. Then, roughness of fractured surfaces have been reconstructed by applying 3D image processing techniques on these big binary images with around half a billion voxels.

Percolation analysis

$\omega_\epsilon(\mathbf{X})$ presented in Eq. (4-1) measures the natural logarithm of the average height variations around each point, on a height field $h(\mathbf{X})$ with its neighbours over a circle with a radius of ϵ. The pair length scale and direction $(\epsilon, n) = (2.d, 12)$ is used to compute Δh:

$$\langle \Delta h(\epsilon)^2 \rangle_\Theta = \frac{1}{n}\sum_{k=0}^{n-1}\Big[h\big(x_i, z_j\big) - h\big(x_i + \epsilon * \cos(2\pi k/n\,), z_j + \epsilon * \sin(2\pi k/n\,)\big)\Big]^2 \tag{4-8}$$

where $\Theta \in [0, 2\pi]$ rad. x_i and z_j are the coordinates of a point on $h(\mathbf{X})$ in crack propagation and crack front directions, respectively.

To verify that damage percolation is the mechanism of fracture initiation at length scales smaller than the critical length scale $\xi \equiv \ell_c$, fractal dimension of percolation clusters on ω_ϵ field is calculated for all rock types. Three different thresholds are applied to keep only a fraction P_{th} of steep cliffs on $\omega_\epsilon(\mathbf{X})$, and then fractal dimension of such cliffs is computed that is showing an universality, which is independent from P_{th}, and verify damage percolation is the underlying mechanism of fracture initiation at small enough length scales.

Multifractal analysis

In order to compute multiscaling spectrum of the rough surfaces, $S_q(\delta r, \theta)$ has been calculated for different directions θ and separations δr as per Eq. (4-2) over admissible coordinates (xo_i, zo_j). xo_i and zo_j are the coordinates of a point on a height field with zero average, $\langle h(\mathbf{X})\rangle_\theta = 0$, in crack propagation and crack front directions, respectively. It is a very time consuming process to compute many moments order q of structure function over all admissible coordinates, and directions with small intervals for large data sets in order of million data points. Therefore, $m = 12$ moments i.e. $q = \{0.2, 0.4, 0.6, 0.8, 1, 1.5, 2, 2.5, 3, 4, 5, 6\}$ and $n = 4$ directions i.e. $\theta = \pi k/n$ rad ($k = 0, 1, \dots, n-1$) have been selected. Moreover, an interval l equal 2 pixels for calculating $S_q(\delta r, \theta)$ is used. Thus, $\Delta h(\delta r)$ has been calculated between

following admissible coordinates $h(xo_{il}, zo_{jl} + \delta r) - h(xo_{il}, zo_{jl})$ for selected q and θ sets. It is notable that for a few smaller subsets $S_q(\delta r, \theta)$ have been calculated among both selected and all admissible coordinates $h(xo_i, zo_j + \delta r) - h(xo_i, zo_j)$, and for different number of θ angles $n = \{4, 12, 36\}$, and the differences between the calculated average scaling properties $\langle S_q(\delta r)\rangle_\theta$ were negligible. Admissible coordinates would be different considering separation and direction. Maximum separation has always been about half of the minimum dimension of the studied surfaces to compute moments at different separations over enough and similar data points. Different domains of discrete separations $\delta r \in [16.5, 9900]$ μm have been analysed to determine the monofractal domain that its minimum is the critical length scale $\xi \equiv \ell_c$.

K_{Ic} determination

Semi-circular bending experiment is suggested by ISRM [19] for measuring fracture toughness of rock materials using NSCB specimens that are rather simple to machine and provide good repeatability. Multiple NSCB specimens for each rock type are tested showing good repeatability and the average apparent fracture toughness K_{Ic} is calculated as follows:

$$K_{Ic} = Y' \frac{P_{max}\sqrt{\pi a}}{DB} \tag{4-9}$$

Where a, B, D, and P_{max} are the notch length, the specimen thickness, the diameter of the NSCB specimen and the maximum applied load, respectively. The notch length of the tested NSCB specimens ranges from 14 to 16 mm, while the notch tip radius ρ is 350 microns. The diameter and the thickness of the specimens range from 74 to 76 mm and 29 to 31 mm, respectively. Finally, Y' gives the non-dimensional stress intensity factor derived using the finite element method while assuming plane-strain conditions (Kuruppu et al. 2014). Its expression follows:

$$Y' = -1.297 + 9.516(s/D) - \big(0.47 + 16.457(s/D)\big)\beta + \big(1.071 + 34.401(s/D)\big)\beta^2 \tag{4-10}$$

in which s is the span length that is between 37 to 38 mm for all conducted experiments while β is equal to $2a/D$.

It is notable that following practical developments (Gomez et al. 2006), if the notch tip radius is smaller than the cohesive length $\rho < \ell_c$, the ISRM suggested method (Kuruppu et al. 2014) is a reliable method for determining apparent fracture toughness of rock materials and the effect of ρ is negligible (Aligholi et al. 2022). From Table 4.2, it can be seen that this criterion is met and the cohesive length of all studied rock types is larger than ρ that is 350 microns.

Creager – Paris solution

C – P solution provides the stress distribution in specimens with a blunted notch of radius ρ:

$$\sigma(x,0) = \frac{2K^{U}}{\sqrt{\pi}} \frac{x+\rho}{(2x+\rho)^{3/2}} \tag{4-11}$$

using the coordinate system depicted in Fig. 4.7 provided that x starts from notch tip. The apparent stress intensity factor K^{U} is measured experimentally following ISRM (Eq. (4-9)).

σ_{tc} determination

Ring specimens with different central hole radii are used to measure the apparent tensile strength of the studied rock materials under different stress concentrations. The minimum diameter of the internal hole that could be drilled into the sandstone and the marble is about 3mm, while it is about 6mm for granites. Rings with four different inner diameters are prepared for the sandstone and the marble, whereas three different ring specimens are prepared for granites. The outer diameter and thickness of the rings are around 75 and 30 mm, respectively. Note that, following the analysis of Fillon (1924), the ratio of the inner to the outer diameter of the tested ring specimens is less than or equal to 0.4 so that the tensile mode of failure dominates over the compressive one (Hobbs 1965). The driving rate of the cross-head for all ring tests is set to 0.05 mm/min to avoid dynamics effects.

Following Torabi et al. (2017), Kirsch's solution together with Hobbs' correction (Hobbs 1965) are used to determine the tensile stress distribution $\sigma_x(y)$ along the loading axis y (see the schematic of the ring specimen shown in Fig. 4.9.a for the definition of the axes x and y):

$$\sigma_x(y) = \frac{\sigma_{\max}}{2}\left(2 - 2\frac{R^2}{y^2} + 12\frac{R^4}{y^4}\right)F_{\text{corr}} \tag{4-12}$$

Here, F_{corr} is a correction factor that should be taken into account for sufficiently large R/R_0 ratios, which follows:

$$F_{\text{corr}} = 1 + \frac{19}{3}\left(\frac{R}{R_0}\right)^2. \tag{4-13}$$

The maximum applied stress $\sigma_{\max}$ provides the tensile stress applied to the inner surface of the specimen right below the point at which load being applied at the moment of failure, and can be calculated by measuring the applied failure load $P_{\max}$:

$$\sigma_{\max} = \frac{P_{max}}{\pi B R_0} \tag{4-14}$$

where B is the ring thickness, while R and R_0 are the inner and outer radii of the ring, respectively Fig. 4.9.a). At least three different specimens for any geometry are tested and the average of calculated $\sigma_{\max}$ values that always showing good repeatability for each rock type/geometry is used for further analyses (Table 4.2).

For determining apparent tensile strength of rings following CFFM, the apparent stress intensity factor of the ring along y axis is integrated over an unknown ℓ_{pz} to satisfy the energy criterion according to Eq. (6). Fig. 4.9.b is schematically showing this procedure. According to CZM, at the moment of failure, the material or intrinsic fracture toughness K_{Ii} calculated as a function of the cohesive stress σ_c over the cohesive length ℓ_c, is equal to the average of the stress intensity factor $K_I(c)$ corresponding to $\sigma_{\max}$ over ℓ_{pz} or apparent fracture toughness $\overline{K_{Ic}}$, i.e. $K_{Ii} = \overline{K_{Ic}}$. D – B formula Eq. (4-4) is a simplified form of CZM considering material toughness as the resistant of a material against propagation of a crack by assuming a constant cohesive stress σ_c over the cohesive length ℓ_c ahead of a through-thickness crack in an infinite

body. For more details and proof of the D – B formula refer to Aligholi et al. (2022). Thus, D – B formula is considering a crack geometry in an infinite body, and ignores other factors like shape of the specimen, loading condition or environmental condition that can change the stress intensity factor. This is why ℓ_c is considered as the ℓ_{pz} of a crack with a function f = 1 controlling the stress intensity factor, and Eq. (4-7) is suggested to generalize D – B formula by taking into account the function *f*.

The apparent stress intensity factor $K_I(c)$ corresponding to σ_{max} of the ring specimens can be calculated as a function of c ranging from 0 to ℓ_{pz} as follows:

$$K_I(c) = \sigma_{max} F_{corr} \sqrt{\pi c} F(s) \tag{4-15}$$

where $F(s)$ is a shape function of s:

$$s = \frac{a}{a + R} \tag{4-16}$$

that for symmetric crack propagation as verified by high speed photography for our ring tests,[36] can be written as follows (Tada et al. 1985):

$$F(s) = (1 - \kappa)F_0(s) + \kappa F_1(s) \tag{4-17}$$

in which $\kappa = -3$,

$$F_0(s) = 0.5(3 - s)[1 + 1.243(1 - s)^3], \tag{4-18}$$

and

$$F_1(s) = 1 + (1 - s)[0.5 + 0.743(1 - s)^2]. \tag{4-19}$$

Putting these formulations in energy criterion lead to the following:

$$\frac{1}{\ell_{pz}} \int_0^{\ell_{pz}} k_I^2(c)dc = \frac{\pi(\sigma_{max} F_{corr})^2}{\ell_{pz}} \int_0^{\ell_{pz}} F^2(s)cdc = k_{Ii}^2 \tag{4-20}$$

Then, by integration:

$$\frac{\pi(\sigma_{\max}F_{\text{corr}})^2}{\ell_{\text{pz}}}\left(0.5c^2+cR+\frac{0.883R^9}{(c+R)^7}+\frac{1.243R^8}{(c+R)^6}-\frac{1.223R^7}{(c+R)^5}-\frac{1.26R^6}{(c+R)^4}+\frac{1.743R^5}{(c+R)^3}-\frac{1.114R^4}{(c+R)^2}-\frac{5.236R^3}{c+R}-0.75R^2ln[c+R]\right)\Big|_0^{\ell_{\text{pz}}}=k_{\text{Ii}}^2 \tag{4-21}$$

Finally, by defining the integral interval from 0 to ℓ_{pz}:

$$\begin{aligned}\frac{\pi(\sigma_{\max}F_{\text{corr}})^2}{\ell_{\text{pz}}}\Bigg(&4.964R^2+0.75R^2ln\,[R]\\&+\frac{1}{(R+\ell_c)^7}\left(-4.964R^9-33.998R^8\ell_{\text{pz}}-76.728R^7{\ell_{\text{pz}}}^2\right.\\&-85.653R^6{\ell_{\text{pz}}}^3-36.869R^5{\ell_{\text{pz}}}^4+19.97R^4{\ell_{\text{pz}}}^5\\&+33.264R^3{\ell_{\text{pz}}}^6+17.5R^2{\ell_{\text{pz}}}^7+4.5R{\ell_{\text{pz}}}^8+0.5{\ell_{\text{pz}}}^9\\&+R^2\left(-0.75R^7-5.25R^6\ell_{\text{pz}}-15.75R^5{\ell_{\text{pz}}}^2-26.25R^4{\ell_{\text{pz}}}^3\right.\\&-26.25R^3{\ell_{\text{pz}}}^4-15.75R^2{\ell_{\text{pz}}}^5-5.25R{\ell_{\text{pz}}}^6\\&\left.\left.-0.75{\ell_{\text{pz}}}^7\right)ln[R+\ell_{\text{pz}}]\right)\Bigg)=k_{\text{Ii}}^2\end{aligned} \tag{4-22}$$

ℓ_{pz} can be determined.

Next, the determined ℓ_{pz} is inserted into the stress criterion, and $\sigma_x(y)$ is replaced by the stress distribution given in Eq. (4-12):

$$\sigma_{\text{tc}}=\frac{1}{\ell_{\text{pz}}}\int_R^{R+\ell_{\text{pz}}}\sigma_x(y)dy=\frac{\sigma_{\max}F_{\text{corr}}}{2\ell_{\text{pz}}}\int_R^{R+\ell_{\text{pz}}}\left(2-\frac{2R^2}{y^2}+\frac{12R^4}{y^4}\right)dy \tag{4-23}$$

Then, by integration:

$$\sigma_{\text{tc}}=\frac{\sigma_{\max}F_{\text{corr}}}{2\ell_{\text{pz}}}\left(-\frac{4R^4}{y^3}+\frac{2R^2}{y}+2y\right)\Big|_R^{R+\ell_{\text{pz}}} \tag{4-24}$$

Finally, by defining the integral interval from R to $R + \ell_{pz}$:

$$\sigma_{tc} = \sigma_{max} F_{corr} \frac{\left(-2R^4 + R^2\left(R + \ell_{pz}\right)^2 + \left(R + \ell_{pz}\right)^4\right)}{\ell_{pz}\left(R + \ell_{pz}\right)^3} \tag{4-25}$$

the apparent tensile strength σ_{tc} of rings can be determined.

Chapter 5: Order of intermittent rock fractured surfaces

According to chaos theory, some underlying patterns can disclose order of disordered systems. In this chapter, we present intermittency of rough rock fractured surfaces is such orderable disorder at intermediate length scales. However, this kind of disorder is more complicated than simple fractal or even multiscaling behaviours. We are dealing with some multifractal spectra that systematically change as a function of the analysed domain. Accordingly, some parameters are introduced that can perfectly take into account such systematic behaviour and fully quantify intermittency of the studied surfaces.

After failure of a single scaling exponent like Hurst exponent *H* (Hurst 1951) or fractal dimension *D* (Mandelbrot 1983) to statistically model multiscale properties of natural phenomena, multifractal formalisms have been developed (Benzi et al. 1984; Halsey et al. 1986; Meneveau and Sreenivasan 1987; Muzy et al. 1993; Frisch 1995) to tackle this issue. What is the origin of multifractal phenomena, and how we can predict their scale-dependent exponents as a non-linear spectrum? These fundamental questions have been addressed in a variety of different fields and led to emergence of new formalisms (Vandewalle and Ausloos 1998; Ivanov et al. 1999; Kantelhardt et al. 2002; Jaffard 2004; Esser et al. 2017). Indeed, the cause of multifractality is scale-dependency of disorder. Rock materials, for instance, are composed of different constituents including minerals, cements and voids. Their minerals are formed from crystals with different crystalline systems. Therefore, there are different degrees of effective anisotropy and heterogeneity in rock materials at different length scales.

If we consider constant boundary conditions, this kind of disorder is the first and foremost cause of roughening of fractured surfaces and the root of multi-affine properties of their Fracture Process Zone (FPZ), as it is reported from experimental studies (Bouchbinder et al. 2006; Bouchaud et al. 2008; Vernede et al. 2015). At small enough length scales or separations $\delta r < \xi$, there is a correlation between height variations $\Delta h(\delta r)$ of fractured surfaces because of local similarities inside different constituents, which is scale-dependence itself. In crystalline igneous rocks like granite, for example, at meso-scale (few hundred microns to a few millimetres) there are different rock-forming minerals with same local properties, but at micro-scale (few hundred nanometres to few hundred microns) there are different crystals with

different properties making a single mineral. These apparently uniform crystals at micro-scale are no longer uniform at nano-scale due to crystal defects. The shorter the separation, the higher the correlation in a particular resolution (Ogilvy and Foster 1989). Because of this spatial correlation, central limit theorem fails, and we observe non-Gaussian distribution of height variations with fat tails (Ponson 2016; Granero-Belinchon et al. 2018). However, for separations larger than a cut-off length $\delta r > \xi$, there is no correlation and multiscaling spectrum of the height variations shows mono-affinity.

Such kind of cut-off lengths are very important in studying the phase transition of natural phenomena (Sornette 2004). From statistical physics point of view, fracture is a mixed-order phase transition (Alava et al. 2006; Shekhawat et al. 2013), and ξ is a cross over length scale indicating a transformation from continuous damage percolation at $\delta r \ll \xi$ to a first order phase transition at $\delta r \gg \xi$ where material can be considered as linear elastic (Bonamy et al. 2006; Morel et al. 2008; Gjerden et al. 2013). Therefore, from mechanical point of view, ξ is reminiscent of effective length of fracture process zone of a moving crack or the cohesive length ℓ_c (Barenblatt 1962; Vernede et al. 2015). More details regarding mechanics of fracture, the mixed-order phase transition and proof of $\xi \equiv \ell_c$ can be found in Chapter 4.

This phase transition argument can be used to exactly determine the cut-off length ξ. Indeed, ξ is the critical length scale at which a transition from multi- to mono-affinity takes place. Variogram analysis by applying height-height correlation function (Barabasi et al. 1992; Ponson et al. 2006b) or structure function (Davis et al. 1994) together with an elaborate domain analysis for different pairs of δr_{min} and δr_{max} are employed to successfully quantify ξ as the minimum of a mono-fractal domain with no intermittency as explained in Chapter 4. In the course of this task, a systematic domain dependent multiscaling behaviour is observed that we would like to discuss about it in this paper, which can throw spotlight on behaviour of disordered systems at intermediate length scales.

For this work, four different rock types including a sandstone, a marble, a fine-grained (FG) granite and a coarse-grained (CG) granite have been studied. The topography of fractured surfaces, illustrated in Fig. 5.1, have been reconstructed from 3D X-ray computed tomography data with a spatial resolution *d* of about 16.5 μm acquired at the Imaging and Medical beamline at the Australian Synchrotron. This method is superior to contact methods affected by the tip geometry of probes (Mazeran et al. 2005; Lechenault et al. 2010).

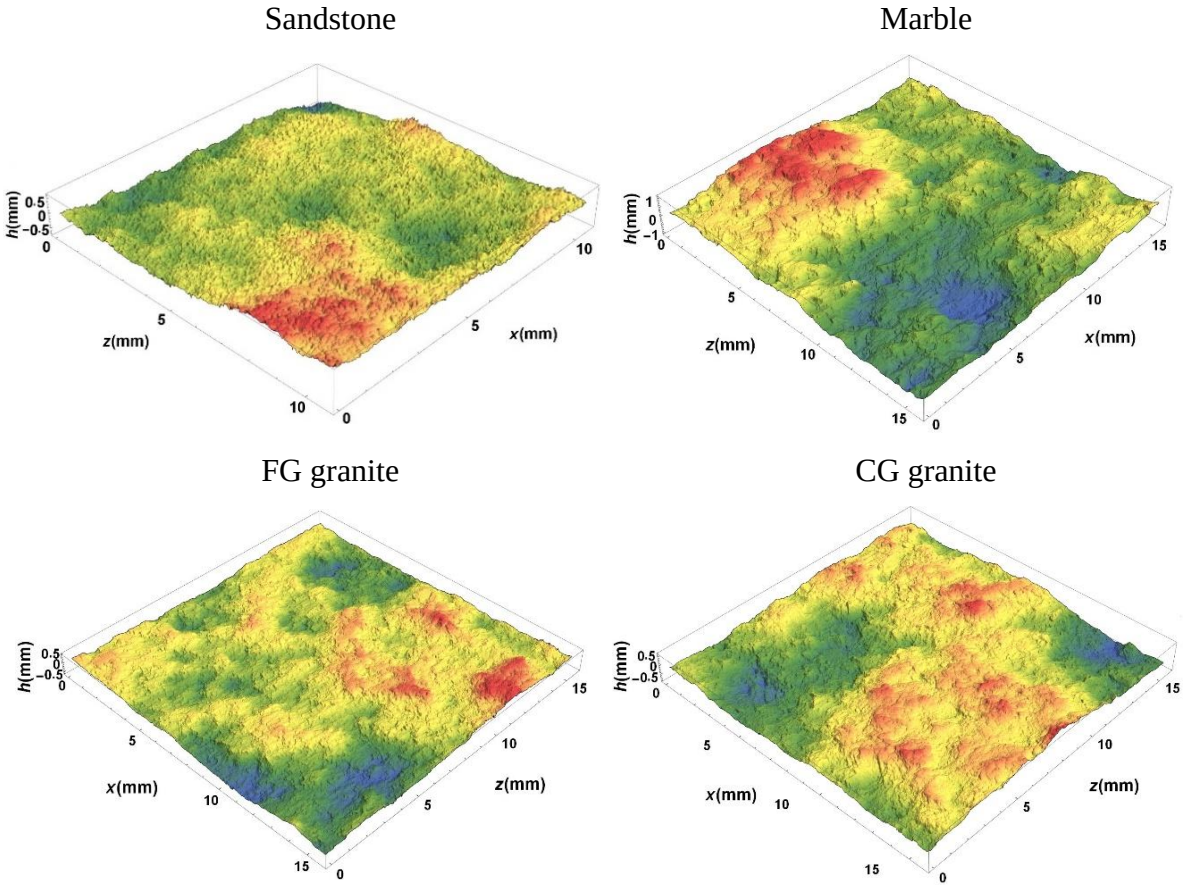

Fig. 5.1. Topographic images of fracture surfaces of sandstone, marble, fine-grained and coarse-grained granites. Square fractured surfaces are represented here for the sake of clarity. The x-axis and z-axis correspond to the crack propagation direction and the crack front direction, respectively.

Following Santucci et al. (2007) qth root of the qth moment of statistical distribution of the height fluctuations known as qth-order structure functions $S_q(\delta r)$ is utilized to demonstrate scale-dependency of roughness of quasi-brittle fractured surfaces, and their transition from mono-affine to multi-affine surfaces at small enough separations:

$$S_q(\delta r) = \langle |\Delta h(\delta r)|^q \rangle^{1/q} = \langle |h(\mathbf{X} + \delta r) - h(\mathbf{X})|^q \rangle_{\mathbf{X}}^{1/q} \propto \delta r^{\zeta_q * 1/q} \quad (5\text{-}1)$$

where angular brackets denote the ensemble average. The superiority of using $S_q(\delta r)$ to calculate generalized Hurst exponent $H(q) = \zeta_q / q$ of turbulent phenomena is discussed by Gilmore et al. (2002), and the advantages of using this method for estimating multiscaling

spectrum is emphasised by Di Matteo (2007). Following (Voss 1988), a relationship between generalized Hurst exponent and fractal dimension D_q can be written as $D_q + H(q) = q + 1$ (at least for positive integer moments). Studied rough surfaces exhibit two distinct scaling regimes: they are almost mono-affine fractals at $\delta r > \xi$, while they are multi-affine fractals at $\delta r < \xi$. Mono-affine fractal regimes can be characterized by $D_q = D_0 + 1$, $H(q) = H$, and $D_0 + H = q$ that are both scale and moment invariance (stationary increment property). Intermittent multi-affine fractal regimes, however, cannot be characterised by a single scale invariance exponent H (the original Hurst exponent) along all separations δr and show different local ζ_q exponents (Schmittbuhl et al. 1995). The average of directional multiscaling spectra of these multi-affine fractal regimes is statistically considered as multifractals for further analyses.

The high precision roughness quantification of the studied fractured surfaces reveals perfect power laws for intermittency of multiscaling spectra of such surfaces. These power laws further verified analytically as they predict a range of 0 to 1 for correlation function of rock roughness.

According to this finding, the intermittency of the studied multifractal spectra of rock FPZ can be quantified by a single parameter, i.e. the exponent of the power law λ. However, as it is discussed such intermittency is depending on the analysed domain. Similar size dependent power laws of intermittency of roughness of burning fronts on papers is reported, and it is argued that statistical distribution of the height differences can be modelled using stable Levy distribution (Balankin and Matamoros 2005). To analyse the effect of range of analysed length scale on the intermittency, the intermittent exponent λ is computed for length scales between a fixed minimum of 50 microns and up to the length of FPZ of the studied, which is 400, 1100, 500 and 900 microns for sandstone, marble, FG granite and CG granite, respectively (Fig. 5.2).

From Fig. 5.2, it can be seen that all spectra are converging in a critical moment order q_c. The reason behind this convergence is that at the q_c, the corresponding structure function is showing perfect power laws for all separations δr (Fig. 5.3). Following this observation, we have tried to find the q_c by fitting power laws for different moment order q. Then, the one with the minimum error is corresponding to the convergence point and will give the q_c. Therefore, the fitted curve with the maximum R-square is corresponding to q_c. Fig. 5.3 is showing the R-square values for different moments and rock types.

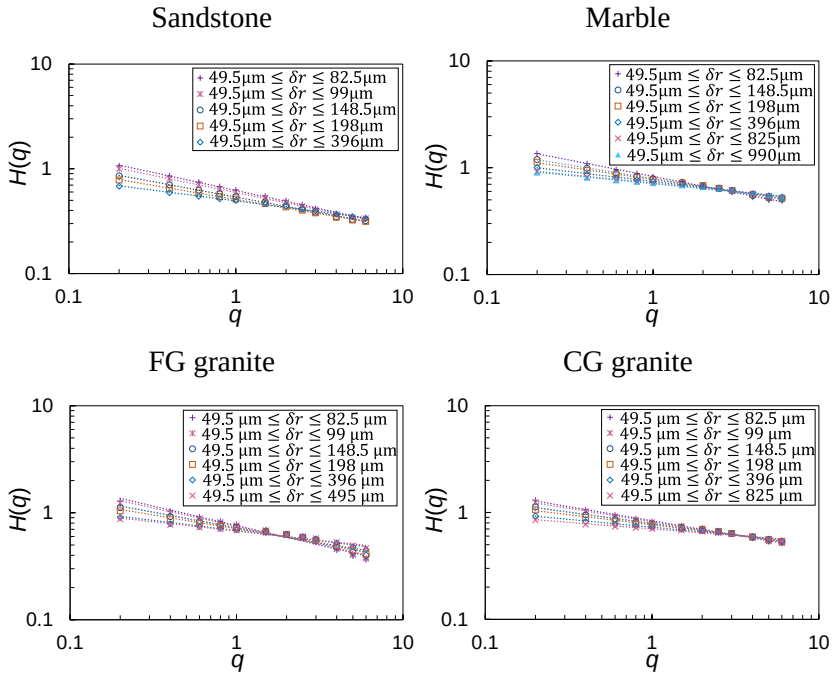

Fig. 5.2. Intermittency of the studied fracture surfaces at different domains.

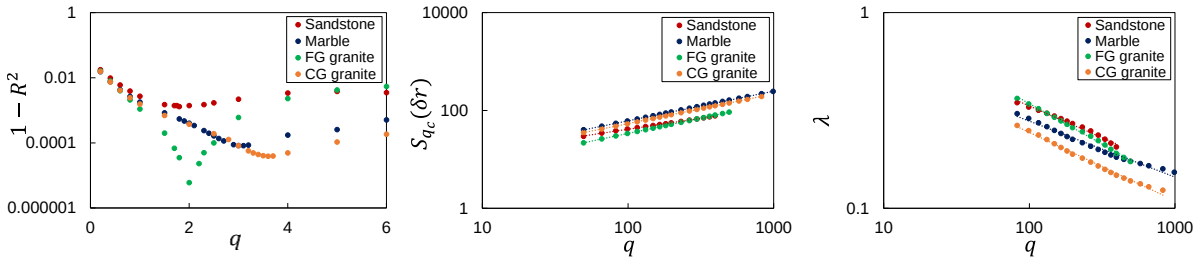

(a) (b) (c)

Fig. 5.3. Analysis of the power law fitting errors associate with moment order q (a); the power law fitting of the critical moment order q_c with the minimum error (b); and (c) intermittent exponent λ as a function of the maximum of the fitting domain δr_{max}.

By this analysis, one point on multifractal spectra is found. Now, it is required to predict how the intermittency is changing in other moment order q. Thus, the intermittent exponent λ as a function of the maximum of the analysed domain $\delta r_{\max}$ (up to the FPZ) is plotted to see if any relationship can be found. Surprisingly, the changes of λ as a function of $\delta r_{\max}$ with a fixed $\delta r_{\min}$ of 50 microns can be formulated by perfect power laws as well (Fig. 5.3). It seems the exponent of these power laws ψ are universal for a fixed minimum. It is notable that other fixed

minima are also showing similar trends but with different ψ values. Therefore, the intermittency of FPZ roughness of the rock materials can be fully formulated by two parameters: the critical moment order q_c and the exponent ψ.

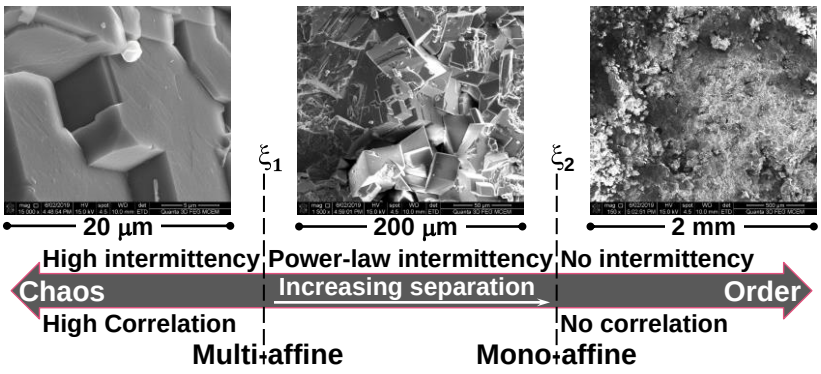

Fig. 5.4. The phase diagram is showing fractured surface of a crystalline rock at different magnifications. It can be clearly seen at high length sclaes smaller than the first cut-off length ξ_1, there is a high correlation (same crystal) and high intermittency (huge height differences between different crystals). Therefore, lognormal distribution of this sparse considerable height differences might be useful for statistical presentation of roughness at this length scales (Nanometre). Stable levy distribution found to be a good means to characterise roughness at intermediate length scales, from ξ_1 to ξ_2, where there is orderable power law intermittency. At length scales larger than the second cut-off length of length of FPZ there is neither correlation nor intermittency.

According to the discussed results, a 1D-phase diagram as a function of length scale is presented in Fig. 5.4 that divides the statistics of roughness in 3 different regimes: complete disorder, orderable disorder and order. It is notable that complete disorder regime cannot be analysed for the studied rock materials because of resolution of the data and can be topic of a future research. The introduced disorder analysis method can model intermittency of data sets at intermediate length scales that would increase the prediction power of current statistical models. For instance, more accurate predictive models can be developed for time series. Ultimately, this can lead to, for example, predict seismic or flood events in short time with higher accuracy.

Analytical verification of the observed power law intermittency

It is observed that heart rate time series display different multiscaling exponents because of long-range correlations (Peng et al. 1995). BDM model is proposed to provide a link between multifractality and long-range correlation of financial time series (Muzy et al. 2000; Bacry et al. 2001):

$$H(q) = H - (q-1)\frac{\lambda_c}{2} \tag{5-2}$$

in which $H \equiv \zeta_1$, and λ_c is slope of correlation function of a multifractal process. It means, $H(q) = H$ if there is no correlation, i.e., $\lambda_c = 0$, which is the case for monofractals. Otherwise, $H(q)$ decrease linearly with q for $\lambda_c > 0$. BDM is a linear model and could not provide a good estimation of non-linear multifractal spectra of the studied rock fractured surfaces. Based on experimental observations a power law is introduced that can exactly predict statistically isotropic multiscaling spectrum of rock FPZ:

$$H(q) = H\left(q^{-\lambda}\right) \tag{5-3}$$

where λ is intermittency (slope of multiscaling spectrum) of a multifractal process.

By applying a log-log transformation Eq. (5-3) can be read as $\log H(q) = -\lambda \log q + \log H$. From Fig. 5.5, it is indisputable that this log-log transformation is showing a perfect linear relationship that is unique to power functions. A comparison among experimental data, BDM model and the proposed model is made in Fig. 5.6, which is showing the success of the proposed model in predicting multiscaling spectra of the rock fractured surfaces at small enough length scales $\delta r < \xi$.

$\omega_\epsilon(\mathbf{X})$ operator has been used for calculating correlation function of height variations of fractured surfaces $\Delta h(\epsilon)$ at some length scales ϵ (Vernede et al. 2015):

$$\omega_\epsilon(\mathbf{X}) = \frac{1}{2}\log(\langle \Delta h(\epsilon)^2 \rangle_\Theta) - \Omega_\epsilon \tag{5-4}$$

where $\log(\Delta h)$ denotes the natural logarithm, whose base value is e. It measures the average height variations around each point, on a height field $h(\mathbf{X})$, with its neighbours over a circle of radius $\epsilon = d * p$ $(p = 1, 2, 3, 4, 5\ px)$. ϵ is product of spatial resolution and number of pixels used for calculating $\Delta h(\epsilon)$; Ω_ϵ is chosen such that the average of $\omega_\epsilon(\mathbf{X})$ over all $\mathbf{X}$ is zero. The pair length scale and direction $(\epsilon, n) = \{(16.5,8), (33,12), (49.5,16), (66,20), (82.5,28)\}$ is used to compute $\langle \Delta h(\epsilon)^2 \rangle_\Theta = \frac{1}{n} \sum_{k=0}^{n-1} \left[h(x_i, z_j) - h(x_i + \epsilon * \cos(2\pi k/n), z_j + \epsilon * \sin(2\pi k/n)) \right]^2$ where $\Theta \in [0, 2\pi)\ rad$. x_i and z_j are the coordinates of a point on $h(\mathbf{X})$ in crack propagation and crack front directions, respectively. Fig. 5.7 is showing the correlation functions $C_\epsilon(\delta r) = \langle \omega_\epsilon(\mathbf{X}) \omega_\epsilon(\mathbf{X} + \delta r) \rangle_\theta$ of ω_ϵ fields averaged over 4 directions $\theta \in [0, \pi) = \pi k/4\ rad\ (k = 0, 1, 2, 3)$. Indeed, $C_\epsilon(\delta r)$ indicates scale-dependency of material's disorder since ω_ϵ quantifies local height variations and removes global slopes caused by macroscopic and dynamic effects (Alava et al. 2006; Bonamy and Bouchaud 2011).

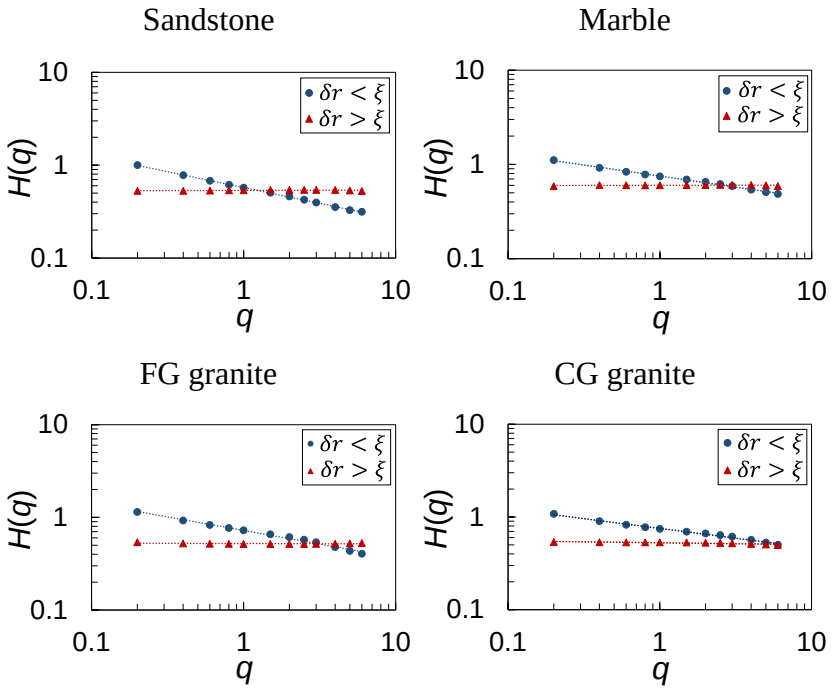

Fig. 5.5. Multiscaling spectra of the rock fractured surfaces. The spectra are computed both below (blue curve) and above (red curve) ξ. Both regimes are predicted with power laws. Intermittency of multifractal regimes ($\delta r < \xi$) are showing perfect power laws with $R^2 \approx 1$ and some exponents between 0.2 and 0.35. Monofractal regimes ($\delta r > \xi$), however, show insignificant intermittency whose exponents are less than 0.02. Hurst exponent values are ranging from 0.5 to 0.6 for monofractal regimes.

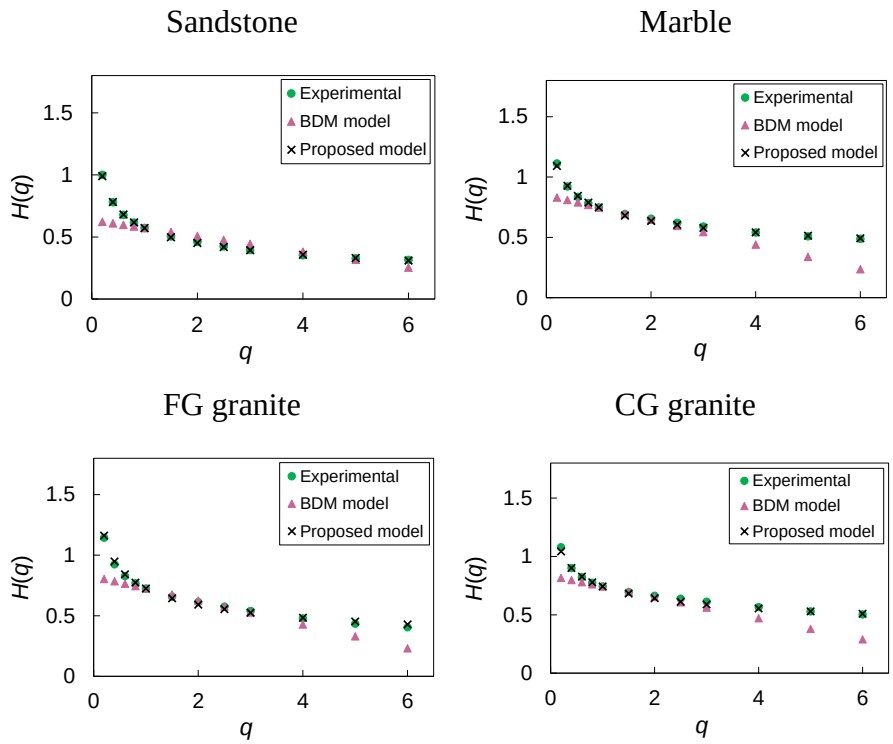

Fig. 5.6. Experimental and predicted multiscaling spectra of the rock fractured surfaces. Predicted spectra by the proposed model are very close to the experimental ones.

It is notable that in BDM model a logarithmic decay of correlation of height differences is considered, and λ_c is the slope of this decay $C_\epsilon(\delta r) = -\lambda_c \log(\delta r/\xi) + \varepsilon$ (under the assumption that $\varepsilon = 0$). It is notable that λ_c is dimensionless since slopes of auto-correlation (dimensionless) and auto-covariance (dimensional) functions are the same.

The observed intermittent power law can be proved analytically as well. From one hand, Eq. 2 can be rewritten as follows:

$$\zeta_q/H = q^{1-\lambda} \tag{5-5}$$

Now, by applying a log-log transformation Eq. (5-5) can be read as $\lambda = 1 - \frac{\log(\zeta_q/H)}{\log(q)}$. On the other hand, as it can be seen from Fig. 5.7, decay of the correlation of ω-field can be fitted by some power laws and slope of this decay or exponent of the power laws can be written as $\lambda_c = -\frac{\log(C_\epsilon(\delta r)) - \varepsilon}{\log(\delta r/\xi)}$. Monofractals are neither correlated nor intermittent, and both λ and λ_c are almost zero for monofractals. Therefore, there should be a relationship between these two exponents for multifractals.

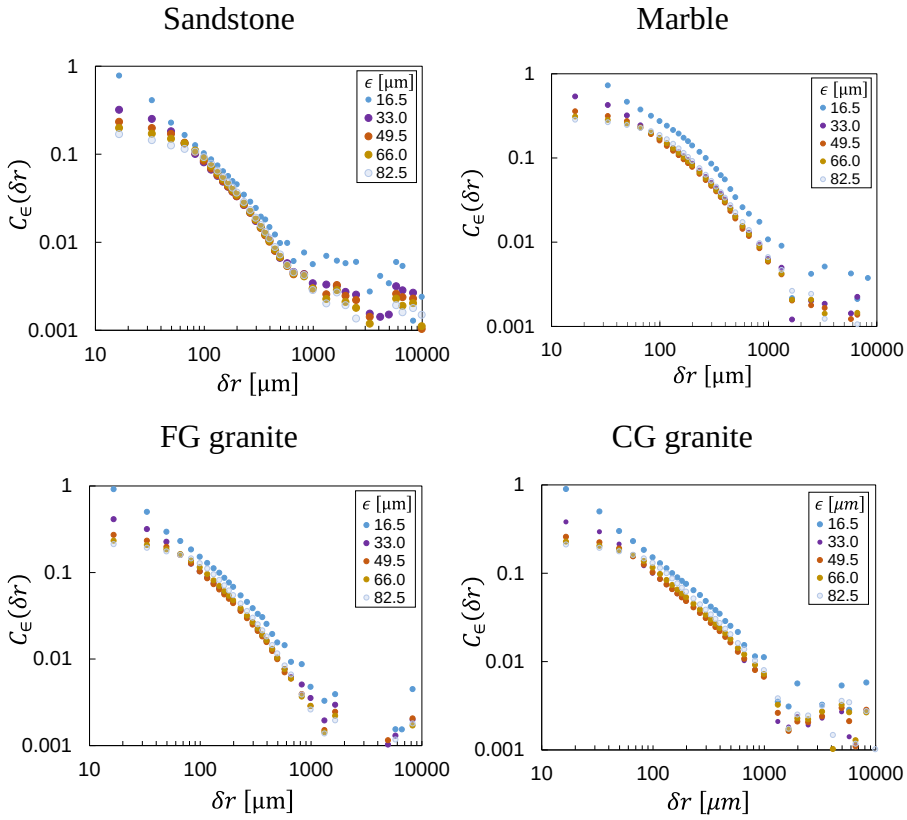

FIG. 5.7. Spatial correlations of ω_ϵ for different rock types. The correlations are represented for ω_ϵ computed at different scales ϵ.

If $\lambda = c * \lambda_c$, then $1 - \frac{\log(\zeta_q/H)}{\log(q)} = -c * \frac{C_\epsilon^*(\delta r)-\varepsilon}{\log(\delta r/\xi)}$, this equation can be rearranged as follows:

$$\frac{\log(\zeta_q/H)}{\log(q)} - \frac{c*C_\epsilon^*(\delta r)}{\log(\delta r/\xi)} = 1 - \frac{c*\varepsilon}{\log(\delta r/\xi)} \tag{5-6}$$

where $C_\epsilon^*(\delta r)$ is auto-correlation function that is normalized by variance of ω_ϵ field. In the monoaffine regime, $\zeta_q/H = q$, there is no correlation $C_\epsilon^*(\delta r) \approx 0$, and Eq. (5-6) read as $1 - 0 = 1$. In the transition zone the correlation from ε at $\delta r = \xi$ would tend to zero as δr tends to infinity. In the multiaffine regime, $\zeta_q/H = q^{1-\lambda}$, there is a correlation $0 < C_\epsilon^*(\delta r) - \varepsilon < 1$, and Eq. (5-6) read as $1 - \lambda + c * \lambda_c = 1$. The question remains open here is that what is the relationship between the slope of correlation function and the intermittency? To answer this question finding a meaningful link between correlation function and structure function is the

first step. Two kind of these links that can trigger some interesting future researches are provided as follows.

The power spectrum, on the one hand, is the Fourier transform of the auto-covariance function of a wide-sense stationary random process (Wiener–Khinchin theorem). Height variations in monofractal regime can be considered as a fractional Brownian motion with stationary increments and their spectral density $S(f)$ scales with the frequency f as a power law: $S(f) \propto f^{-\beta}$ where $\beta = 2H(2) + 1$ (Flandrin 1989). On the other hand, the spectral density is proportional to second-moment of distribution of height variations $\langle|\Delta h(\delta r)|^2\rangle \propto \delta r^{\alpha}$ where $\alpha = 2H(2) = \beta - 1$ (Di Matteo 2007). For monofractals a relationship between $H(q) = H$ and β can be defined as $D_q = q + 1 - H = q + \frac{3-\beta}{2}$ (Voss 1988). However, when it comes to multifractals with nonstationary increments this link between correlation function and structure function needs some modifications. In other words, like generalized fractal dimension and Hurst exponent, a generalization for spectral analysis is required. Wigner-Ville spectral analysis is introduced as the unique generalized spectrum for spectral analysis of non-stationary processes (Martin and Flandrin 1985). There is also a statistical relationship between structure function and correlation function: $\langle|\Delta h(\delta r)|^2\rangle = 2\big(\sigma^2 - C_{\epsilon}(\delta r)\big)$ where $\sigma^2 = \langle h(\mathbf{X})^2\rangle \approx \langle h(\mathbf{X} + \delta r)^2\rangle$ is variance of a height map. This equation is working very well for second moment, but the question is how we can expand it for other moments. Moreover, this relationship ignores the effect of local averaging on the height map (to compute ω_{ϵ} field). Along with this theoretical issue, it seems the coefficient c plays a very important role in understanding multifractal phenomena and can be used to estimate crossover length of multiphase phenomena. Further measurements in different fields is required to have a better comprehension about the proposed model in this study.

Chapter 6: Conclusions and future work

In this chapter the most important contributions of this research is summarised. Moreover, the ongoing research of this PhD is introduced and some directions for future research is presented.

6.1. Conclusions

The most important contributions of this research is to effectively determine length of fracture process zone of rock materials and investigating the effect of intrinsic (microstructure) and extrinsic features (loading rate) on ℓ_{pz}. The presented framework could be combined with other techniques to understand multiscale materials behaviour under different loading and environmental conditions. Moreover, it can be used for analysing the effect of geometry on critical tensile strength σ_{tc} that a sample or structure can bear. Indeed, the cohesive stress of material together with geometry of the sample or structure, and experimental or environmental condition set the ℓ_{pz} and σ_{tc}.

Determining multifractal behaviour of roughness of rock fractured surfaces and providing a link between statistical physics of fractured surfaces of such materials and their fracture mechanics by quantifying the cohesive length $\xi \equiv \ell_c$ is another important contribution of this research. ℓ_c is the basic parameter that was required to be quantified for further developments. It is used to verify the quantified ℓ_{pz} by means of mechanical models. The proposed multifractal model can be used for quantifying ℓ_{pz} of a moving crack or cohesive length ℓ_c, intrinsic tensile strength or cohesive stress σ_c and fracture toughness of materials by roughness analysis.

The link between rock physics and fracture mechanics can be used as a valuable tool to model and predict fracture propagation in any project dealing with fracture controlling, such as geothermal energy, hydrocarbon reservoirs, induced seismicity, waste disposal, mining, and tunnelling in geo-mechanics, as well as plethora of other fields in material science and mechanical engineering.

Following the results of this study, it turns out that plane disk specimens without stress concentrators cannot be used to measure tensile strength of rock materials, and tensile strength is underestimated if plane specimens are used. It is shown ring specimens can be used to successfully measure apparent tensile strength of rock materials. Moreover, brittle nature of rock materials is a major issue for fabricating a sharp notch in SCB specimens to successfully determine material fracture toughness. It is verified that notch mechanics and practical developments in similar materials can be used to rectify the notch root radius effect on determining fracture toughness of rock materials. However, if the notch root radius is smaller than the cohesive length, the ISRM suggested method (Kuruppu et al. 2014) is a reliable method for determining fracture toughness of rock materials.

Finally, the physics of fractured surfaces are investigated at length scales smaller than $\xi \equiv \ell_c$, and the order of intermittency of rough rock fractured surfaces is discovered at intermediate length scales. The introduced disorder analysis method can model intermittency of data sets at these length scales that would increase the prediction power of current statistical models. For instance, more accurate predictive models can be developed for time series analysis. Ultimately, this can lead to, for example, predict seismic or flood events in short time with higher accuracy.

6.2. Future work

It is discussed in Chapter 4 that after a threshold the fracture toughness K_{Ic} of rock materials increase with loading rate. As it goes from its name K_{Ic} or critical stress intensity factor is a measure of stress concentration that can be changed as a function of material geometry or loading rate and change the behaviour of material in K dominance region that ℓ_c is within it. As opposed to K_{Ic}, at quasi-statics loading rate the cohesive stress σ_c is material dependent and independent of loading rate. However, it is suggested that at dynamic loading rates the properties of material and accordingly σ_c will change (Zhao 2000). Therefore, in a future research it will be investigated by determining σ_c of fractured surfaces of the same rock types broken under dynamic loading rates using roughness analysis. Sixteen fractured surfaces including 4 surface for each of the four studied rock types broken under a wide range of quasi-static and dynamic loading rates will be analysed using the developed multifractal model for determining their ℓ_c and σ_c values for such purpose.

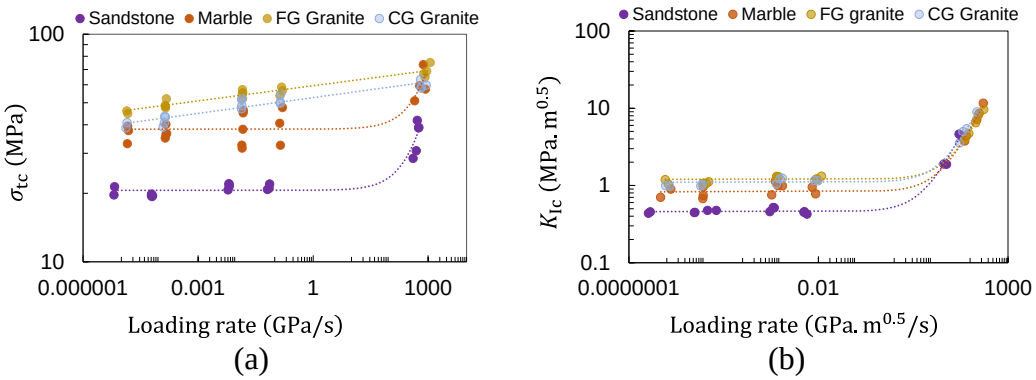

Fig. 6.1. Loading rate against apparent tensile strength (a); and mode I fracture toughness (b).

Moreover, the mechanical behaviour of the studied rock materials are determined under different loading rates (Fig. 6.1). The Dynamic Increase Factor (DIF) can be clearly seen from this figure for both apparent fracture toughness and tensile strength. However, this observation cannot give us any information about ℓ_c and σ_c.

It seems multiscale behaviour of materials is related to both intrinsic and extrinsic features. The nominal intrinsic features are always constant at different scales, but their response to mechanical loading under different extrinsic conditions is different. In other words, extrinsic features can activate different scales. Strain rate is one of the main external parameters that can change the mechanical response of rock materials with same nominal intrinsic features under same environmental conditions. There are good review papers regarding strain rate dependent behaviour of rock materials (Zhang and Zhao 2014; Xia and Yao 2015). Therefore, the relationship between multiscale physical properties of rock materials and strain rate will be investigated in the future research as well. Theoretically, under different strain rates the amount of energy flux to the crack front is different. Therefore, at higher strain rates crack front can depines the material at smaller scales (Zhang and Zhao 2013; Barras et al. 2017; Chopin et al. 2018).

According to outcomes of the first phase of this research, based on intrinsic features of different rock types, a transition from non-linear inelastic fracture mechanics to LEFM is expected to take place in a range of length scales between 10 micrometres to 20 millimetres (Fig. 6.2). Appendix B. is presenting some numerical examples regarding the multiscale

analysis of intrinsic features of materials and quantifying their heterogeneity and anisotropy. It is supposed that the critical length scale at which transition takes place is a function of extrinsic and environmental conditions.

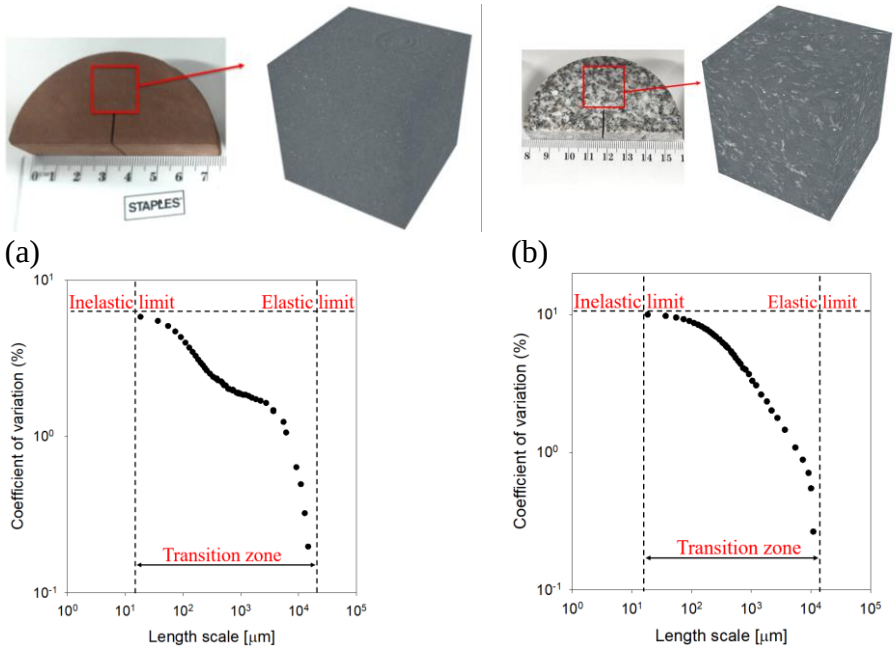

Fig. 6.2. Homogenization of selected parts from NSCB specimens of a sandstone (a, c); and a CG granite (b, d).

Appendices

Appendix A: *Photomicrographs of fractured surfaces of different rock types*

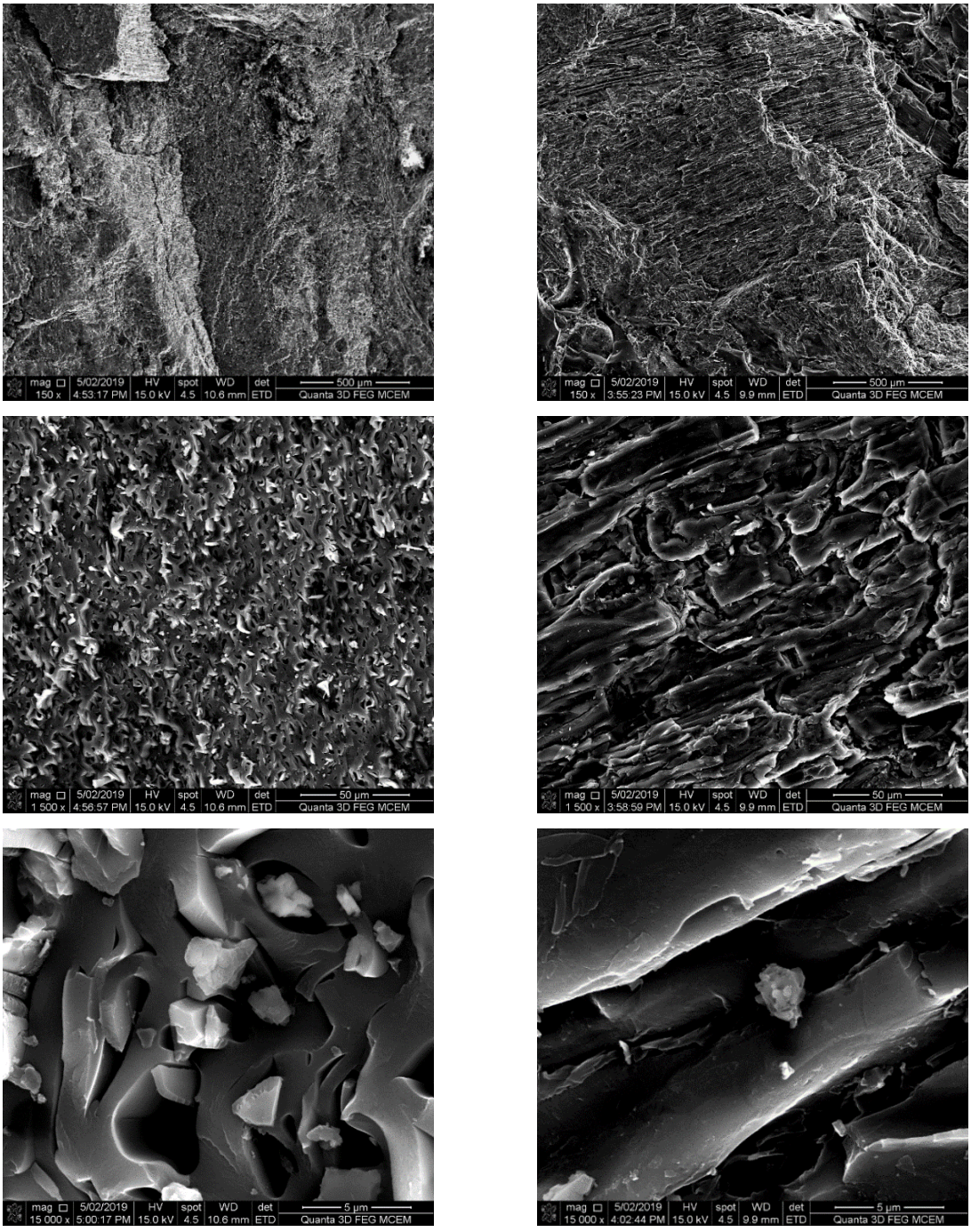

Fig. A.1. SEM photos of Coal. The left column is showing the microstructure of a coal fractured surface which is perpendicular to the direction of tabulated carbon structure at different

magnifications (all photos have the same centre); while the right column is showing the fractured surface of the same material which is parallel to the direction of tabulated carbon structure at different magnifications (all photos have the same centre).

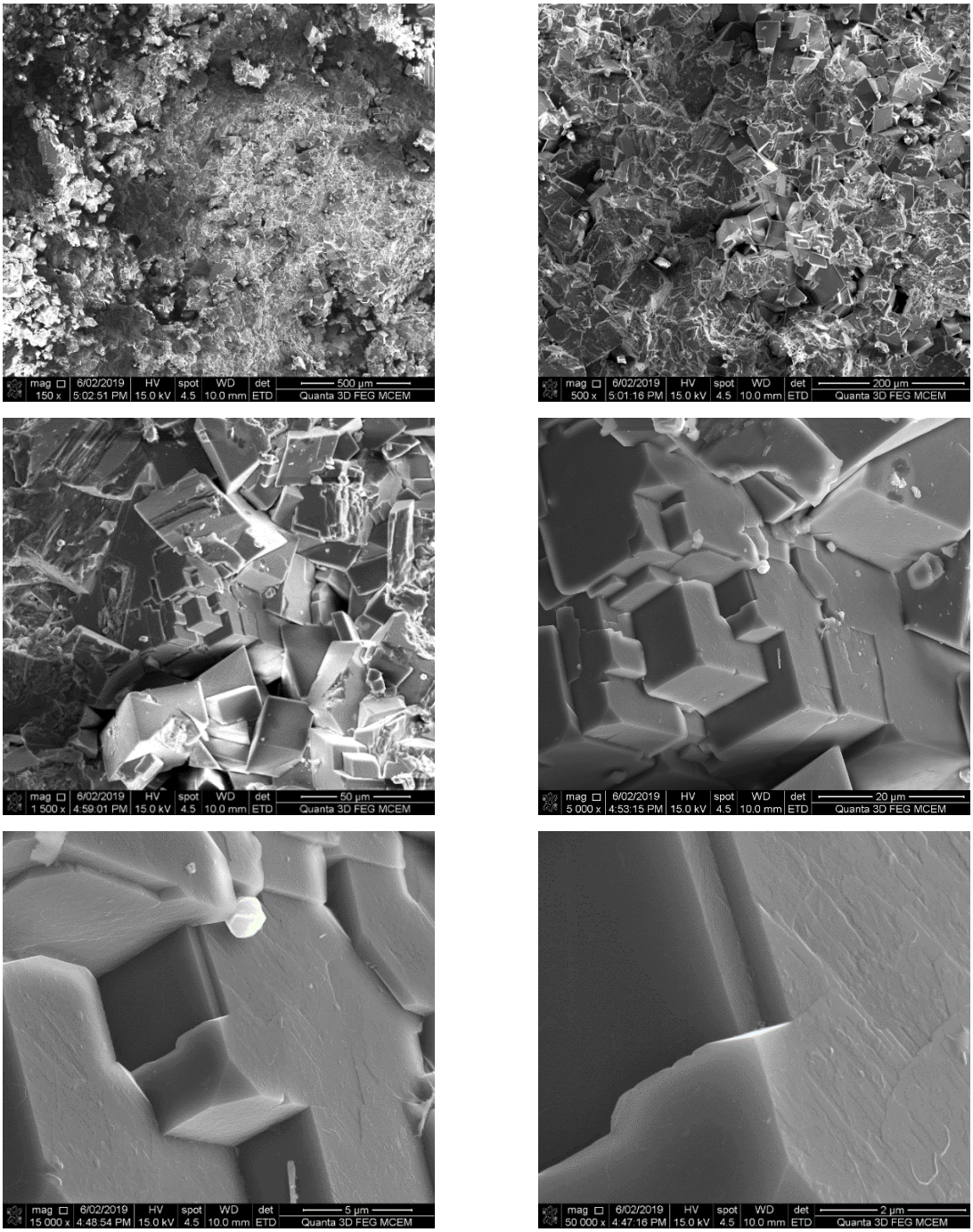

Fig. A.2. Multiscale properties of fractured surface of a crystalline limestone with quite large crystals at different magnifications (all photos have the same centre); the importance of crystalline structure of calcite crystals and their cleavage directions on roughness of this surface is obvious.

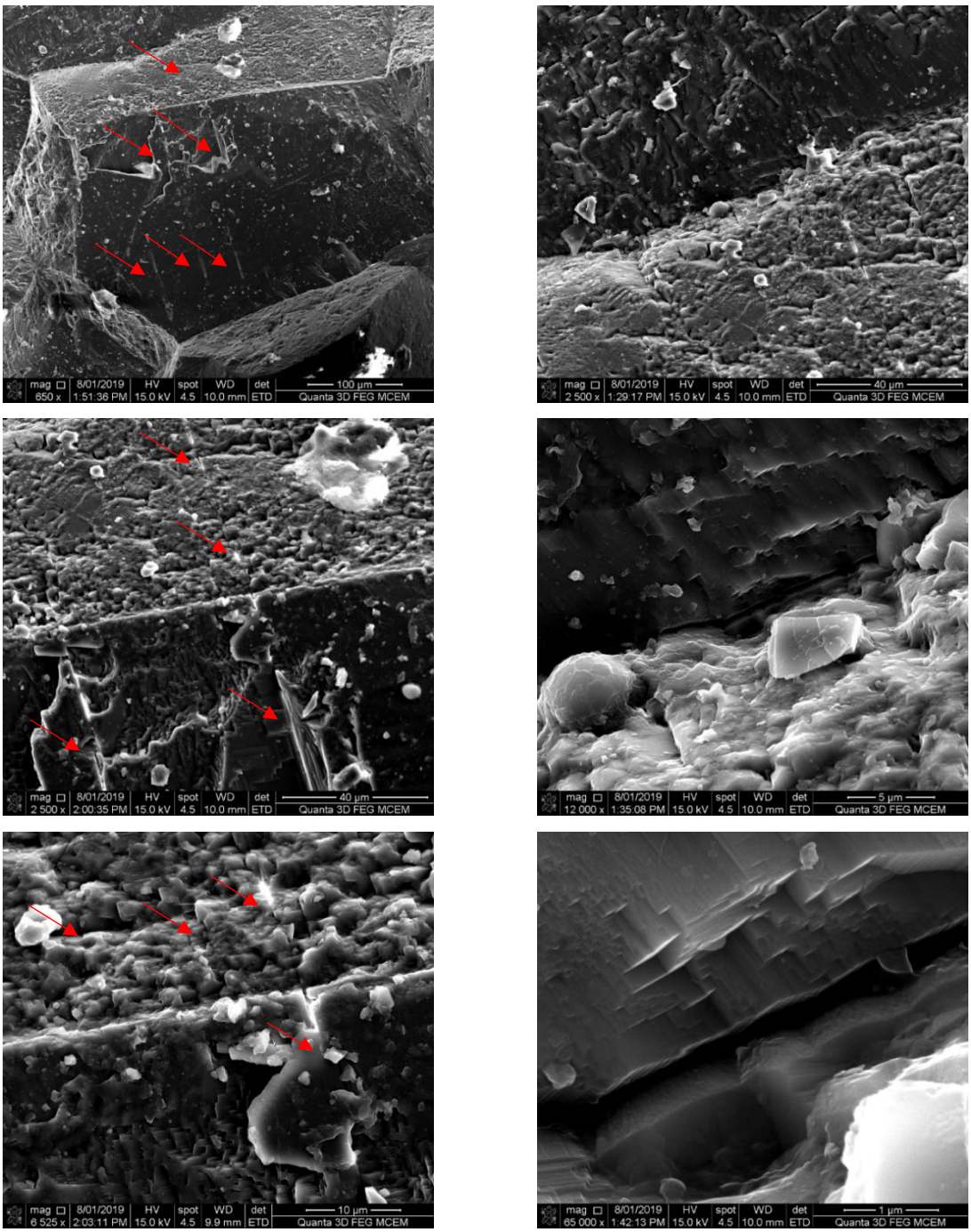

Fig. A.3. Multiscale properties of fractured surface of a crystalline marble. The left column is showing the parallel cleavage surfaces of a quite large calcite crystal at different magnifications (all photos have the same centre); and the right column is showing the common fracture patterns in marble which is being formed with such cleavages in three directions at right angles (90º) at different magnifications (all photos have the same centre).

Appendix B: *Quantifying heterogeneity and anisotropy of some simulated materials*

To understanding the multiscale behaviour of materials, first we need to know how their structure begin to change from one length scale to another. For better understanding of the problem, some 3D media have been simulated with different sizes, degrees of heterogeneity and anisotropy. The voxels of simulated materials have values between zero and one. In order to see how the structure of the simulated materials would change at different scales, we have used asymptotic homogenization method. In this procedure, different number of voxels have grouped together to show the structure of materials at different length scales. For instance, if the initial size of a sample were 100^3 voxels, it would be reduced to 50^3 voxels when we group every 2^3 voxels together. It is notable that values of new voxels (grouped voxels) are the mean values of the voxels before grouping. Fig. B.1 is showing the asymptotic homogenization of a simulated isotropic heterogeneous material with uniform distribution. It resembles scanning materials or media using X-ray CT or other tomographic techniques with different resolutions. Therefore, considering the structural complexity of a material when we start to use lower resolutions (higher length scales) to scan the same sample it begins to become more homogeneous (Figs. B.1 and Fig. B.2). From Fig. B.2, which shows probability density function (PDF) and cumulative distribution function (CDF) of the same sample in Fig. B.1 and at different length scales, it can be clearly seen that when the resolution is lower, the sample is nominally more homogeneous. In the following some examples will presented to simulate the heterogeneity and anisotropy of some artificial materials at different length scales.

Example 1: simulating an isotropic heterogeneous medium using uniform distribution at different sizes. This example shows the effect of sample size on characteristic length scale determination. Four different sample sizes have been selected from 4^3 to 100^3 voxels. Fig. B.3 can schematically show the importance of a representative sample. From this figure, it is obvious that considering the amount of heterogeneity of the materials and size of its constituents the representative size should be different to characterise it. Fig. B.4 shows the multiscale behaviour of this simulated material, but with different sample sizes. Based on this example, representative size should be fulfilled to obtain CL. This representative size might be different considering different engineering or scientific applications. However, obtaining a real representative size is difficult and might need large samples. This is why, most of the laboratory

tests should repeat multiple times on different samples from same material and the average value is being used to characterise the material.

As it can be seen from Fig. B.4, for the isotropic medium with uniform distribution after grouping more than about 20^3 voxels together the coefficient of variation became less than one percent. This scale is almost the CL of the system and it is homogenized if we assume the system will grow with same structure in every direction. From this example, it can be deduced for predicting multiscale behaviour of the simulated material the samples should at least be larger than the CL, otherwise there should be statistical errors. Fig. B.4 shows the CL of the simulated samples with the size of 40^3 voxels, which have smaller size than the nominal CL (almost 20^3 voxels) of the material, can be obtained by averaging characteristic length scales of different samples. Please note that Coefficient of Variations is a measure of material heterogeneity and is standard deviation of all voxels over their average.

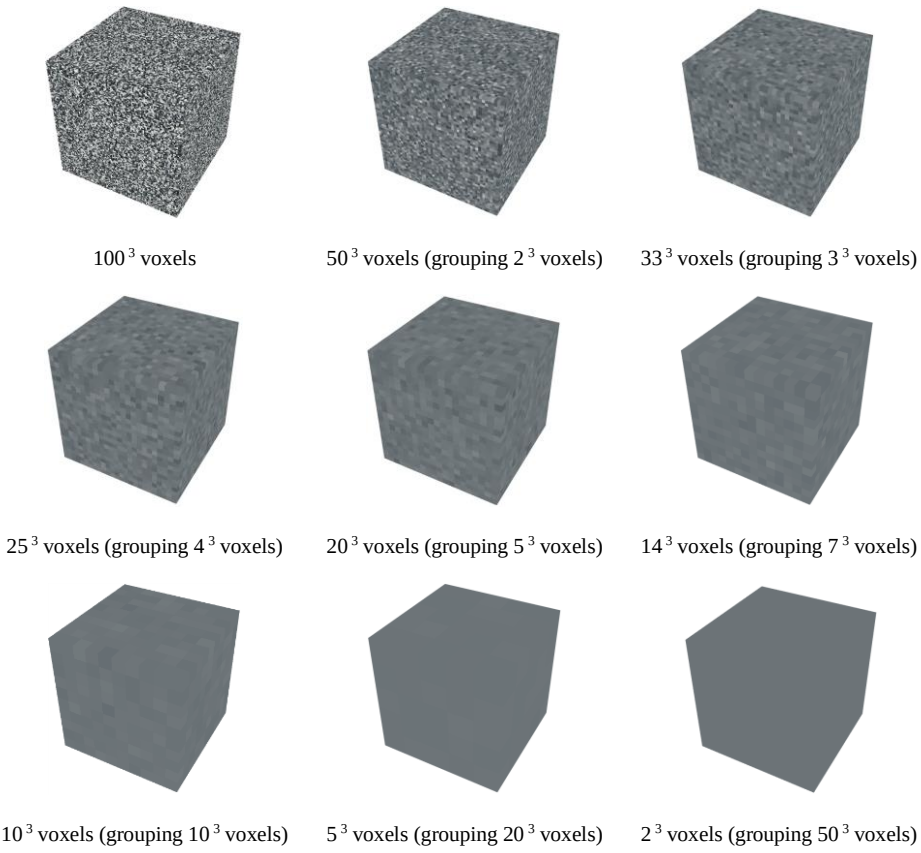

Fig. B.1. Asymptotic homogenization of a simulated medium with uniform distribution [values of voxels are between zero (black) and one (white)].

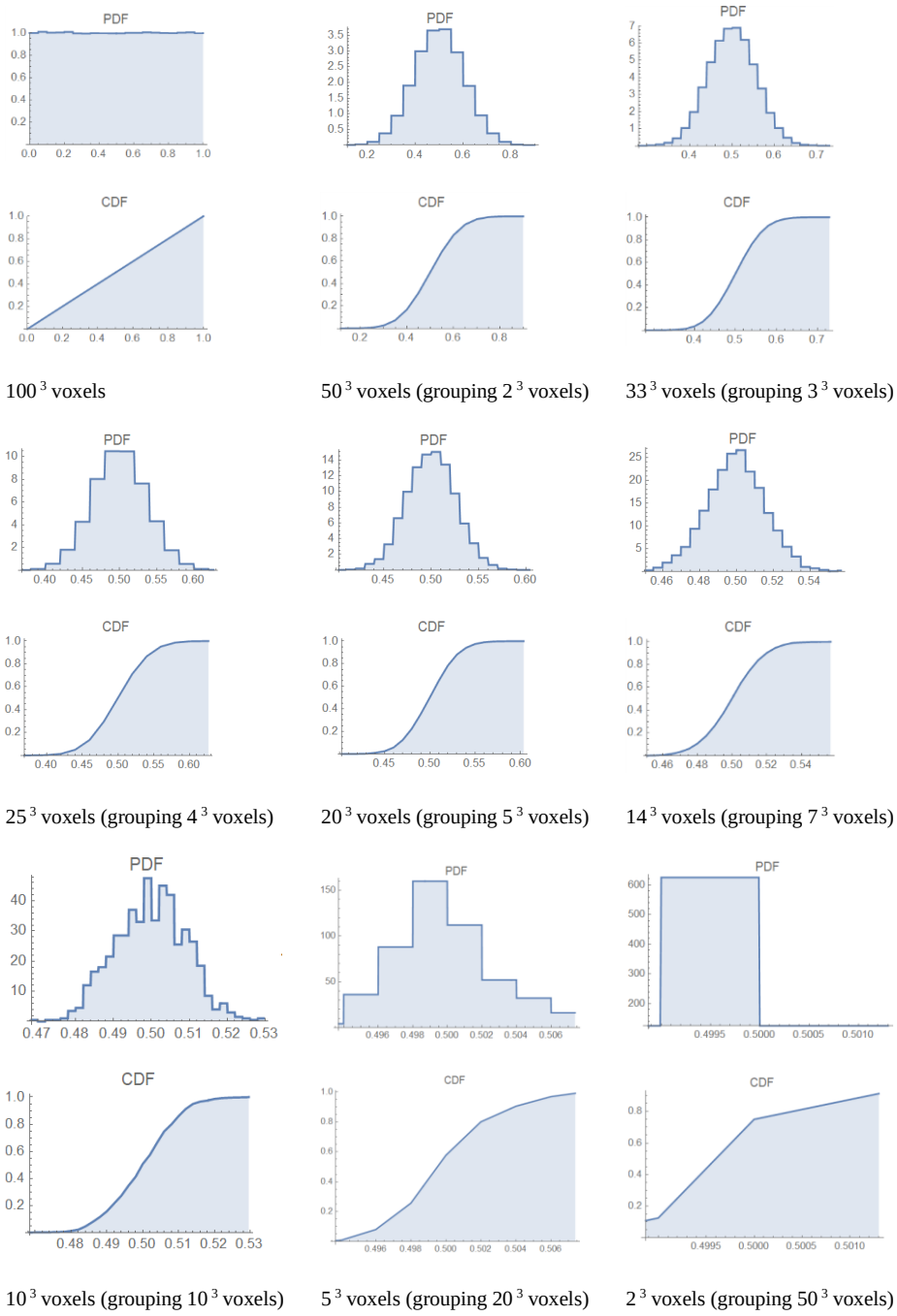

Fig. B.2. Probability density function (PDF) and cumulative distribution function (CDF) of the voxel values of a simulated material with uniform distribution at different length scales.

Example 2: simulating some isotropic heterogeneous medium using different random distributions. Normal and Weibull distributions have been used to simulate materials with different degrees of heterogeneity. Fig. B.5 is showing the homogenization of some simulated materials with different normal distributions. These examples can show the effect of heterogeneity on CL, the higher the standard deviation, the larger the CL. Same as normal

distribution the effect of different levels of heterogeneity introduced by Weibull distribution can be clearly seen on the CL (Fig. B.6). Based on this statistical work, the characteristic size in isotropic media depends on distribution and fabric of different constituents and phases as well as the size of them. Therefore, it seems the presented formulas for predicting multiscale behaviour of materials by knowing their CL, can be statistically proved for isotropic heterogeneous materials with same distribution throughout the body. For such kind of ideal materials, CL can be considered as RVE. However, natural materials cannot be considered neither isotropic nor continuously distributed with a same function across all length scales.

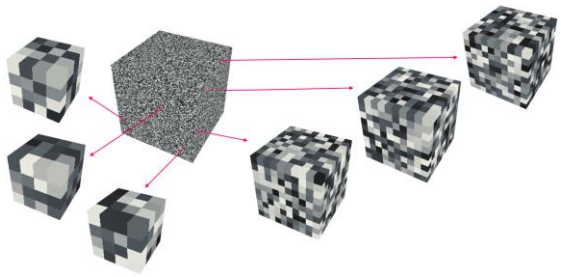

Fig. B.3. Different sample sizes from 4^3 to 100^3 voxels from a simulated heterogeneous medium with uniform distribution.

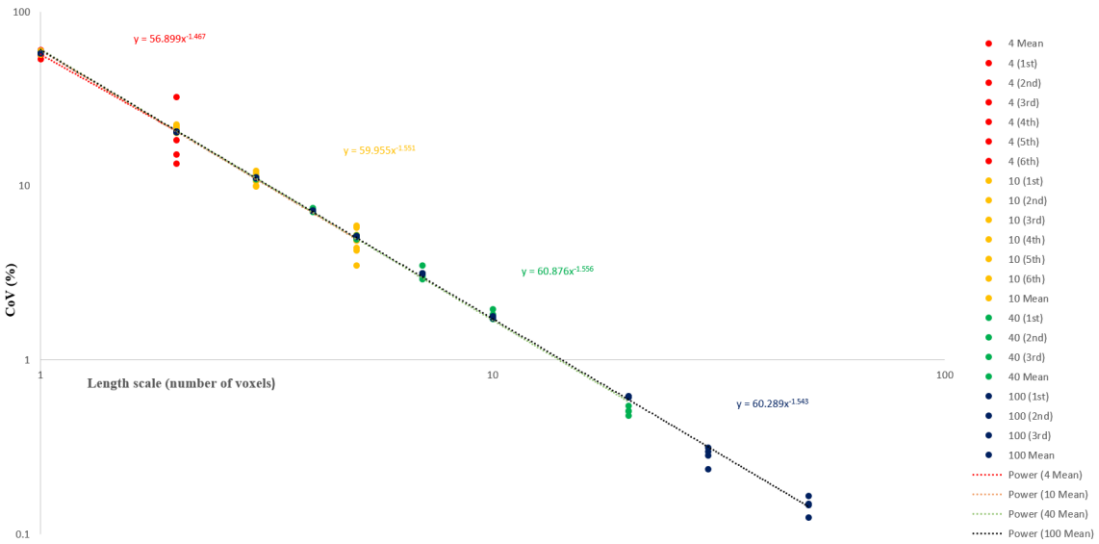

Fig. B.4. The importance of representative sample size on determining multiscale behaviour of a simulated heterogeneous medium with uniform distribution and its CL.

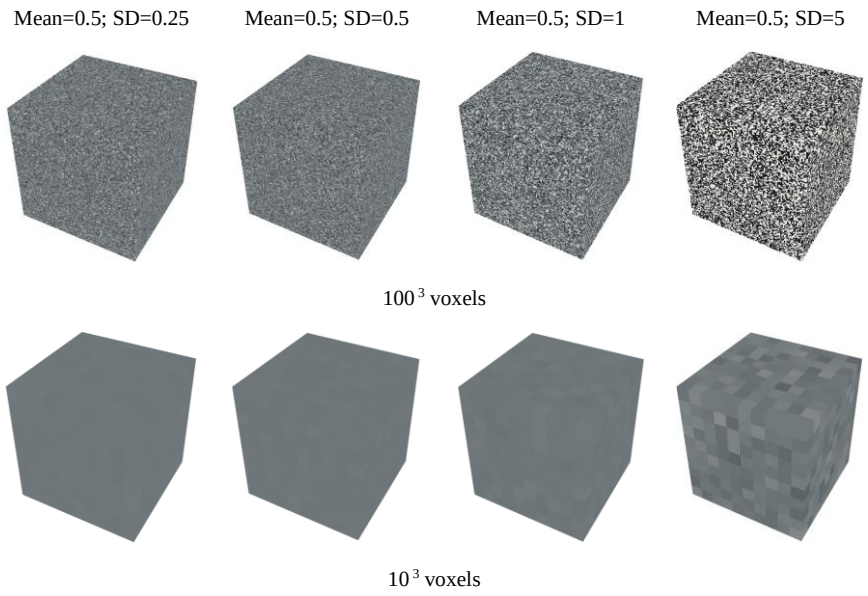

Fig. B.5. Homogenization of some media with different degrees of heterogeneity simulated using normal distributions with different standard deviations (in each case the minimum value is white and the maximum is black).

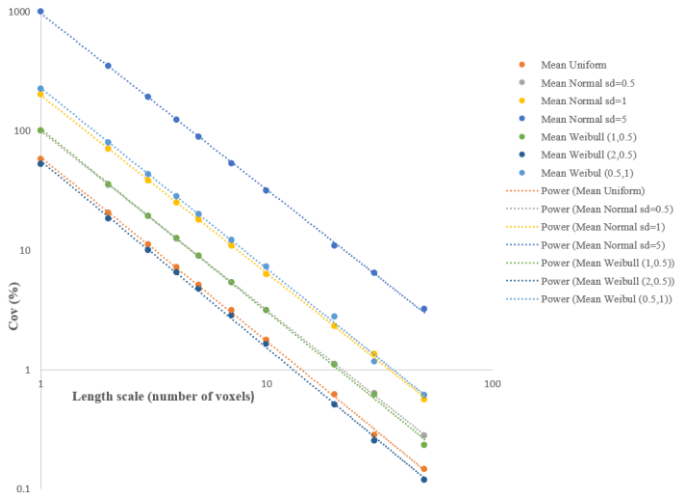

Fig. B.6. Homogenization of some simulated isotropic heterogeneous media with different distributions (normal distributions with different standard deviations and Weibull distributions with different shape and scale parameters).

Example 3: simulating asymptotic homogenization of an anisotropic medium. Figs. B.7 and B.8 are showing the asymptotic homogenization of a simulated anisotropic medium made of two periodic layers. As it is evident from statistical simulations, as opposed to isotropic materials (Figs. B.4 and B.6), anisotropic ones are showing nonlinear asymptotic

homogenization. This is showing the importance of directional dependency of materials multiscale physical properties. The method introduced by Yun et al. (2013) has been adopted to identify relative anisotropies. It is notable that after lots of examination on simulated three-dimensional materials the errors of this method have detected and eliminated in this study.

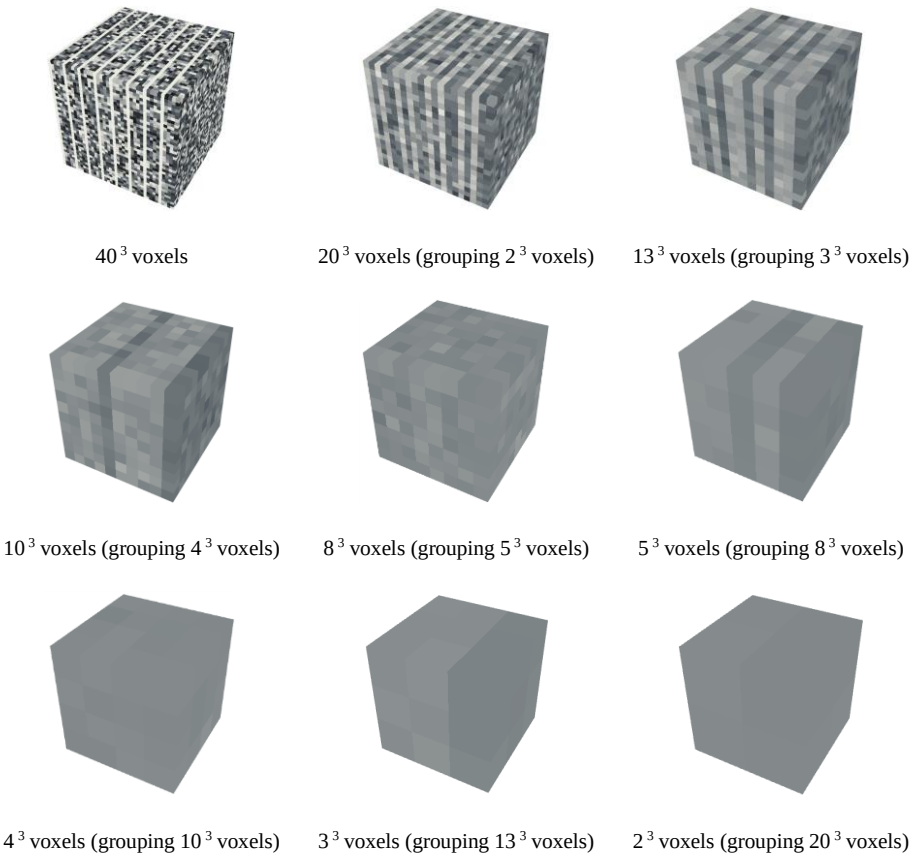

Fig. B.7. Asymptotic homogenization of an anisotropic medium made of two periodic layers.

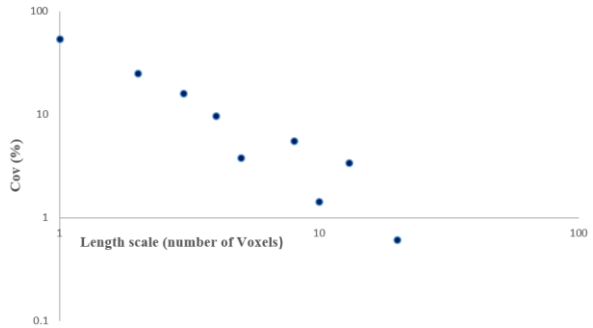

Fig. B.8. Nonlinear asymptotic homogenization of the simulated anisotropic medium.

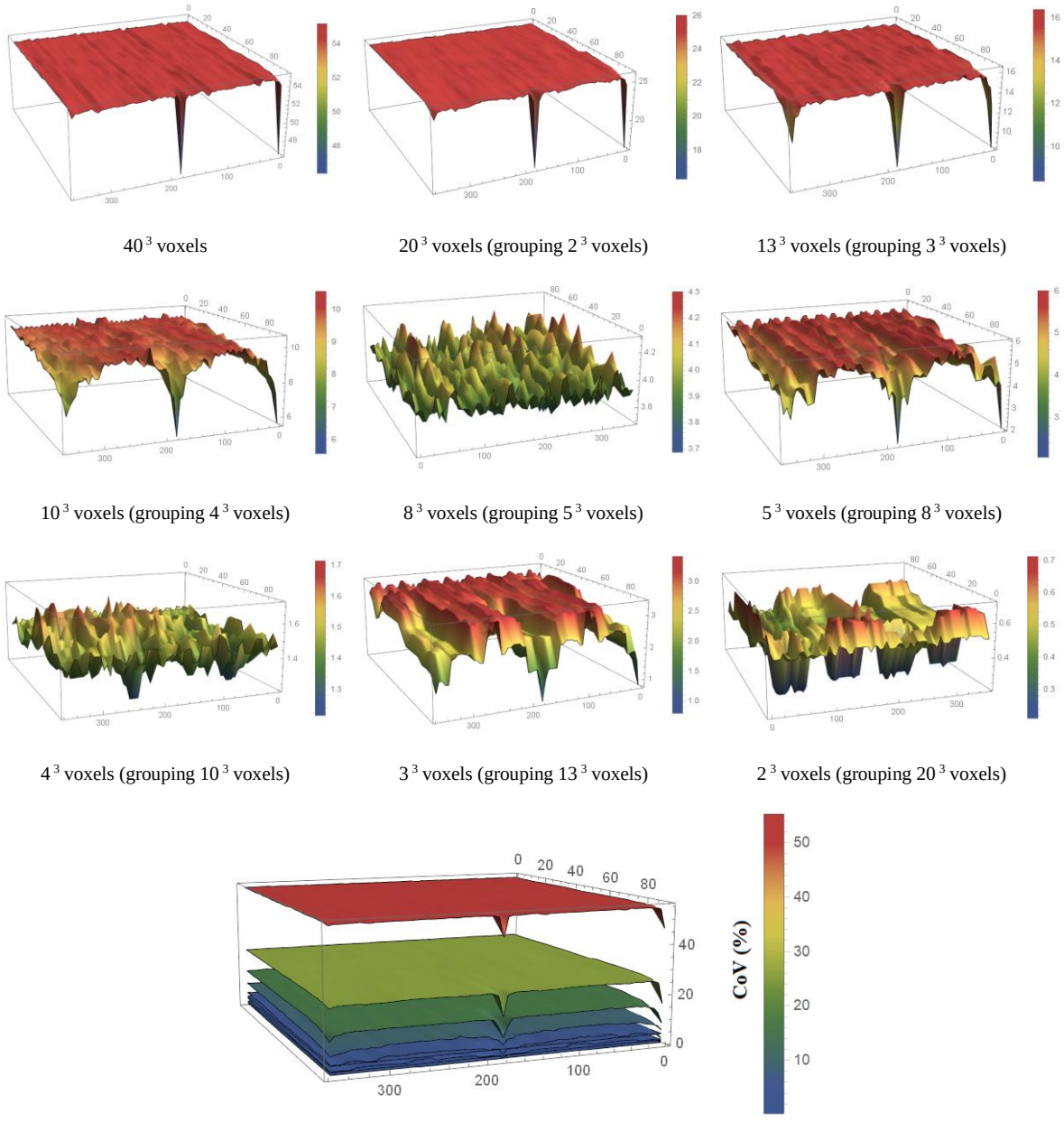

Fig. B.9. Asymptotic homogenization of the simulated anisotropic medium made of two periodic layers at each direction (trends from 0 to 359 and plunges from 0 to 90 at 5-degree intervals).

Fig. B.9 is showing the amount of heterogeneity (CoV) of this simulated anisotropic material at different length scales and directions, and Fig. B.10 is demonstrating the amount of anisotropy of the simulated material from its centre of mass. From these simple examples, it can be seen that the multiscale analysis is very promising to find CL of a media, which is related to its sample size and the resolution of the method used for tomography. Furthermore, there is no general formulation for multiscale behaviour of different materials and depending on

microstructural features the behaviour of different materials at different scales, locations and directions are different with respect to corresponding CLs.

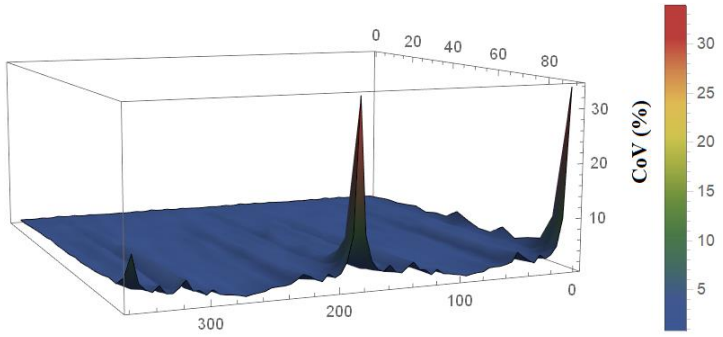

Fig. B.10. The amount of anisotropy of the simulated medium at each direction from its centre of mass.

References

Alava MJ, Nukala PK, Zapperi S (2006) Statistical models of fracture. Adv. Phys. 55:349–476.

Aligholi S, Lashkaripour GR, Ghafoori M, TrighAzali S (2017a) Evaluating the relationships between NTNU/SINTEF drillability indices with index properties and petrographic data of hard igneous rocks. Rock Mech. Rock Eng. 50(11):2929–2953.

Aligholi S, Lashkaripour GR, Ghafoori M (2017b) Strength/Brittleness classification of igneous intact rocks based on basic physical and dynamic properties. Rock Mech. Rock Eng. 50(1):45–65.

Aligholi S, Lashkaripour GR, Ghafoori M (2018) Estimating engineering properties of igneous rocks using semi-automatic petrographic analysis. Bull. Eng. Geol. Environ. 78:2299–2314.

Aligholi S, Ponson L, Torabi AR, Zhang QB (2022) A new methodology inspired from the theory of critical distances for determination of inherent tensile strength and fracture toughness of rock materials. Int. J. Rock Mech. Min. Sci. 152:105073.

Bacry E, Delour J, Muzy JF (2001) Multifractal random walk. Phys. Rev. E 64:026103.

Bakhvalov N, Panasenko G (1989) Homogenization: Averaging Processes in Periodic Media Kluwer, Dordrecht.

Balankin AS, Matamoros DM (2005) Anomalous roughness of turbulent interfaces with system size dependent local roughness exponent. Phys. Rev. E 71:056102.

Barabasi AL, Szepfalusy P, Vicsek T (1991) Multifractal spectra of multi-affine functions. Physica A 178:17.

Barabasi AL, Bourbonnais R, Jensen M, Kertész J, Vicsek T, Zhang YC (1992) Multifractality of growing surfaces. Phys. Rev. A 45:R6951.

Barenblatt GI (1959) The formation of equilibrium cracks during brittle fracture. General ideas and hypotheses. Axially-symmetric crack. J. Appl. Math. Mech. 23(3):pp. 622–636.

Barenblatt GI (1962) The mathematical theory of equilibrium cracks in brittle fracture. Adv. Appl. Mech. 7:55–129.

Bargmann S, Klusemann B, Markmann J , Schnabel JE, Schneider K, Soyarslan C, Wilmers J. (2018) Generation of 3D representative volume elements for heterogeneous materials: a review. Prog. Mater. Sci. 2018; 96:322–84.

Barras F, Geubelle PH, Molinari JF (2017) Interplay between process zone and material heterogeneities for dynamic cracks. Phys. Rev. Lett. 119(14):144101.

Bazant ZP, Kazemi MT (1990) Determination of fracture energy, process zone length and brittleness number from size effect, with application to rock and concrete. Int. J. Fract. 44:111–31.

Bazant ZP (1997) Scaling of quasibrittle fracture: Hypotheses of invasive and lacunar fractality, their critique and Weibull connection. Int. J. Fract. 83(1):41–65.

Bazant ZP, Planas J (1997) Fracture and Size Effect in Concrete and Other Quasibrittle Materials. CRC Press, Boca Raton Florida.

Bazant ZP et al. (2004) Quasibrittle fracture scaling and size effect. Materials and Structures (RILEM) 37:547–568.

Benzi R, Paladin G, Parisi G, Vulpiani A (1984) On the multifractal nature of fully developed turbulence and chaotic systems. J. Phys. A 17:3521.

Bieniawski ZT (1975) The point-load test in geotechnical practice. Eng. Geol. 9(1):1–11.

Bonamy D, Ponson L, Prades S, Bouchaud E, Guillot C (2006) Scaling exponents for fracture surfaces in homogeneous glass and glassy ceramics. Phys. Rev. Lett. 97:135504.

Bonamy D, Santucci S, Ponson L (2008) Crackling dynamics in material failure as the signature of a self-organized dynamic phase transition. Phys. Rev. Lett. 101:045501.

Bonamy D, Bouchaud E (2011) Failure of heterogeneous materials: A dynamic phase transition? Phys. Rep. 498:1–44.

Bostanabad R, Zhang Y, Li X, Kearney T, Brinson LC, Apley DW, Liu WK, Chen W (2018) Computational microstructure characterization and reconstruction: review of the state-of-the-art techniques. Prog. Mater. Sci. 95:1–41.

Bouchaud JP, Bouchaud E, Lapasset G, Planes J (1993) Models of fractal cracks. Phys. Rev. Lett. 71:2240–2243.

Bouchaud E, Lapasset G, Planes J (1990) Fractal Dimension of Fractured Surfaces: A Universal Value? Europhys. Lett. 13:73.

Bouchaud E (1997) Scaling properties of cracks, J. Phys. Condens. Matter 9 4319–4344.

Bouchaud E, Bouchaud JP, Fisher DS, Ramanathan S, Rice JR (2002) Can crack front waves explain the roughness of cracks? J. Mech. Phys. Solids 50:1703–1725.

Bouchaud E, Boivin D, Pouchou JL, Bonamy D, Poon B, Ravichandran G (2008) Fracture through cavitation in a metallic glass. Europhys. Lett. 83:66006.

Bouchbinder E, Procaccia I, Santucci S, Vanel L (2006) Fracture Surfaces as Multiscaling Graphs. Phys. Rev. Lett. 96:055509.

Bruno G, Kachanov M, Sevostianov I, Shyam A (2019) Micromechanical modeling of non-linear stress-strain behavior of polycrystalline microcracked materials under tension. Acta Mater. 164:50–59.

Carpinteri A, Chiaia B (1995) Multifractal Natural of Concrete Fracture Surface and Size Effects on Nominal Fracture Energy, Mater. Struct. 28:435–443.

Carpinteri A, Chiaia B, Ferro, G (1995) Size Effects in Nominal Tensile Strength of Concrete Structures: Multifractality of Material Ligaments and Dimensional Transition From Order to Disorder. Mater. Struct. 28:311– 317.

Carpinteri A, Pugno N (2005) Are scaling laws on strength of solids related to mechanics or to geometry? Nat. Mater. 4:421–423.

Carpinteri A, Cornetti P, Puzzi S (2006) Scaling laws and multiscale approach in the mechanics of heterogeneous and disordered materials. Appl. Mech. Rev. 59:283–304.

Chopin J, Bhaskar A, Jog A, Ponson L (2018) Depinning Dynamics of Crack Fronts. Phys. Rev. Lett. 121:235501.

Cioranescu D, Donato P (1999) An introduction to homogenization, Oxford Lecture Series in Mathematics and Applications 17, Oxford.

Cornetti P, Pugno N, Carpinteri A, Taylor D (2006) Finite fracture mechanics: a coupled stress and energy failure criterion. Eng. Fract. Mech. 73:2021–2033.

Creager M, Paris P (1967) Elastic field equations for blunt cracks with reference to stress corrosion cracking. Int. J. Frac.t Mech. 3:247–252.

Darlington WJ, Ranjith PG, Choi SK (2011) The effect of specimen size on strength and other properties in laboratory testing of rock and rock-like cementitious brittle materials. Rock Mech. Rock Eng. 44(5):513–529.

Davis A, Marshak A, Wiscombe W, Cahalan R (1994) Multifractal characterizations of nonstationarity and intermittency in geophysical fields: Observed, retrieved, or simulated. J. Geophys. Res. Atmos. 99:8055–8072.

Di Matteo T (2007) Multi-scaling in finance. Quant. Finance 7, 21–36.

Dugdale DS (1960) Yielding of steel sheets containing slits. J. Mech. Phys. Solids, 8(2):100–104.

Dutler N, Nejati M, Valley B, Amann F, Molinari G (2018) On the link between fracture toughness, tensile strength, and fracture process zone in anisotropic rocks. Eng. Fract. Mech. 201:56–79.

Esser C, Kleyntssens T, Nicolay S (2017) A multifractal formalism for non-concave and non-increasing spectra: The leaders profile method. Appl. Comput. Harm. Anal. 43:269–291.

Fakhimi A, Tarokh A (2013) Process zone and size effect in fracture testing of rock. Int. J. Rock Mech. Min. Sci. 60:95–102.

Fakhimi A, Lin Q, Labuz JF (2018) Insights on Rock Fracture from Digital Imaging and Numerical Modeling. Int. J. Rock Mech. Min. Sci. 107:201–207.

Filon LNG (1924) The stresses in a circular ring. Sel Engng Pap Instn Civ Engrs. Paper No. 12.

Fineberg J, Marder M (1999) Instability in dynamic fracture. Phys. Rep. 313: 1–108.

Flandrin P (1989) On the spectrum of fractional Brownian motions. IEEE Trans. Inf. Theory 35:197–199.

Frisch U (1995) Turbulence: The Legacy of A. N. Kolmogorov. Cambridge University Press, Cambridge.

Gao K, Chung ET, Gibson RL, Fu S, Efendiev Y (2015) A numerical homogenization method for heterogeneous, anisotropic elastic media based on multiscale theory. Geophysics 80 (4) D385–D401.

Gilmore M, Yu C, Rhodes T, Peebles W (2002) Investigation of rescaled range analysis, the Hurst exponent, and long-time correlations in plasma turbulence. Phys. Plasmas 9(4)1312–1317.

Gjerden KS, Stormo A, Hansen A (2013) Universality Classes in Constrained Crack Growth. Phys. Rev. Lett. 111:135502.

Gomez FJ, Guinea GV, Elices M (2006) Failure criteria for linear elastic materials with Unotches. Int. J. Fract. 141:99–113.

Granero-Belinchon C, Roux SG, Garnier NB (2018) Kullback-Leibler divergence measure of intermittency: Application to turbulence. Phys. Rev. E 97:013107.

Guerra C, Scheibert J, Bonamy D, DalmasD (2012) Understanding fast macroscale fracture from microcrack post mortem patterns. Proc. Nat. Acad. Sci. 109:390–394.

Halsey TC, Jensen MH, Kadanofr LP, Procaccia I, Shraiman BI (1986) Fractal measures and their singularities: The characterization of strange sets. Phys. Rev. A 33:1141.

Hansen A, Schmittbuhl J (2003) Origin of the Universal Roughness Exponent of Brittle Fracture Surfaces:Stress-Weighted Percolation in the Damage Zone. Phys. Rev. Lett. 90:045504.

Hobbs DW (1965) An assessment of a technique for determining the tensile strength of rock. Br. J. Appl. Phys. 16:259–268.

Hoek E, Brown ET (1997) Practical estimates of rock mass strength. Int. J. Rock Mech. Min. Sci. 34(8):1165–1186.

Hu R, Oskay C (2019) Multiscale nonlocal effective medium model for in-plane elastic wave dispersion and attenuation in periodic composites. J. Mech. Phys. Solids 124:220-243.

Hurst HE (1951) Long-term storage capacity of reservoirs. Trans. Am. Soc. Civ. Eng. 116:770–799.

Irwin GR (1958) Fracture. In: Flügge S (ed) Handbuch derphysik, vol. 6., Springer, Berlin.

Ivanov PC, Nunes Amaral LA, Goldberger AL, Havlin S, Rosenblum MG, Struzik ZR, Stanley HE (1999) Multifractality in human heartbeat dynamics. Nature 399:461–465.

ISRM. The complete ISRM suggested methods for rock characterization, testing and monitoring: 1974–2006. In: R. Ulusay, J.A. Hudson (eds) Suggested methods prepared by the commission on testing methods, International Society for Rock Mechanics, compilation arranged by the ISRM Turkish National Group. Kozan Ofset, Ankara: 2007.

Jaffard S (2004) Wavelet Techniques in Multifractal Analysis, in Fractal Geometry and Applications: A Jubilee of Benoit Mandelbrot, edited by M. Lapidus and M. van Frankenhuysen, Proc. of Symp. in Pure Mathematics, AMS.

Jiang F, Vecchio KS (2009) Hopkinson bar loaded fracture experimental technique: a critical review of dynamic fracture toughness tests. Appl. Mech. Rev. 62(6):060802–060839.

Kanit T, Forest S, Galliet I, Mounoury V, Jeulin D. (2003) Determination of the size of the representative volume element for random composites: statistical and numerical approach, Int. J. Solids Struct. 40:3647–3679.

Kanoute P, Boso DP, Chaboche JL, Schrefler BA (2009) Multiscale methods for composites: a review. Arch. Comput. Methods Eng. 16(1):31–75.

Kantelhardt JW, Zschiegner SA, Koscielny-Bunde E, Havlin S, Bunde A, Stanley HE (2002) Multifractal detrended fluctuation analysis of nonstationary time series. Physica A 316(1):87–114.

Karihaloo BL, Abdalla HM, Xiao QZ (2006) Deterministic size effect in the strength of cracked concrete structures. Cem. Concr. Res. 36:171–88.

Kietov V, Henschel S, Krüger L, (2019) AE analysis of damage processes in cast iron and high-strength steel at different temperatures and loading rates, Eng. Fract. Mech. 210:320–341.

Kumar S, Curtin WA (2007) Crack interaction with microstructure. Mater. Today 10:34–44.

Kuruppu MD, Obara Y, Ayatollahi MR, Chong KP, Funatsu T (2014) ISRM-Suggested method for determining the mode I static fracture toughness using semi-circular bend specimen. Rock Mech. Rock Eng. 47(1):267–274.

Leary PC (2003) Fractures and Physical Heterogeneity in Crustal Rock. In: Goff J.A., Holliger K. (eds) Heterogeneity in the Crust and Upper Mantle. Springer, Boston, MA.

Lechenault F, Pallares G, George M, Rountree C, Bouchaud E, Ciccotti M (2010) Effects of Finite Probe Size on Self-Affine Roughness Measurements. Phys. Rev. Lett. 104:025502.

Leguillon D (2002) Strength or toughness? A criterion for crack onset at a notch. Eur. J. Mech. A/Solids 21:61–72.

Maloy KJ, Hansen A, Hinrichsen EL, Roux S (1992) Experimental measurements of the roughness of brittle cracks. Phys. Rev. Lett. 68:213.

Mandelbrot BB (1983) The Fractal Geometry of Nature. Freeman, New York.

Mandelbrot BB, Passoja DE, Paullay AJ (1984) Fractal character of fracture surfaces of metals. Nature 308:721–722.

Masoumi H, Saydam S, Hagan PC (2016) Unified size-effect law for intact rock. Int. J. Geomech. 16(2): 04015059.

Martin W, Flandrin P (1985) Wigner-Ville spectral analysis of nonstationary processes. IEEE Trans. Acoust., Speech, Signal Process. 33(6):1461–1470.

Matous K, Geers MGD, Kouznetsova VG, Gillman A (2017) A review of predictive nonlinear theories for multiscale modeling of heterogeneous materials. J. Comput. Phys. 330:192–220.

Mazeran P, Odoni L, Loubet J (2005) Curvature radius analysis for scanning probe microscopy. Surf. Sci. 585:25–37.

Meneveau C, Sreenivasan KR (1987) Simple multifractal cascade model for fully developed turbulence. Phys. Rev. Lett. 59:1424.

Morel S, Bonamy D, Ponson L, Bouchaud E (2008) Transient damage spreading and anomalous scaling in mortar crack surfaces. Phys. Rev. E 78:016112.

Muralidhara S, Raghu Prasad BK, Singh RK (2013) Size Independent Fracture Energy Release Rate in Plain Concrete Beams. Eng. Fract. Mech. 98:284–295.

Muzy JF, Delour J, Bacry E (2000) Modelling fluctuations of financial time series: from cascade process to stochastic volatility model. Eur. Phys. J. B 17:537–548.

Muzy JF, Bacry E, Arneodo A (1993) Multifractal formalism for fractal signals: The structure-function approach versus the wavelet-transform modulus-maxima method. Phys. Rev. E 47:875.

Needleman A (1988) Material rate dependence and mesh sensitivity in localization problems. Comput. Methods Appl. Mech. Eng. 67:69–85.

Ogilvy JA, Foster JR (1989) Rough surfaces: gaussian or exponential statistics? J. Phys. D 22:1243–1251.

Otsuka K, Date H (2000) Fracture process zone in concrete tension specimen. Eng. Fract. Mech. 65:111–31.

Paggi M, Corrado M, Reinoso J (2018) Fracture of solar-grade anisotropic polycrys- talline Silicon: a combined phase field-cohesive zone model approach. Comput. Methods Appl. Mech. Eng. 330:123–148.

Parisio F, Tarokh A, Makhnenko R, Naumov D, Miao XY, Kolditz O, Nagel T (2019) Experimental characterization and numerical modelling of fracture processes in granite, Int. J. Solids Struct. 163:102–116.

Peng CK, Havlin S, Stanley HE, Goldberger AL (1995) Quantification of scaling exponents and crossover phenomena in nonstationary heartbeat time series. Chaos 5(1):82–87.

Ponson L, Bonamy D, Bouchaud E (2006a) Two-dimensional scaling properties of experimental fracture surfaces. Phys. Rev. Lett. 96:035506.

Ponson L, Auradou H, Vie P, Hulin JP (2006b) Low Self-Affine Exponents of Fractured Glass Ceramics Surfaces. Phys. Rev. Lett. 97:125501.

Ponson L, Auradou H, Pessel M, Lazarus V, Hulin JP (2007) Failure mechanisms and surface roughness statistics of fractured Fontainebleau sandstone. Phys. Rev. E 76.

Ponson L (2016) Statistical aspects in crack growth phenomena: how the fluctuations reveal the failure mechanisms. Int. J. Fract. 201:11–27.

Ramanathan S, Fisher DS (1997) Dynamics and instabilities of planar tensile cracks in heterogeneous media. Phys. Rev. Lett. 79:877.

Santucci S, Maloy KJ, Delaplace A, Mathiesen J, Hansen A, Bakke JOH, Schmittbuhl J, Vanel L, Ray P (2007) Statistics of fracture surfaces. Phys. Rev. E 75:016104.

Schmittbuhl J, Schmitt F, Scholtz C (1995) Scaling invariance of crack surfaces. J. Geophys. Res. 100(B4):5953–5973.

Sevostianov I, Kachanov M (2019) On the effective properties of polycrystals with intergranular cracks. Int. J. Solids Struct. 156–157:243–250.

Sharon E, Cohen G, Fineberg J (2001) Propagating solitary waves along a rapidly moving crack front. Nature 410 68–71.

Shekhawat A, Zapperi S, Sethna JP (2013) From Damage Percolation to Crack Nucleation Through Finite Size Criticality. Phys. Rev. Lett. 110:185505.

Silberschmidt V (1996) Fractal and Multifractal Characteristics of Propagating Cracks. Journal de Physique IV, Paper C6-287.

Sornette D (2004) Critical Phenomena in Natural Sciences. Springer, Berlin, 2nd ed.

Srivastava A, Ponson L, Osovski S, Bouchaud E, Tvergaard V, Needleman A (2014) Effect of inclusion density on ductile fracture toughness and roughness. J. Mech. Phys. Solids 63:62–79.

Tada H, Paris P, Irwin G (1985) The Stress Analysis of Cracks. Handbook. second ed., Paris Productions Incorporated, St. Louis Missouri.

Tanne E, Li T, Bourdin B, Marigo JJ, Maurini C (2018) Crack nucleation in variational phase-field models of brittle fracture, J. Mech. Phys. Solids 110:80–99.

Tartar L (2010) The General Theory Of Homogenization, Lecture notes of the Unione Matematica Italiana, 7, Springer.

Taylor D (2007) The theory of critical distances: a new perspective in fracture mechanics. Elsevier.

Torabi AR, Etesam S, Sapora A, Cornetti P (2017) Size effects on brittle fracture of Brazilian disk samples containing a circular hole. Eng. Fract. Mech. 186:496–503.

Vandewalle N, Ausloos M (1998) Multi-affine analysis of typical currency exchange rates. Eur. Phys. J. B 4:257–261.

Van Vliet MR, Van Mier JG (2000) Experimental investigation of size effect in concrete and sandstone under uniaxial tension. Eng. Fract. Mech. 65(2):165–188.

Vernede S, Ponson L, Bouchaud JP (2015) Turbulent fracture surfaces: A footprint of damage percolation? Phys. Rev. Lett. 114:215501.

Vogler D, Walsh SDC, Bayer P, Amann F (2017) Comparison of surface properties in natural and artificially generated fractures in a crystalline rock. Rock Mech. Rock Eng. 50:2891–2909.

Voss R (1988) Fractals in Nature: From Characterization to Simulation. Springer, New York, USA.

Wang Y, Bui HH, Nguyen GD, Ranjith PG (2019) A new SPH-based continuum framework with an embedded fracture process zone for modelling rock fracture. Int. J. Solids Struct. 159:40–57.

Weibull W (1939) A statistical theory of the strength of materials. Ph.D. dissertation, Royal Swedish Academy of Engineering Science, Stockholm, Sweden.

Weinan E (2011) Principles of Multiscale Modeling. Cambridge, UK: Cambridge University Press.

Xia K, Yao W (2015) Dynamic rock tests using split Hopkinson (kolsky) bar system - a review. J. Rock Mech. Geotech. Eng. 7(1):27–59.

Yun ST, Jeong YJ, Kim KY, Min KB (2013) Evaluation of rock anisotropy using 3D X-ray computed tomography. Eng. Geol. 163:11–19.

Zhang QB, Zhao J (2013) Effect of loading rate on fracture toughness and failure micromechanisms in marble. Eng. Fract. Mech. 102:288–309.

Zhang QB, Zhao J (2014) A review of dynamic experimental techniques and mechanical behaviour of rock materials. Rock Mech. Rock Eng. 47:1411–1478.

Zhao J (2000) Applicability of Mohr–Coulomb and Hoek–Brown strength criteria to the dynamic strength of brittle rock. Int. J. Rock Mech. Min. Sci. 371115–1121.

Zhou YX, Xia K, Li XB, Li HB, Ma GW, Zhao J, Zhou ZL, Dai F (2012) Suggested methods for determining the dynamic strength parameters and mode-I fracture toughness of rock materials. Int. J. Rock Mech. Min. Sci. 49:105–12.

Zhu XK, Joyce JA (2012) Review of fracture toughness (G, K, J, CTOD, CTOA) testing and standardization. Eng. Fract. Mech. 85:1-46.

Zietlow WK, Labuz JF (1998) Measurement of the intrinsic process zone in rock using acoustic emission. Int. J. Rock Mech. Min. Sci. 35(3):291–9.